Development of solid polymer electrolyte with excellent lithium dendrite suppression ability for all solid-state lithium metal batteries

by

Changlin Liu

Graduate School of Science and Technology

Hirosaki University

2023

ABSTRACT

With the development of renewable energy and electric vehicles, high energy density power sources have received more and more attentions. All solid-state lithium (Li) metal batteries (ASSLMBs) with the advantages of low flammability, non-volatile, and high energy density have become one of the most promising directions. However, the industrial application of ASSLMBs with long lifespan, excellent cycling stability, and low cost is still hindered by several issues, such as the uncontrolled growth of Li dendrite, degradation of interface contact, and low ion conductivity of electrolytes. In particular, Li dendrite growth is thought as the cause of continous formation of solid-electrolyte interphase (SEI) and "dead Li", which directly lead to a decrease of coulombic efficiency (CE). Therefore, high capacity retention and long cycle life are both based on excellent Li dendrite suppression ability of solid-state electrolyte (SSE). In this view, development of new SSEs, which possess an acceptable ion conductivity, a wide electrochemical stability window (ESW), high mechanical strength and a good Li dendrite suppression ability even combined with the high-loading cathode is of great importance.

In this study, a poly(ether block amide) (PEBA) based solid-state polymer electrolyte (SPE) with lithium bis-(trifluoromethanesulfonyl)imide (LiTFSI) as the Li salt is developed. It is found that the PEBA 2533-20% LiTFSI electrolyte possesses an ion conductivity of 3.0×10^{-5} S cm^{-1} at 25 ℃. Especially, the Li dendrite suppression ability of SEI is greatly enhanced since it provides abundant amide groups to activate $TFSI^-$ anions and further enriches lithium fluoride (LiF) content in the SEI layer, which endows the full-cell with enhanced cyclability. As a result, the fabricated solid-state Li/PEBA 2533-20% LiTFSI/$LiFePO_4$ (areal capacity: 0.15 mAh cm^{-2}) battery remains 94% of its maximum capacity (127.5 mAh g^{-1}) at a rate of 0.5 C and 60 ℃ after 200 cycles. In particular, the full cell can cycle for almost 1000 cycles without short circuit. Therefore, the PEBA based electrolyte could promote the LiF enriched SEI layer into a platform to suppress the growth of Li dendrite toward ASSLMBs with a long lifespan.

In order to further enhance the Li dendrite suppression ability of PEBA 2533 based SPE, aluminum oxide (Al_2O_3) nanoparticles are used as the solid plasticizer. In the case of addition of 3wt% Al_2O_3 nanoparticles, ion conductivity of the obtained PEBA 2533-20wt% LiTFSI-3wt% Al_2O_3 SPE was 3.57×10^{-5} S cm^{-1} at 25 ℃. Furthermore, the Li

symmetrical battery assembled with it shows excellent cycling stability (1000 h) at 0.1 mA cm^{-2}. While, the assembled all-solid-state Li/PEBA 2533-20% LiTFSI-3wt% Al_2O_3/$LiFePO_4$ (areal capacity: 0.15 mAh cm^{-2}) battery maintains 94.9% of the maximal capacity (133.9 mAh g^{-1}@0.1 mA cm^{-2}) at 60 ℃ even after 650 cycles with a superior average CE of 99.84%. By using X-ray photoelectron spectroscope (XPS), self-aggregation layer (SAL) of polyamide 12 (PA12) of PEBA 2533 is discovered, which should contribute to promoting the robustness of LiF enriched SEI layer. In addition, it is considered that the state of interface between SPE and cathode should be the cause of voltage polarization of the full cell.

Commonly, the larger the amount of Li deposited is, the more obvious the volume effect will be, and the more difficulty of it is to suppress Li dendrites. The excellent Li dendrite suppression ability of PEBA based SPE has been demonstrated with PEBA 2533 as the polymer matrix. However, the excellent performance of the batteries is based on low-loading cathode (0.15 mAh cm^{-2}). In the last work, PEBA 4033 based SPEs with LiTFSI as the Li salt are prepared and the ion conductivity of PEBA 4033-40wt% LiTFSI SPE achieves 3.49×10^{-5} S cm^{-1} at 25 ℃. Besides, the SPEs with Al_2O_3 nanofillers are also prepared and used to assemble the ASSLMBs combining with the high-loading $LiFePO_4$ cathode (1.5 mAh cm^{-2}). Thereafter, the effects of solvent evaporation temperature on battery performance are investigated and as a result, a higher CE is realized at higher solvent evaporation temperature.

ACKNOWLEDGEMENTS

First of all, I would like to express my sincere gratitude and deepest appreciation to Professor Dr. Guoqing Guan for providing me an opportunity to work towards PhD degree at Hirosaki University, as well as professional suggestions, guidances, supports, and feedbacks during my Ph.D program.

I would like to thank Professor Abuliti Abudula for his all guidances and kind advices on my research.

I would like to thank Professor Xiaogang Hao, Department of Chemical Engineering, Taiyuan University of Technology, China, for his encouragement and the application of Materials Studio software.

I would like to thank Dr. Qiang Zhao and Dr. Xiaowei An, for their technical supports.

I am also thankful to all professors and staffs at Institute of Regional Innovation (IRI) and Graduated School of Science and Technology, Hirosaki University, for all kind supports.

I would like to extend my sincere thanks to all members in our group, PhD alumni and classmates for all their suggestions and discussions.

I would like to thank my parents and my wife for their love, support and understanding during the hard three years.

Finally, I would like to acknowledge the scholarship from the State Scholarship Fund of China Scholarship Council.

Thank you all.

Changlin Liu

TABLE OF CONTENTS

LIST OF TABLES

LIST OF FIGURES

CHAPTER 1 Introduction

Total energy consumption in the world continues to rise with economic developing, and it has been already reached to 595.15 EJ by 2021. At present, traditional energy including coal, oil and natural gas still occupies the main part (~82.3%), which accounts for the majority of total CO_2 emmision[1]. Currently, most of the oil is consumed by transportation, such as automobile and truck. Thus, the development of an electrified transportation should be an extremely important way to achieve the social CO_2 reduction goal[2]. Fortunately, since 2000, renewables have been developed rapidly, and its proportion has increased from less than 1% to more than 6% in 2021[1]. Meanwhile, electric vehicles have been also developed rapidly in recent years. However, the construction of an electrified society puts forward higher requirements for battery systems with high energy density, high safety, and long cycle life. It has induced extensive research efforts [3-5]. Normally, the battery is composed of cathode, anode, and electrolyte. For the Li-ion battery (LIB) with liquid electrolyte, a separator is needed to avoid the contact of cathode and anode. But the use of flammble liquid electrolyte poses a huge safety risk, both in energy storage and electric vehicles. Besides, the growing pursuit for high energy density drives the cathode material from the general cathodes (such as $LiCoO_2$ and $LiFePO_4$) to high capacity cathodes, and the anode material from graphite to Li metal[6,7]. However, Li metal anode (LMA) has poor cyclability in liquid electrolytes due to its high reactivity and rapid dendrite growth during the charging and discharging process[8-10].

Considering the bottleneck of LIBs, various SSEs such as solid sulfide electrolytes [11-13], solid oxide electrolytes [14-16], solid halide electrolytes [17,18] and solid-state polymer electrolytes (SPEs) [19-22] have received extensive researches. Sulfide solid electrolytes, such as $Li_{10}GeP_2S_{12}$ (LGPS), have high ionic conductivity, which is even

close to that of the liquid electrolytes[23]. Nevertheless, those sulfide-based electrolytes are unstable at water atmosphere and uncompatible with high-voltage cathode material[24-28]. Solid oxide electrolytes, such as $Li_7La_3Zr_2O_{12}$ (LLZO), have better chemical stability with electrode materials comparing with sulfide solid electrolytes but are brittle and have severe contact problems with cathode[29]. Thus, the surface wettability is usually improved with liquid electrolytes[30,31]. As a competitive electrolyte, solid halide electrolytes have a high ion conductivity at room temperature ($>10^{-3}$ S cm^{-1}) [32-35]. On the other hand, when combined with LMA, continuous decomposition of solid halide electrolytes could happen without passivation layer formation[36,37]. In addition, hydrolysis reaction during the preparation process also hinders the application of solid halide electrolytes[38,39].

Fortunately, SPEs are more economical, easier to manufacture, and more highly flexible to improve the contact with electrodes. Actually, the polymer as an ion conductive matrix in SPEs has been investigated by Wright in the early 1970s[40]. But the technological interest in polymer electrolytes is increased until Armand et al.[41] proposed them as a new class of electrolytes in solid state batteries (SSBs). Although numerous polymers have been adopted for ASSLMBs, PEO hosting a Li salt, LiX, e.g., LiTFSI, Lithium bisfluorosulfonimide (LiFSI), Lithium trifluoromethanesulfonate ($LiCF_3SO_3$), Lithium perchlorate ($LiClO_4$), Lithium tetrafluoroborate ($LiBF_4$), and Lithium hexafluoroarsenate ($LiAsF_6$), is the most studied one[42-47]. However, in the application of SPEs-based ASSLMBs, there are at least three main issues, i.e., (1) limited ionic conductivity restricted by the low mobility of polymer segments at room temperature (RT); (2) uncontrolled Li dendrite growth during the plating and stripping process; (3) contact degradation between the SPE and cathode due to the volume variation. All these issues are still needed to be addressed.

To date, Li dendrite and cathode contact problems have been the main barriers for high energy density, high safty, and long cycle life SPEs-based ASSLMBs application[48,49]. Li dendrite growth is thought as the cause of continous formation of SEI and “dead Li”, which directly leads to a decrease of CE[48]. Therefore, high capacity retention and long cycle life are both based on excellent Li dendrite suppression ability of SPEs. Additionally, structure of cathode uesd in the LIBs is not suitable for the SPEs-based ASSLMBs due to the insufficient contact between SPEs and cathode materials, which is caused by the strong mechanical strength of polymer. Thus, it is expected that a new cathode with electrolyte inside can be developed for enhancing its ion conductivity, and a new SPEs with excellent Li dendrite suppression ability can also be developed for improving the cycling stability and further accelerate the application of ASSLMBs.

1.1 Ion conduction in SPEs

For the SPEs, considerable ionic conductivity is a prerequisite for their application in the battery devices, which exerts a critical effect on the rate performance of the ASSLMBs. Therefore, exploration of ion conduction mechanism in SPEs is the premise for developing high ion conductivity electrolytes. To date, several ion conduction theories have been developed for the SPEs, such as ion hopping, polymer segment migration, and interfacial ion conduction[50,51]. In this section, several models such as Arrhenius, Vogel-Tamman-Fulcher (VTF), and free volume are summarized for the design of SPEs.

1.1.1 Ion transfer mechanism

Generally, the SPEs are composed of inorganic salts and polymer matrix usually containing functional groups such as -O-, -S-, -N-, -P-, -C=O, and -NH_2. Those functional groups can promote the dissociation of salts into ions via electrostatic

interaction based on the Lewis acid-base properties[52]. For facilitating the dissociation of Li salts, high dielectric constant of polymer and low lattice energy of Li salts are both needed[53]. Based on the above theoretical ananysis, ion conductivty (σ) of SPEs can be calculated as follows[54].

$$\sigma = \sum n_i q_i \mu_i \qquad (1)$$

where n_i represents the concentration of carriers, q_i is the charge number of mobile ions, and μ_i represents the mobility of carries.

As shown in this formula, enhancing the dissociation of Li salts and expanding the amorphous region proporation of polymer is useful for increasing the concentration and mobility of carriers. Figure 1.1[50] illustrates the ion transfer mechanism in amorphous regions of polymer matrix. The motion of ions in polymer matrix can be described as follows: hopping between coordinating sites is one of the ways of ion transportation. In addition, ions that interact with polymer functional groups can also transport by coupling with the segments of polymer chains. Therefore, it is believed that amorphous region in polymer matrix mainly contributes to the transport of ions due to the mobility of polymer segments in amorphous regions. Thus, ionic conductivity of SPEs is strongly dependent on the crystallinity of polymer. In addition, ion hopping and polymer segment migration are both temperature dependent. It determines that SPEs own a low ion conductivity at room temparature, which makes the enhancement of ion conductivity becomes an popular reasearch topic.

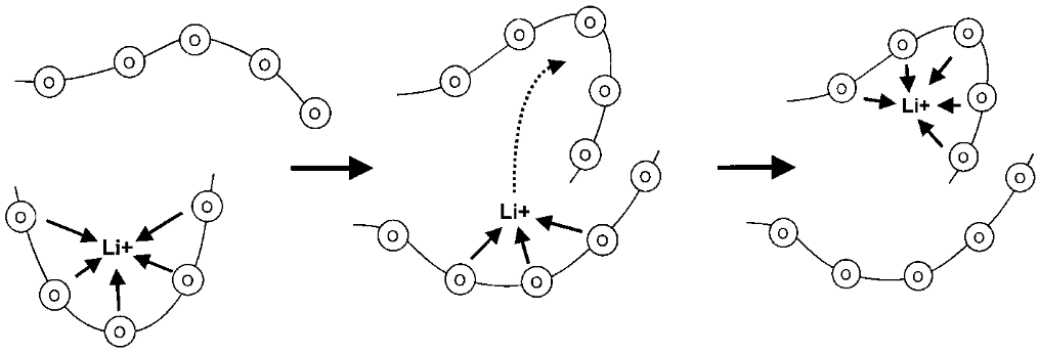

Figure 1.1 Schematic illustration of Li-ion-conduction mechanisms in amorphous phase of SPE[50].

The ionic conduction properties of SPEs can be studied by electrochemical impedance spectroscopy (EIS) with a small potential (5~10 mV) to ensure a linear current-voltage relationship, and the ionic conductivity σ is calculated by equation (2):

$$\sigma = \frac{L}{RA} \qquad (2)$$

where R (Ω) represents the obtained resistance measured by the EIS technique, L (cm) is the thickness of electrolyte, and A (cm^2) stands for the electrolyte effective area.

However, the ion transfer mechanism in composite polymer electrolytes (CPEs) is more complex when compared with those in the SPEs composed of polymer matrix and salts. The CPEs are divided into two categories based on the type of fillers. The ion-conducting mechanism of CPEs with passive fillers (SiO_2, Al_2O_3, and ZrO_2) is the same as that of SPEs. In this type of CPEs, the crystallinity and glass transition temperature (T_g) of polymer are decreased due to the modification of polymer structure. Moreover, the functional groups of passive fillers can enhance the dissociation of salts based on the Lewis acid-base theory and further increase the content of free ions. Although the ionic conductivity of SPEs can be improved greatly with the addition of passive fillers, the ion conduction of CPEs is still caused by the mobile segments of polymer matrix. For another category of CPEs, active fillers (LLZO, $Li_{0.34}La_{0.56}TiO_3$ (LLTO), and

LATP) are adopted. In this case, the ion transfer mechanism becomes extremely complex due to the combination of both organic and inorganic conductors. In addition to the same function as passive fillers, additional Li ion pathway is thought to be constructed to contribute the improvement of ionic conductivity. As shown in Figure 1.2a[51], a surface layer (~3 nm) is observed by the transmission electron microscope (TEM), which can serve as the space charge region. Herein, the formation of space charge region can be simulated with the phase-field method based on the Poisson-Cahn equations[55]. The schematic illustration of Ga-LLZO is shown in Figure 1.2b[51], in which the interface between the active particles and polymer matrix is the space charge region as the Li ion pathway.

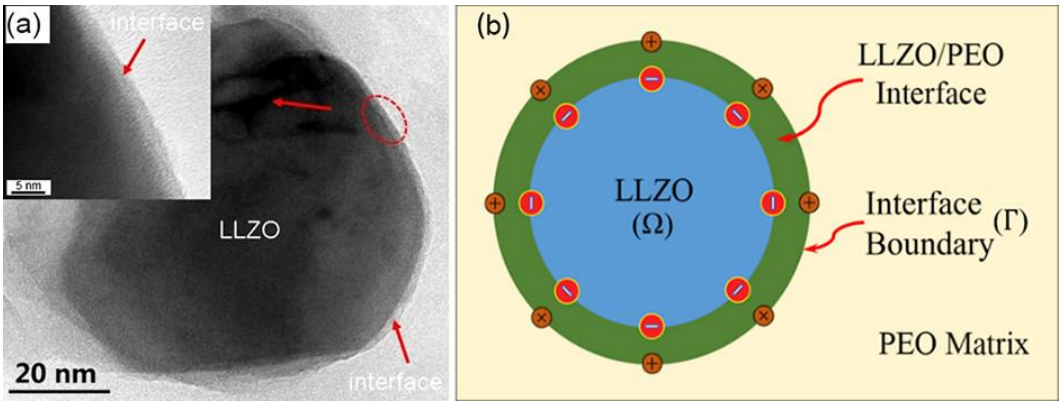

Figure 1.2 Space charge region at the Ga-LLZO/PEO interface. (a) TEM images of the Ga-LLZO/PEO interface. (b) Schematic illustration of Ga-LLZO nanoparticle in the PEO:Ga-LLZO composite. The domain of the Ga-LLZO nanoparticle Ω is surrounded by the Ga-LLZO/PEO int interface Γ[51].

1.1.2 Ion conduction models

In the SPEs, ion conductivities are usually quantified via Arrhenius and Vogel-Tammann-Fulcher models. The Arrhenius model shown as follows is more suitable for the ion conduction description of SPEs with high-crystallinity rigid solid systems[56-58] and follows the hopping mechanism[59].

$$\sigma(T) = Aexp\left(\frac{-Ea}{K_B T}\right) \quad (3)$$

where A is the pre-exponential parameter, T Kalvin temperature, and k_B Boltzmann constant.

Generally, with the decrease of T_g, flexibility of polymer chains can be enhanced. Hence, the selection of polymer matrix is crucial in the development of SPEs. The complex structure-property correlation of polymer matrix determines the ion-conducting mechanism. The Vogel-Tammann-Fulcher (VTF) equation derived by quasi-thermodynamics with free volume and configurational entropy is suitable for SPEs[60]. The relationship between ionic conductivity and temperature is described by equation (4):

$$\sigma(T) = \sigma_0 T^{\frac{1}{2}} exp\left(-\frac{B}{T - T_0}\right) \quad (4)$$

where B (EA/k) is the pseudo-activation energy, T_0 is the reference temperature (10∼50 K below T_g), σ_0 is the pre-exponential factor.

1.1.3 Li-ion transference number (t_{Li+})

Basically, SPEs are composed of polymer matrix and salts. The salt dissociates into anions and cations under the interaction with polymer, and the ions can be conducted through the polymer chains under an electric field. The SPEs containing both the mobile cations and its counter anions are dual-ion conductors, by which the Li ion and its counter anion can both easily move in it, causing a low t_{Li+}. Generally, t_{Li+} in the SPE can be analyzed with the AC impedance method by using a symmetric Li/SPE/Li cell and calculated with the formula as follows.

$$t_{Li+} = \frac{I_{ss}(\Delta v - I_0 R_0)}{I_0(\Delta v - I_{SS} R_{SS})} \quad (5)$$

in which, I_0 and I_{ss} are the initial and steady currents respectivity. R_0 and R_{ss} are the initial and steady impedance respectivity. ΔV represents AC amplitude.

Currently, for most SPEs, the values of t_{Li+} are near 0.4, which restricts the development of high-performance ASSLMBs[61,62]. Theoretically, low t_{Li+} value is caused by the stronger interaction between Li^+ and chemical groups in the polymer than anions[63,64]. It directly results in the polarization in the SPEs during the charging and discharging process. Therefore, enhancing Li^+ mobility and restricting anion migration are the direct way to improve the t_{Li+} of SPEs. Thereafter, significant effects of polymer structure and Li salt concentration on t_{Li+} improvement are proved[65,66].

Actually, the single-ion conducting SPE with the fixed anions on the polymer chain owns high t_{Li+} theoretically[62]. In the single-ion conducting SPEs, cations are the only mobile species. However, the single-ion conductor with high t_{Li+} near to 1.0 is simultaneously combined with a low ionic conductivity. Thus, the battery can only work at a high temperature with the relatively high t_{Li+} as well as high ionic conductivity. To date, the development of single-ion conductors showing both high ionic conductivity and high t_{Li+} at ambient temperature still remains challenge.

1.1.4 Space-charge theory

Generally, the battery assembled with anode, cathode, and SPEs contains several interfaces inside, such as anode-SPE interface and cathode-SPE interface. Normally, chemical potentials of carriers in different materials are significantly different, which promotes the migration and redistribution at the interface area. Thereafter, a stable region formed with the accumulation and depletion of carriers, which is called space-charge layer (SCL)[67-73]. Of course, the transition of SPEs from isotropic to anisotropy state during the charging and discharging process can also be thought as a SCL. Thus, the SCL inside battery is complex and makes great influence on Li^+ migration.

In this theory, the region near cathode is thought as quasi-neutral region and the

region near anode side is called SCL. While, ion tranfers in the quasi-neutral region and SCL are driven by diffusion and electric field respectively. Importantly, the SCL near anode is thought as the cause of Li dendrite growth[74]. Consequently, new SPEs which can regulate the distribution of both anions and cations are of great importance for the suppression of Li dendrite[75,76]. Immobilizing anions is one of the effective ways to improve the cycling performance of batteries, and even less than 10% anion could be immobilized, the cell owns much extended cycle life[77,78]. As aforementioned, single-ion conducting SPEs with much more anions immobilized should have better performance in Li dendrite suppression. Meanwhile, it normally possesses a lower ionic conductivity. Thus, balance of ion conductivity and Li deposition performance is of great importance.

1.2 Categories of SPEs

SPEs with alkali-metal salts dissociated in polymer matrix was first discovered by Wright in 1973[40]. Then, in 1979, Armand and co-workers[79] envisioned the potential of SPEs through the investigation of PEO based electrolyte. Since then, research on SPEs for Li battery has improved tremendously. From that time, SPEs are thought to be safe due to the absence of liquid solvents and flexible with various shapes, and their light weight can also improve the energy density of battery. However, for practical application of ASSLMBs in electrochemical devices, the SPEs must fulfil some other prerequisites[80]:

1) Ionic conductivity higher than 10^{-4} S cm^{-1}.
2) Chemical and electrochemical stability with the Li anode or cathode material during cycling.
3) Thermal and mechanical stability during charge and discharge processes.
4) Low cost, simple fabrication process, and environmentally friendly.

Normally, SPEs are dual-ion conducting electrolytes and composed of various polymer matrices and Li salts. In order to make the polymer function as host in the SPEs, the polymer must possess polar groups with lone-pair electrons for bonding with the cation. Various polymers such as Polyethylene oxide (PEO), polyacrylonitrile (PAN), poly(vinylidenefluoride) (PVDF), poly(methyl methacrylate) (PMMA), Poly propylene carbonate (PPC), poly(vinylidenefluoride-co-hexafluoropropylene) (PVDF-HFP), and cellulose, as shown in Figure 1.3[81] have been adopted as SPEs matrix.

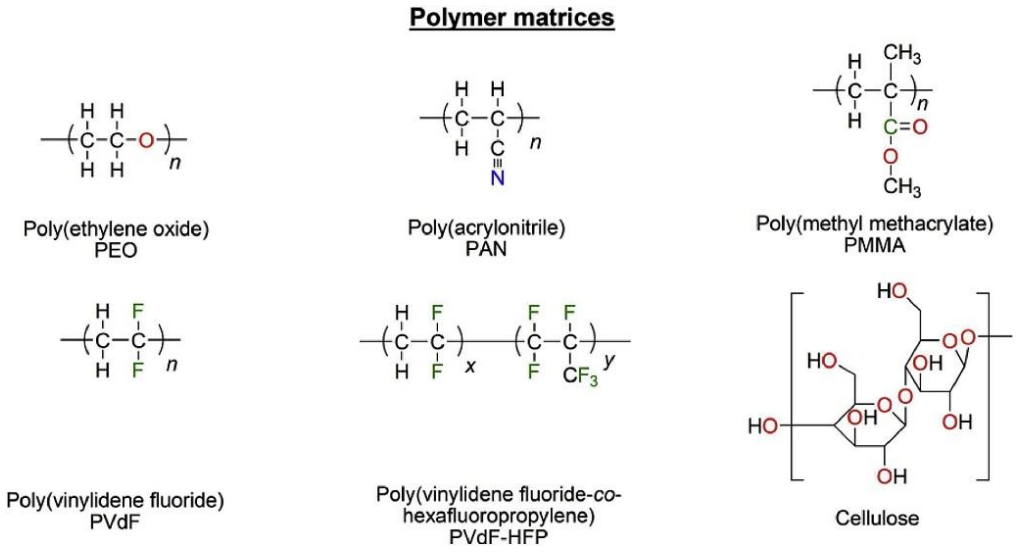

Figure 1.3 Chemical structures of commonly-studied polymer matrices for solid composite electrolytes[81].

Unfortunately, SPEs usually show poor ion conductivity at room tempearture due to the poor mobility of polymer segments as discussed before. Ion conductivities of several typical SPEs are shown in Table 1.1.

Table 1.1 Ionic conductivities of various SPEs

Polymer matrix	Li salt	Ion conductivity (10^{-4} S cm^{-1})	Temperature (℃)	Ref.
PEO	LiTFSI	0.417	25	[82]
PVDF-HFP	LiTFSI	0.0016	25	[83]
PAN	$LiClO_4$	0.06	RT	[84]
PPC	LiTFSI	0.011	RT	[85]
PVDF	$LiClO_4$	0.36	RT	[86]
PMMA	$LiClO_4$	0.039	30	[87]

While, different architectures of SPEs normally lead to differences in interfacial compatibility, SEI composition, Li dendrite suppression, and ionic conductivity. Therefore, in-depth understanding of the composition and structure of SPEs is critical for ASSLMBs development. To present, enormous CPEs have been developed for improving the performance of ASSLMBs through blending, grafting, copolymerization, and fillers addition.

1.2.1 Nanoparticle filling

CPEs have been extensively studied due to their ability to simultaneously improve the ionic conductivity and shear modulus of SPEs. As a representative strategy, inorganic nanoparticles which can disorder the crystallization of polymers is adopted as the filler to facilitate the dissociation of Li salts due to its plastification effect. In addition, it can also improve the mechanical property of SPEs. The inorganic fillers are usually divided into passive fillers (ZrO_2, Al_2O_3, SiO_2, TiO_2, CuO) and solid inorganic electrolytes (LLTO, LLZO, LATP, LAGP). Additionally, ion conduction performance of CPE is also affected by filler dimension.

The mostly used nanoparticles are thought as zero-dimensional (0D) fillers,such as ZrO_2, Al_2O_3, SiO_2, TiO_2, CuO. Addition of inorganic nanoparticles can decrease the crystallinity of polymer and enhance the dissociation of Li salts based on the Lewis

acid-base interactions. Croce et al.[88] obtained ionic conductivities of 10^{-4} S cm^{-1} at 50 °C and 10^{-5} S cm^{-1} at 30 °C, respectively, with the doping of TiO_2 and Al_2O_3 fillers in PEO-$LiClO_4$ electrolyte. Cui's group[89] prepared SiO_2 nanoparticles with high monodispersity through an *in-situ* hydrolysis technology, by which the crystallinity of PEO can be decreased so that high ionic conductivity (10^{-4} S cm^{-1} to 10^{-5} S cm^{-1} at RT) was achieved. However, Tan et al.[90] compared the effect of SiO_2 and Al_2O_3 addition on PMMA based CPEs, and found that the addition of Al_2O_3 enhanced the ionic conductivity of CPEs, but the addition of SiO_2 made no difference. Jayathilaka et al.[91] further revealed that chemical groups on the Al_2O_3 nanoparticles play the main role in the enhancement of ionic conductivity of SPEs. Acidic groups always exhibit the highest enhancement followed by basic, neutral, and weakly acidic ones. In general, passive nanoparticle fillers really enhance the ionic conductivity and mechanical properties of SPEs. Apart from these nanopartcles, metal-organic frameworks (MOFs) are also used as fillers in CPE. MOFs can be converted into Li^+ conductors by storing Li^+ in the nanopores, which makes it an ideal filler for enhancing SPE performance. Considering the Lewis acidic interaction between MIL-53(Al) and $N(SO_2CF_3)_2^-$ anions, PEO-MIL-53(Al)-LiTFSI with increased ion conductivity (3.39×10^{-3} S·cm^{-1} at 120 °C) was prepared by Zhu et al.[92]. Meanwhile, the thermal stability and mechanism strength of PEO are both improved due to the cross-linking of MIL-53(Al) nanoparticles.

Apart from aforementioned inert nanoparticles, solid inorganic electrolytes such as LLZO, LLTO, LATP, LAGP[93-95] are more effective due to the intrinsic high ionic conductivity (higher than 10^{-4} S cm^{-1} at RT) apart from impeding crystallization and improving mechanical properties of SPEs. Among all the solid inorganic fillers, LLZO is favored for the chemical stability with Li anode and high oxidation potential[96].

Chen et al.[97] obtained the ionic conductivity of 1.9×10^{-5} S cm^{-1} at 30 °C when using PEO_{18}-LiTFSI-7.5% LLZO CPEs, which is much higher than that using PEO_{18}-LiTFSI (2.92×10^{-6} S cm^{-1} at 25 °C). For further understanding the Li^+ transfer mechanism inside the CPE, Finite element calculations were conducted and proved that the interface between polymer and ceramic particles has positive effect on ion conduction[98,99]. However, some other researches show that Li^+ can also transfer through the ceramic particles[98,100].

To present, three pathways for Li^+ transporation are proved, namely, polymer matrices, fillers, and polymer/filler interfaces. Therefore, one-dimensional (1D), two-dimensional (2D), and three-dimensional (3D) fillers with longer continuous pathways may reduce the junction crossing existed in CPE with 0D fillers. Electrospinning LLZO fibers are adopted to blend with PEO, and the hybrid electrolytes also exhibit enhanced Li-ion conductivity of 1.59×10^{-4} S cm^{-1} at ambient temperature[101]. Effects of LLZO nanowires orientation on ion conductivity of PAN-$LiClO_4$ electrolyte are also investigated and the ionic conductivity can reach to 5.4×10^{-6} S·cm^{-1} at RT with the random nanowires addition, which is 15 times of the electrolyte without LLZO nanowires. In addition, the ionic conductivity can be further improved to 6.05×10^{-5} S·cm^{-1} with the nanowires arranged[102]. It proved that orientation of nanowires make great influence on the improvement of CPE ionic conductivity.

Graphene oxide (GO) as the representative of 2D materials is also adopted as the filler for ionic conductivity enhancing in CPE[103]. GO with abundant functional groups can not noly decrease the crystallinity of PEO but also accelarate the dissociation of Li salt in the PEO-$LiClO_4$-GO electrolyte[104]. Thus, the ion conductivity of CPE is significantly improved to ~10^{-5} S·cm^{-1} with only 1wt% GO addition.

Considering the significant ionic conductivity improvement of SPEs with 0D, 1D, and 2D fillers, 3D nanofiller network, which can avoid the aggregation phenomenon occurred on low dimensional fillers, is expected to further enhance the properties of CPE. Actually, continuous fast Li-ion conduction pathways can be formed by blending PEO with 3D garnet framework, by which the enhanced Li-ion conductivity (1.2×10^{-4} S cm^{-1} at 30 °C), excellent thermal, mechanical, and electrochemical stabilities are achieved[105]. Apart from the conductive ceramic frameworks, inert ceramic frameworks can also be used for CPE preparation. Continuous ceramic/polymer interfaces have been constructed with PEO and aluminum framwork, and the ion conductivity is enhanced to 5.82×10^{-4} S cm^{-1}[106]. More researches about ionic conductivity improving are shown in Table 1.2.

Table 1.2 Polymer electrolyte modification by nanofilling

Dimension	Polymer matrix	Additive	Ion conductivity (S cm^{-1})	Temperature (℃)	Ref.
0D	PAN	ZrO_2	1.16×10^{-3}	25	[107]
	PMMA	TiO_2	3.0×10^{-4}	30	[108]
	PEO	AlF_3	1.58×10^{-4}	30	[109]
	PEO	$Li_7La_3Zr_2O_{12}$	3.9×10^{-4}	25	[110]
	PEO	Al-LLZO	4.4×10^{-4}	30	[111]
	PEO	Ta-LLZO	4.8×10^{-4}	60	[112]
	PVDF	Ta-LLZO	5.0×10^{-4}	25	[113]
	PEO	LATP	1.7×10^{-4}	20	[93]
	PEO	LAGP	6.76×10^{-4}	60	[95]
	PEO	$Li_{10}GeP_2S_{12}$	1.21×10^{-3}	80	[114]
1D	PVDF-HFP	SiO_2	1.08×10^{-3}	25	[115]
	PAN	LLTO	2.4×10^{-4}	25	[116]
	PEO	LLTO	2.4×10^{-4}	25	[117]
	PAN	LLZO	1.31×10^{-4}	25	[100]
	PEO	Ta-LLZO	2.13×10^{-4}	25	[118]
2D	PEO	Graphene oxide	$\sim10^{-5}$	25	[104]
	PEC	Montmorillonite	3.5×10^{-4}	25	[119]

	PVDF-HFP	Carbon nitride	2.3×10^{-4}	30	[120]
	PVDF-HFP	Hydroxide	2.2×10^{-4}	25	[121]
	PEO	g-C_3N_4	1.7×10^{-5}	30	[122]
3D	PVDF-PEO	Gd-doped CeO_2	2.3×10^{-4}	30	[123]
	PEO	AAO	5.82×10^{-4}	25	[106]
	PEO	PVDF	$\sim10^{-5}$	30	[124]
	PEO	Aramid nanofiler	8.8×10^{-5}	25	[125]
	PEO	Al-LLZO	2.5×10^{-4}	25	[99]
	PEO	Ta-LLZO	1.17×10^{-4}	30	[126]
	PEGMEA	Li_6PS_5Cl	4.6×10^{-4}	25	[127]

In general, addition of nanoparticles into the polymer matrix can improve the ionic conductivity of SPEs by inhibiting polymer crystallinity and accelarating Li salt dissociation, especially for 1D, 2D, and 3D materials with continuous pathways. Additionally, the mechanical strength, electrochemical stability and thermal stability can also be enhanced significantly. Thus, filling nanoparticles is an optional and potential solution for improving the performance of SPEs.

1.2.2 Ionic liquids adding

Normally, the ion conductivity of SPEs is much lower than that of liquid electrolyte at room temperature, which restricts the application of ASSLMBs. In order to improve the ionic conductivity of SPEs at room temperature, the less flammable ionic liquid is adopted as the additive for improving the ionic conductivity of SPEs. Therefore, ionic liquid-polymer composite electrolyte proposed by Passerini et al. received more and more researches[128-130].

The ionic conductivity of PEO_{18}LiTFSI electrolyte was enhanced from 5.6×10^{-6} S cm^{-1} to $\sim10^{-4}$ S cm^{-1} by using (N-methyl-N-proylpiperidinum bis(fluormethanesulfonyl)imide (PP13FSI) ionic liquid as the additive at 25 ℃[131]. In addition, the grain boundary resistance of PEO can also be decreased with the addition of PP13FSI ionic liquid, which is the cause of increased ionic

conductivity[132]. Apart from the ionic conductivity, the Li dendrite suppression ability of electrolyte is another important factor that hinders the application of ASSLMBs. Imanishi et al. [133] compared the performances of Li symmetrical batteries assembled with PEO_{18}LiTFSI and PEO_{18}LiTFSI-PP13FSI electrolytes respectivity, and revealed that the short-circuit time was extended from 15 h to 37 h at the current density of 1.0 mA cm^{-1}. However, the mechanical strength will decrease with the addition of ionic liquid. Thus, the development of SPEs with high ion conductivity and mechanical strength is still urgent and at the same time, searching for the polymer matrix which is suitable for the Li anode to generate stable SEI layer is also important for the application of ASSLMBs.

1.2.3 Polymer blending, crosslinking, and copolymerizing

In addition to the aforementioned solutions, blending, copolymerization, and crosslinking are all promising methods to improve the ionic conductivity as well as mechanical properties of SPEs. The polymers commonly used in SPEs include PEO, PAN, PVDF, PMMA, PPC, and PVDF-HFP, and all the polymers have their own characteristics. Polymer blending by combining two or more polymers is the simplest way to improve the ionic conductivity, mechanical property, and electrochemical stability of SPEs due to the combination of advantages from different polymers.

The PEO-based electrolyte with good interfacial stability when combined with Li metal is mostly used to blend with other polymers[134,135]. Comparing with the low ionic conductivity of PEO-based electrolyte, PAN-based electrolyte possesses higher ionic conductivity at room temperature. However, its mechanical strength is poor. In this view, blending of polymers is a promising and feasible solution to combine the advantages together. For example, Wu et al.[136] blended PVDF-HFP with Poly(3-{2-[2-(2-hydroxyethoxy) ethoxy] ethoxy}methyl-3′-methyloxetane) (PHEMO) together as

a new polymer matrix, and the ionic conductivity can reach up to 1.64×10^{-4} S cm^{-1} at RT. The crystalline and thermal properties of PEO-based electrlyte blended with PPC were tested and proved that both the crystallinity and the T_g of the electrolyte decrerased. Therefore, a high ionic conductivity (6.83×10^{-5} S·cm^{-1}) was realized at RT[137]. Besides, cross-linked SPEs are also effective to enhance ionic conductivity and suppress Li dendrite growth contributing to the amorphous phase increase and 3D network. Cross-linked polyethylene (PE)/PEO electrolytes with low-modulus ($G' \approx 1.0\times10^5$ Pa at 90 °C) can also exhibit excellent Li dendrite suppression ability with a high ionic conductivity (>1.0×10^{-4} S cm^{-1} at 25 °C)[138]. What should be pointed out is that high modulus is not necessary for suppressing Li dendrites. Perhaps the interfacial SEI stability caused by the confinement migration of polymer segments is the key to suppressing dendrites. Moreover, copolymer contains at least two types of monomers could provide ionic conduction and mechanical support functionalities separately. Excellent Li dendrite suppression ability is demonstrated by using polystyrene-block-polyethylene oxide (SEO) block copolymer electrolytes[139]. While, the SPE prepared by mixing poly(ether block amide) (PEBA) 4011 and $LiClO_4$ has a ionic conductivity of 1.0×10^{-6} S cm^{-1}[140]. In general, SPEs enhanced with various methods still can not meet the requirements of commercial application, especially due to the low ionic conductivity at RT compared with liquid electrolyte, which really restricts the rate performance of ASSLMBs.

1.2.4 Gel polymer electrolytes (GPEs)

In order to accelerate the application of ASSLMBs, gel polymer electrolytes (GPEs) as a new type of electrolyte is developed to conquer the ionic conductivity issue. Normally, GPEs are composed of polymer network and liquid electrolyte[141-143]. Thus, the GPEs possess a high ionic conductivity close to that of liquid electrolyte and

acceptable mechanical strength. In addition, the interface contact, leakage of electrolyte and flammability issues are also solved.

Commonly, there are several strategies for GPEs` preparation, such as cross-linking, physical gelation, and polymerization[142]. Moreover, the polymerization strategy can be further divided into ex situ and in situ methods. For the ex situ preparation of GPEs, phase inversion and casting are the most popular methods[144-147]. However, poor interface contact and the resulting interface resistance still exist. In addition, the volatilization of organic solvent is inevitable. Therefore, in situ preparation of GPEs through polymerizing is investigated and excellent battery performance has been proved[148,149]. Kang et al. [150] prepared the pentaerythritol tetraacrylate (PETEA)-based GPE and realized a extremely high ionic conductivity (1.13×10^{-2} S cm^{-1}). In order to balance the mechanical strength and improve the thermal stability of GPE, Guo et al. [151] prepared a poly(vinylene carbonate) (PVC) based GPE via in situ method and realized a high ionic conductivity (4.4×10^{-3} S cm^{-1}) at 20 °C. However, polymerization rate is difficult to control during the in situ preparation process, which directly restricts the consistency of ASSLMBs.

As discussed above, although there are many solutions to improve the ionic conductivity, mechanical property, and electrochemical stability of SPEs, the compatibility for electrolyte-electrode interface is still full of challenge.

1.3 Compatibility of SPEs

1.3.1 Compatibility with anode

Li metal with the lowest formal potential of -3.045 V vs. Standard hydrogen electrode (SHE) is very active to react with salt anions, liquid solvents, and impurities in the electrolyte to form a stable SEI layer, which can effectively hinder the continuation of the reaction. However, during the repeated charge-discharge process, the SEI layer will

be damaged and rebuilt again and again, which could result in the continuous consumption of anions, and further lead to the decrease of ionic conductivity of SPEs. In addition, the increased roughness of electrode surface inevitably causes the inhomogeneous distribution of electrical fields and Li plating. As such, Li dendrite will grow from these defects firstly and result in low coulombic efficiency, bad interface contact, short cycling life and safety problems. In particular, as shown in Figure 1.4[48], "dead Li" deposites at the anode surface could hinder the movement of Li ions.

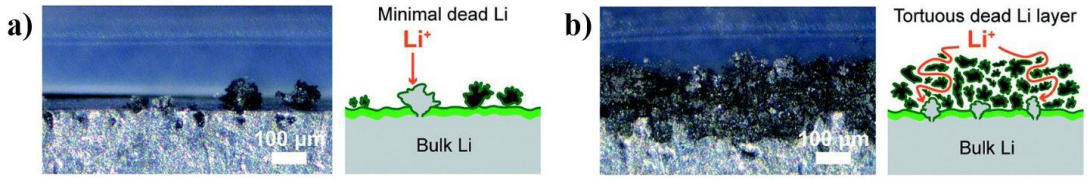

Figure 1.4 (a) Earlier cycles and (b) later cycles show that amore tortuous pathway is present after the accumulation of a thick dead Li layer on the electrode surface[48].

Although SPEs can generally make intimate interfacial contact with Li anode, they still cannot inhibit Li dendrites. As aforementioned, high modulus contributes to the suppression of Li dendrites but leads to poor interface contacts with both anode and cathode, which reflects the trade-off between the interface contact and Li dendrite suppression. Therefore, in order to realize the application of Li-air batteries, there are at least two requirements: (1) the interface between anode and SPEs must be stable enough without destroying the SEI layer and keep intimate contact during the repeated charge-discharge process; (2) the SPEs must possess high modulus to hinder the growth of Li dendrites at considerable current density.

Various strategies have been adopted to suppress the growth of Li dendrite, such as using inorganic fillers, blending different polymers, copolymerization and crosslink. However, the Li dendrite problem has only been alleviated to a certain extent, and is still not solved. Thus, development of novel SPEs remains extremely urgent and

important, especially new-type salts, additives, and combination of polymer groups. Moreover, it must be pointed out that the selection of solutions usually requires multiple considerations.

1.3.2 Compatibility with anode

Ideally, the SPEs should be thermodynamically stable against anode and cathode. As shown in Figure 1.5a[152], the potential range of electrodes is from μ_a to μ_c, and the energy gap (E_g) between the lowest unoccupied molecular orbital (LUMO) and the highest occupied molecular orbital (HOMO) is defined as the electrochemical window of SPEs. In order to avoid the electrochemical reactions between the SPE and electrodes, the potential range of electrodes should be within E_g. The electrochemical windows of several representative SPEs and inorganic electrolytes are summarized in Figure 1.5b[153].

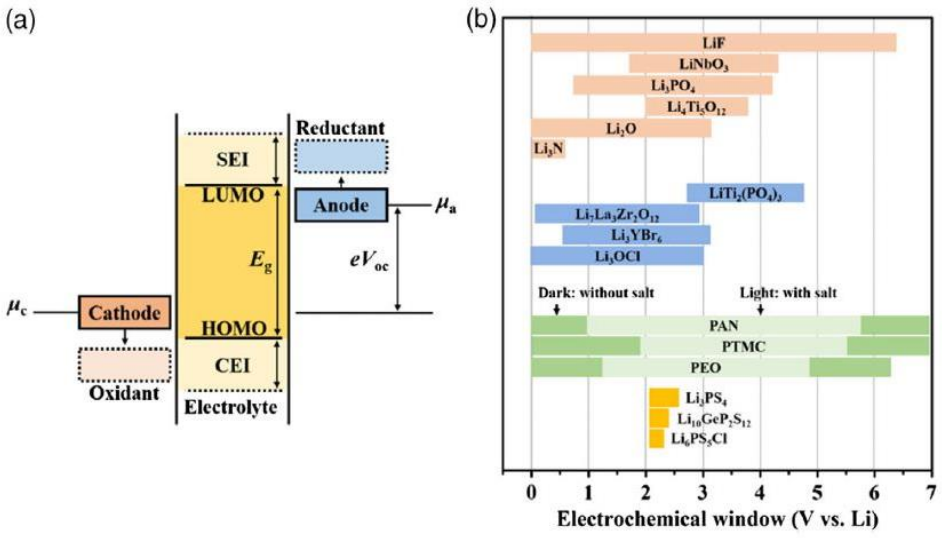

Figure 1.5 a) Relation between energy gap (μ_a-μ_c) and the LUMO-HOMO window of an SSE[152]. b) Electrochemical windows of various electrolytes[153].

PEO based electrolytes have been reported to be stable even at 4.2 V[154], however, the upper limit of its electrochemical window may be overestimated due to the

imperfect contact between electrolyte and cathode, and testing methods also make a great difference[155]. Thus, an accurate and unified testing method is needed. Apart from the electrochemical stability of SPEs contacted with cathode materials, the contact property between SPEs and electrode is also significant for the improvement of ASSLMBs.

Actually, the traditional cathode is designed for LIBs using liquid electrolyte. However, when the liquid electrolyte is changed to SPEs, the contact problem appears due to the strong mechanical strength of SPEs. Thus, a new cathode which possesses high ionic conductivity is urgently needed for the application of ASSLMBs. Ye et al. [156] prepared the $LiCoO_2$-$Li_{6.6}La_3Zr_{1.6}Ta_{0.4}O_{12}$ (LCO-LLZTO) composite cathode with a high areal capacity (>3.0 mAh cm^{-2}) through a water-based method, and high specific capacity (~120 mAh g^{-1}) is realized at the current density of 0.05 mA cm^{-2} and 60 °C. However, specific capacity of the full cell decreases rapidly to lower than 70 mAh g^{-1} only 11 cycles later, and the mechanism is still unclear. In addition, Ihrig et al. [49] tried to enhance the contact between electrolyte and cathode by infiltration of SPE into $LiFePO_4$-$Li_{1.5}Al_{0.5}Ti_{1.5}(PO_4)_3$ (LFP-LATP) composite cathode. The cycling performance of the full cell assembled with this cathode shows a high specific capacity (>160 mAh g^{-1}) after 8 cycles, which reveals that the cathode and SPE is fully contacted, but during the first 8 cycles. Moreover, the contact between cathode and SPE is improved gradually, which demonstrates that the interface is not perfect at the first cycle. Additionally, the specific capacity begins to decrease after 30 cycles, and the mechanism is still unlear. Based on the aforementioned analysis, there are still many obstacles for the application of ASSLMBs, especially for the high-loading cathode batteries. It should be pointed out that the application of ASSLMBs is the first step even in a low current density and high temperature.

1.4 Preparation methods of SPEs

Generally, the properties of SPEs are closely related to the preparation method and fabrication process. Solution casting, electrospinning, and phase inversion are several popular methods for the SPE preparation. Among all the mentioned methods, the solution casting is the most conventional and easy way. At first, the solution containing both polymer and salts is casted onto a suitable substrate. Then, the solvent is evaporated at RT or elevated temperature in an oven. Sometimes, the casting procedure is also conducted in a glovebox. After drying, the as-prepared SPE can be used directly. As for the electrospinning method, it can be used to produce films with a fiber morphology. And the thermal stability of electrospinning films is much better than that prepared by solution-casting method. However, many parameters relating to the preparation such as solution viscosity, surface tension, and polymer molecular weight need to be optimized in the electrospinning process. In addition, the setup conditions (e.g., flow rate, applied voltage) of electrospinning are also very complex.

The phase inversion technique is suitable to prepare SPEs with porous structure. Solangi et al.[157] prepared the PVDF-HFP based SPEs by using this method. Herein, firstly, the solution containing PVDF-HFP, CeO_2 and N-Methylpyrrolidone (NMP) solvent was stirred for 24 h, and then coated onto the glass-plate. Hereafter, it was immersed in water for solvent extraction and then soaked in $LiClO_4$ solution for 6 h. Finally, the as-prepared SPE possessed a conductivity of 2.5×10^{-5} S cm^{-1} at 25 °C. While, dry-mixing is a new way to prepare SPEs without using solvent, which is usually combined with the hot-pressing. The PEO-based SPE has been prepared with this method with a ionic conductivity of 10^{-5} S cm^{-1} at RT[158]. As stated above, the solution casting should be more convenient than the electrospinning, dry-mixing and phase inversion techniques for SPE preparation.

1.5 Objective of this study

Normally, excellent long-cycle performance, rate performance, and temperature properties are the basis for ASSLMBs application. As reviewed above, there are still several obstacles on the road of ASSLMBs` industrial application, especially with the SPEs. Li dendrite growth during the charge-discarge process is thought as the main problem, especially at high current density, which really restricts the rate performance of ASSLMBs. Besides, after the continues stripping and plating process, the interface between LMA and SPEs degradates gradually, which directly results in the growth of Li dendrite, increase of interface resistance, continous growth of SEI layer and "dead Li" phenomenon. The objectives of this study are to develop new SPEs, which possess acceptable ion conductivity, a wide electrochemical stability window, high mechanical strength and good Li dendrite suppression ability even combined with the high-loading cathode. Furthermore, the mechanism behind the excellent battery performance will be discussed based on the experimental and calculation results.

1.6 Scope of this dessertation

The introduction is considered as Chapter 1, in which the progress of ASSLMBs, preparation of SPEs, and mechanisms relating to the lithium ion transfer in the SPEs are reviewed and discussed.

Chapter 2 presents the preparation process of PEBA 2533 based electrolyte with LiTFSI as the Li salt and the cycling performance of the full battery assembled with LMA and $LiFePO_4$ cathode. The thermal stability, electrochemical stability and crystalline property are all investigated. In addition, the formation mechanism of LiF-enriched SEI layer is also studied based on the DFT calculation results.

Chapter 3 presents the effects of Al_2O_3 nanoparticles on the properties of PEBA2533 based SPE and the performance of ASSLMBs assembled with the improved SPE.

Besides, by comparing the cycling performance of ASSLMB and the plating and stripping performance, the cause of increased interface resistance is analyzed. More importantly, the differences of PA segments distribution on the surface and inside the membrane are characterized by XPS technique.

Chapter 4 focus on the verification of Li dendrite suppression ability of PEBA 4033 based SPEs according to the cycling performance of ASSLMBs assembled with high-loading cathode, and the effects of SPEs preparation temperature on battery performance are also investigated. Furthermore, the effects of LiTFSI content and solvent evaporation temperature on crystal behavior of PA 12 are investigated.

Finally, general conclusions of this research and suggestions for future work are summarized in Chapter 5.

References

[1] BP GROUP, BP statistical review of world energy, 2022.

[2] D. J. Mackay, Sustainable energy-without the hot air; UIT cambridge, U.K., 2009.

[3] D. Zhai, K. C. Lau, H.-H. Wang, J. Wen, D. J. Miller, J. Lu, F. Kang, B. Li, W. Yang, J. Gao, E. Indacochea, L. A. Curtiss, K. Amine, Interfacial effects on lithium superoxide disproportionation in Li-O_2 batteries, Nano Lett. 15 (2015) 1041-1046.

[4] G.A. Elia, J. Hassoun, A polymer lithium-oxygen battery, Sci. Rep. 5 (2015) 12307.

[5] Y. Li, Y. Bai, X. Bi, J. Qian, L. Ma, J. Tian, C. Wu, F. Wu, J. Lu, K. Amine, An effectively activated hierarchical nano-/microspherical $Li_{1.2}Ni_{0.2}Mn_{0.6}O_2$ cathode for long-life and high-rate lithium-ion batteries, ChemSusChem 9 (2016) 728-735.

[6] P. G. Bruce, S. A. Freunberger, L. J. Hardwick, J.-M. Tarascon, Li-O_2 and Li-S batteries with high energy storage, Nat. Mater. 11 (2011) 19-29.

[7] F. Wu, H. Wang, Y. Bai, Y. Li, C. Wu, G. Chen, L. Liu, Q. Ni, X. Wang, J. Zhou, Hierarchical microspheres and nanoscale particles: Effects of morphology on electrochemical performance of $Li_{1.2}Mn_{0.54}Ni_{0.13}Co_{0.13}O_2$ cathode material for lithium-ion batteries, Solid State Ionics. 300 (2017) 149-156.

[8] X.-B. Cheng, R. Zhang, C.-Z. Zhao, F. Wei, J.-G. Zhang, Q. Zhang, A review of solid electrolyte interphases on lithium metal anode, Adv. Sci. 3 (2016) 1500213.

[9] Y. Jie, X. Ren, R. Cao, W. Cai, S. Jiao, Advanced liquid electrolytes for rechargeable Li metal batteries, Adv. Funct. Mater. 30 (2020) 1910777.

[10] J. Cui, T.-G. Zhan, K.-D. Zhang, D. Chen, The recent advances in constructing designed electrode in lithium metal batteries, Chin. Chem. Lett. 28 (2017) 2171.

[11] M. Murayama, N. Sonoyama, A. Yamada, R. Kanno, Material design of new lithium ionic conductor, thio-LISICON, in the Li_2S-P_2S_5 system, Solid State Ionics. 170 (2004) 173-80.

[12] T. Ohtomo, F. Mizuno, A. Hayashi, K. Tadanaga, M. Tatsumisago, Electrical and electrochemical properties of Li_2S-P_2S_5-P_2O_5 glass-ceramic electrolytes, J. Power Sources 146 (2005) 715-718.

[13] M. Nagao, H. Kitaura, A. Hayashi, M. Tatsumisago, Characterization of all-solid-state lithium secondary batteries using $Cu_xMo_6S_{8-y}$ electrode and Li_2S–P_2S_5 solid electrolyte, J. Power Sources 189 (2009) 672-675.

[14] J. B. Goodenough, H.-P. Hong, J. A. Kafalas, Fast Na^+-ion transport in skeleton structures, Mater. Res. Bull. 11 (1976) 203-220.

[15] L. Latie, G. Villeneuve, D. Conte, G. Le Flem, Ionic conductivity of oxides with general formula $Li_xLn_{1/3}Nb_{1-x}Ti_xO_3$ (Ln= La, Nd), J Solid State Chem. 51 (1984) 293-299.

[16] K. Fu, Y. Gong, G. T. Hitz, D. W. McOwen, Y. Li, S. Xu, Y. Wen, L. Zhang, C. Wang, G. Pastel, J. Dai, B. Liu, H. Xie, Y. Yao, E. D. Wachsman, L. Hu, Three-dimensional bilayer garnet solid electrolyte based high energy density lithium metal-sulfur batteries, Energy Environ. Sci. 10 (2017) 1568-1575.

[17] X. Li, J. Liang, X. Yang, K. R. Adair, C. Wang, F. Zhao, X. Sun, Progress and perspectives on halide lithium conductors for all-solid-state lithium batteries, Energy Environ. Sci. 13 (2020) 1429-1461.

[18] J. Liang, X. Li, K. R. Adair, X. Sun, Metal halide superionic conductors for all-solid-state batteries, Acc. Chem. Res. 54 (2021) 1023-1033.

[19] X. Yang, F. Zhang, L. Zhang, T. Zhang, Y. Huang, Y. Chen, A high-performance graphene oxide-doped ion gel as gel polymer electrolyte for all-solid-state supercapacitor applications, Adv. Funct. Mater. 23 (2013) 3353-3360.

[20] J. Zhang, J. Zhao, L. Yue, Q. Wang, J. Chai, Z. Liu, X. Zhou, H. Li, Y. Guo, G. Cui, L. Chen, Safety-reinforced poly(propylene carbonate)-based all-solid-state

polymer electrolyte for ambient-temperature solid polymer lithium batteries, Adv. Energy Mater. 5 (2015) 1501082.

[21] X. Ban, W. Zhang, N. Chen, C. Sun, A high-performance and durable poly(ethylene oxide)-based composite solid electrolyte for all solid-state lithium battery, J. Phys. Chem. C 122 (2018) 9852-9858.

[22] U. H. Choi, S. Liang, M. V. O'Reilly, K. I. Winey, J. Runt, R. H. Colby, Influence of solvating plasticizer on ion conduction of polysiloxane single-ion conductors, Macromolecules 47 (2014) 3145-3153.

[23] N. Kamaya, K. Homma, Y. Yamakawa, M. Hirayama, R. Kanno, M. Yonemura, T. Kamiyama, Y. Kato, S. Hama, K. Kawamoto, A. Mitsui, A lithium superionic conductor, Nat. Mater. 10 (2011) 682-686.

[24] H. Park, S. Yu, D. J. Siegel, Predicting charge transfer stability between sulfide solid electrolytes and Li metal anodes, ACS Energy Lett. 6 (2021) 150-157.

[25] H. Muramatsu, A. Hayashi, T. Ohtomo, S. Hama, M. Tatsumisago, Structural change of Li_2S-P_2S_5 sulfide solid electrolytes in the atmosphere, Solid State Ionics 182 (2011) 116-119.

[26] Y. Nikodimos, C.-J. Huang, B. W. Taklu, W.-N. Su, B. J. Hwang, Chemical stability of sulfide solid-state electrolytes: stability toward humid air and compatibility with solvents and binders, Energy Environ. Sci. 15 (2022) 991-1033.

[27] F. Walther, R. Koerver, T. Fuchs, S. Ohno, J. Sann, M. Rohnke, W. G. Zeier, J. Janek, Visualization of the interfacial decomposition of composite cathodes in argyrodite-based all-solid-state batteries using time-of-flight secondary-ion mass spectrometry, Chem. Mater. 31 (2019) 3745-3755.

[28] C. Wang, Y. Zhao, M. Zheng, X. Li, X. Sun, All-solid-state lithium batteries enabled by sulfide electrolytes: from fundamental research to practical engineering

design, Energy Environ. Sci. 14 (2021) 2577-2619.

[29] Y. Nikodimos, W.-N. Su, B. W. Taklu, S. K. Merso, T. M. Hagos, C.-J. Huang, H. G. Redda, C.-H. Wang, S.-H. Wu, C.-C. Yang, B. J. Hwang, Resolving anodic and cathodic interface-incompatibility in solid-state lithium metal battery via interface infiltration of designed liquid electrolytes, J. Power Sources 535 (2022) 231425.

[30] M. R. Busche, T. Drossel, T. Leichtweiss, D. A. Weber, M. Falk, M. Schneider, M.-L. Reich, H. Sommer, P. Adelhelm, J. Janek, Dynamic formation of a solid-liquid electrolyte interphase and its consequences for hybrid-battery concepts, Nat. Chem. 8 (2016) 426-434.

[31] C. Wang, Q. Sun, Y. Liu, Y. Zhao, X. Li, X. Lin, M. N. Banis, M. Li, W. Li, K. R. Adair, D. Wang, J. Liang, R. Li, L. Zhang, R. Yang, S. Lu, X. Sun, Boosting the performance of lithium batteries with solid-liquid hybrid electrolytes: Interfacial properties and effects of liquid electrolytes, Nano Energy 48 (2018) 35-43.

[32] G. Xu, L. Luo, J. Liang, S. Zhao, R. Yang, C. Wang, T. Yu, L. Wang, W. Xiao, J. Wang, J. Yu, X. Sun, Origin of high electrochemical stability of multi-metal chloride solid electrolytes for high energy all-solid-state lithium-ion batteries, Nano Energy 92 (2022) 106674.

[33] J. Liang, X. Li, S. Wang, K. R. Adair, W. Li, Y. Zhao, C. Wang, Y. Hu, L. Zhang, S. Zhao, S. Lu, H. Huang, R. Li, Y. Mo, X. Sun, Site-occupation-tuned superionic Li_xScCl_{3+x} halide solid electrolytes for all-solid-state batteries, J. Am. Chem. Soc. 142 (2020) 7012-7022.

[34] Z. Liu, S. Ma, J. Liu, S. Xiong, Y. Ma, H. Chen, High ionic conductivity achieved in $Li_3Y(Br_3Cl_3)$ mixed halide solid electrolyte via promoted diffusion pathways and enhanced grain boundary, ACS Energy Lett. 6 (2020) 298-304.

[35] C. Yu, Y. Li, K. R. Adair, W. Li, K. Goubitz, Y. Zhao, M. J. Willans, M. A. Thijs,

C. Wang, F. Zhao, Q. Sun, S. Deng, J. Liang, X. Li, R. Li, T.-K. Sham, H. Huang, S. Lu, S. Zhao, L. Zhang, L. Eijck, Y. Huang, X. Sun, Tuning ionic conductivity and electrode compatibility of Li_3YBr_6 for high-performance all solid-state Li batteries, Nano Energy 77 (2020) 105097.

[36] Y. Zhu, X. He, Y. Mo, Origin of outstanding stability in the lithium solid electrolyte materials: Insights from thermodynamic analyses based on first-principles calculations, ACS Appl. Mater. Interfaces 7 (2015) 23685-23693.

[37] W. Ji, D. Zheng, X. Zhang, T. Ding, D. Qu, A kinetically stable anode interface for Li_3YCl_6-based all-solid-state lithium batteries, J. Mater. Chem. A 9 (2021) 15012-15018.

[38] X. Li, J. Liang, J. Luo, M. N. Banis, C. Wang, W. Li, S. Deng, C. Yu, F. Zhao, Y. Hu, T.-K. Sham, L. Zhang, S. Zhao, S. Lu, H. Huang, R. Li, K. R. Adair, X. Sun, Air-stable Li_3InCl_6 electrolyte with high voltage compatibility for all-solid-state batteries, Energy Environ. Sci. 12 (2019) 2665-2671.

[39] W. Li, J. Liang, M. Li, K. R. Adair, X. Li, Y. Hu, Q. Xiao, R. Feng, R. Li, L. Zhang, S. Lu, H. Huang, S. Zhao, T.-K. Sham, X. Sun, Unraveling the origin of moisture stability of halide solid-state electrolytes by in situ and operando synchrotron X-ray analytical techniques, Chem. Mater. 32 (2020) 7019-7027.

[40] D. E. Fenton, Complexes of alkali metal ions with poly (ethylene oxide), Polymer 14 (1973) 589.

[41] M. B. Armand, Polymer electrolytes, Annu. Rev. Mater. Sci. 16 (1986) 245-261.

[42] W. Gorecki, M. Jeannin, E. Belorizky, C. Roux, M. Armand, Physical properties of solid polymer electrolyte PEO(LiTFSI) complexes, J. Phys.: Condens. Matter 7 (1995) 6823.

[43] W. Wang, Z. Fang, M. Zhao, Y. Peng, J. Zhang, S. Guan, Solid polymer

electrolytes based on the composite of PEO-LiFSI and organic ionic plastic crystal, Chem. Phys. Lett. 747 (2020) 137335.

[44] S. Klongkan, J. Pumchusak, Effects of the addition of $LiCF_3SO_3$ salt on the conductivity, thermal and mechanical properties of PEO-$LiCF_3SO_3$ solid polymer electrolyte, Int. J. Chem. Eng. Appl. 6 (2015) 165-168.

[45] J. Gurusiddappa, W. Madhuri, R. P. Suvarna, K. P. Dasan, Studies on the morphology and conductivity of PEO/$LiClO_4$, Mater. Today: Proc. 3 (2016) 1451-1459.

[46] E. M. Fahmi, A. Ahmad, N. N. M. Nazeri, H. Hamzah, H. Razali, M. Y. A. Rahman, Effect of $LiBF_4$ salt concentration on the properties of poly (ethylene oxide)-based composite polymer electrolyte, Int. J. Electrochem. Sci. 7 (2012) 5798-5804.

[47] Q. Liu, B. Peng, M. Shen, B. Hu, Q. Chen, Polymer chain diffusion and Li^+ hopping of poly (ethylene oxide)/$LiAsF_6$ crystalline polymer electrolytes as studied by solid state NMR and ac impedance, Solid State Ionics 255 (2014) 74-79.

[48] K.-H. Chen, K. N. Wood, E. Kazyak, W. S. LePage, A. L. Davis, A. J. Sanchez, N. P. Dasgupta, Dead lithium: mass transport effects on voltage, capacity, and failure of lithium metal anodes, J. Mater. Chem. A 5 (2017) 11671-11681.

[49] M. Ihrig, E. Dashjav, A. M. Laptev, R. Ye, D. Grüner, M. Ziegner, P. Odenwald, M. Finsterbusch, F. Tietz, D. Fattakhova-Rohlfing, O. Guillon, Increasing the performance of all-solid-state Li batteries by infiltration of Li-ion conducting polymer into LFP-LATP composite cathode, J. Power Sources 543 (2022) 231822.

[50] W. H. Meyer, Polymer electrolytes for lithium-ion batteries, Adv. Mater. 10 (1998) 439-448.

[51] Z. Li, H.-M. Huang, J.-K. Zhu, J.-F. Wu, H. Yang, L. Wei, & X. Guo, Ionic conduction in composite polymer electrolytes: case of PEO: Ga-LLZO composites, ACS Appl. Mater. Interfaces 11 (2019) 784-791.

[52] W. S. Young, W. F. Kuan, T. H. Epps III, Block copolymer electrolytes for rechargeable lithium batteries, J. Polym. Sci. Part B Pol. Phys. 52 (2014) 1-16.

[53] Q. Zhou, J. Ma, S. Dong, X. Li, G. Cui, Intermolecular chemistry in solid polymer electrolytes for high-energy-density lithium batteries, Adv. Mater. 31 (2019) 1902029.

[54] D. J. Bannister, G. R. Davies, I. M. Ward, J. E. McIntyre, Ionic conductivities for poly(ethylene oxide) complexes with lithium salts of monobasic and dibasic acids and blends of poly(ethylene oxide) with lithium salts of anionic polymers, Polymer, 25 (1984) 1291-1296.

[55] D. S. Mebane, R. A. De Souza, A generalised space-charge theory for extended defects in oxygen-ion conducting electrolytes: from dilute to concentrated solid solutions, Energ. & Environ. Sci. 8 (2015) 2935-2940.

[56] C. Zhang, S. Gamble, D. Ainsworth, A. M. Z. Slawin, Y. G. Andreev, P. G. Bruce, Alkali metal crystalline polymer electrolytes, Nat. Mater. 8 (2009) 580-584.

[57] M. Liu, S. Zhang, E. R. H. van Eck, C. Wang, S. Ganapathy, M. Wagemaker, Improving Li-ion interfacial transport in hybrid solid electrolytes, Nat. Nanotechnol. 17 (2022) 959-967.

[58] Y. Xia, N. Xu, L. Du, Y. Cheng, S. Lei, S. Li, X. Liao, W. Shi, L. Xu, L. Mai, Rational design of ion transport paths at the interface of metal-organic framework modified solid electrolyte, ACS Appl. Mater. Interfaces 12 (2020) 22930-22938.

[59] M. A. Ratner, P. Johansson, D. F. Shriver, Polymer electrolytes: Ionic transport mechanisms and relaxation coupling, MRS Bull. 25 (2011) 31-37.

[60] M. H. Cohen, D. Turnbull, Molecular transport in liquids and glasses, J. Chem. Phys. 31 (1959) 1164-1169.

[61] C.-H. Tsao, Y.-H. Hsiao, C.-H. Hsu, P.-L. Kuo, Stable lithium deposition generated from ceramic-cross-linked gel polymer electrolytes for lithium anode, ACS

Appl. Mater. Interfaces 8 (2016) 15216-15224.

[62] Q. Ma, H. Zhang, C. Zhou, L. Zheng, P. Cheng, J. Nie, W. Feng, Y.-S. Hu, H. Li, X. Huang, L. Chen, M. Armand, Z. Zhou, Single lithium-ion conducting polymer electrolytes based on a super-delocalized polyanion, Angew. Chem. Int. Ed. 55 (2016) 2521-2525.

[63] Y. Shen, G.-H. Deng, C. Ge, Y. Tian, G. Wu, X. Yang, J. Zheng, K. Yuan, Solvation structure around the Li^+ ion in succinonitrile-lithium salt plastic crystalline electrolytes, Phys. Chem. Chem. Phys. 18 (2016) 14867-14873.

[64] D. H. C. Wong, J. L. Thelen, Y. Fu, D. Devaux, A. A. Pandya, V. S. Battaglia, N. P. Balsara, J. M. DeSimone, Nonflammable perfluoropolyether-based electrolytes for lithium batteries, Proc. Natl. Acad. Sci. 111 (2014) 3327.

[65] K. Kimura, J. Motomatsu, Y. Tominaga, Correlation between solvation structure and ion-conductive behavior of concentrated poly(ethylene carbonate)-based electrolytes, J. Phys. Chem. C 120 (2016) 12385-12391.

[66] K. Kimura, Y. Tominaga, Understanding electrochemical stability and lithium ion-dominant transport in concentrated poly(ethylene carbonate) electrolyte, ChemElectroChem 5 (2018) 4008-4014.

[67] H. Wang, J. Zhu, Y. Su, Z. Gong, Y. Yang, Interfacial compatibility issues in rechargeable solid-state lithium metal batteries: A review. Sci China Chem. 64 (2021) 879-898.

[68] K. Lehovec, Space-charge layer and distribution of lattice defects at the surface of ionic crystals, J. Chem. Phys. 21 (1953) 1123-1128.

[69] K. L. Kliewer, J. S. Koehler, Space charge in ionic crystals. I. general approach with application to NaCl, Phys. Rev. 140 (1965) A1226-A1240.

[70] C. Wagner, The electrical conductivity of semi-conductors involving inclusions of

another phase, J. Phys. Chem. Solids 33 (1972) 1051-1059.

[71] T. Jow, J. B. Wagner, The effect of dispersed alumina particles on the electrical conductivity of cuprous chloride, J. Electrochem. Soc. 126 (1979) 1963-1972.

[72] J. Maier, Space charge regions in solid two-phase systems and their conduction contribution-I. conductance enhancement in the system ionic conductor-'inert' phase and application on AgC1:Al_2O_3 and AgC1:SiO_2, J. Phys. Chem. Solids 46 (1985) 309-320.

[73] J. Maier, Space charge regions in solid two phase systems and their conduction contribution-II contact equilibrium at the interface of two ionic conductors and the related conductivity effect, Ber. Bunsen. Phys. Chem. 89 (1985) 355-362.

[74] C.-Z. Zhao, X.-Q. Zhang, X.-B. Cheng, R. Zhang, R. Xu, P.-Y. Chen, H.-J. Peng, J.-Q. Huang, Q. Zhang, An anion-immobilized composite electrolyte for dendrite-free lithium metal anodes, Proc. Natl. Acad. Sci. 114 (2017) 11069-11074.

[75] M. D. Tikekar, S. Choudhury, Z. Tu, L. A. Archer, Design principles for electrolytes and interfaces for stable lithium-metal batteries, Nat. Energy 1 (2016) 16114.

[76] Z. Tu, M. J. Zachman, S. Choudhury, S. Wei, L. Ma, Y. Yang, L. F. Kourkoutis, L. A. Archer, Nanoporous hybrid electrolytes for high-energy batteries based on reactive metal anodes, Adv. Energy Mater. 7 (2017) 1602367.

[77] N. Jayaprakash, W. D. Jones, S. S. Moganty, L. A. Archer, Composite lithium battery anodes based on carbon@Co_3O_4 nanostructures: Synthesis and characterization, J. Power Sources 200 (2012) 53-58.

[78] Y. Lu, K. Korf, Y. Kambe, Z. Tu, L. A. Archer, Ionic-liquid-nanoparticle hybrid electrolytes: Applications in lithium metal batteries, Angew. Chem. Int. Ed. 53 (2014) 488-492.

[79] M. B. Armand, J. M. Chabagno, M. J. Duclot, Fast ion transport in solids, North Holland: Amsterdam 131 (1979).

[80] D. Y. Voropaeva, S. A. Novikova, A. B. Yaroslavtsev, Polymer electrolytes for metal-ion batteries, Russ. Chem. Rev. 89 (2020) 1132-1155.

[81] X. Judez, H. Zhang, C. Li, G. G. Eshetu, J. A. González-Marcos, M. Armand, L. M. Rodriguez-Martinez, Solid electrolytes for safe and high energy density lithium-sulfur batteries: promises and challenges, J. Electrochem. Soc. 165 (2017) A6008-A6016.

[82] P.A.R.D Jayathilaka, M.A.K.L Dissanayake, I. Albinsson, B.-E. Mellander, Effect of nano-porous Al_2O_3 on thermal, dielectric and transport properties of the $(PEO)_9LiTFSI$ polymer electrolyte system, Electrochim. Acta 47 (2002) 3257-3268.

[83] L. Cong, Y. Li, W. Lu, J. Jie, Y. Liu, L. Sun, H. Xie, Unlocking the Poly (vinylidene fluoride-co-hexafluoropropylene)/$Li_{10}GeP_2S_{12}$ composite solid-state Electrolytes for Dendrite-Free Li metal batteries assisting with perfluoropolyethers as bifunctional adjuvant, J. Power Sources 446 (2020) 227365.

[84] W. Jia, Z. Li, Z. Wu, L. Wang, B. Wu, Y. Wang, Y. Cao, J. Li, Graphene oxide as a filler to improve the performance of PAN-$LiClO_4$ flexible solid polymer electrolyte, Solid State Ionics 315 (2018) 7-13.

[85] S. Hua, M.-X. Jing, C. Han, H. Yang, H. Chen, F. Chen, L.-L. Chen, B.-W. Ju, F.-Y. Tu, X.-Q. Shen, S.-B. Qin, A novel titania nanorods-filled composite solid electrolytewith improved room temperature performance for solid-state Li-ion battery, Int. J. Energy Res. 43 (2019) 7296-7305.

[86] M. Wu, D. Liu, D. Qu, Z. Xie, J. Li, J. Lei, H. Tang, 3D coral-like LLZO/PVDF composite electrolytes with enhanced ionic conductivity and mechanical flexibility for solid-state lithium batteries, ACS Appl. Mater. Interfaces 12 (2020) 52652-52659.

[87] P. Pal, A. Ghosh, Investigation of ionic conductivity and relaxation in plasticized PMMA-$LiClO_4$ solid polymer electrolytes, Solid State Ionics 319 (2018) 117-124.

[88] F. Croce, G. B. Appetecchi, L. Persi, B. Scrosati, Nanocomposite polymer electrolytes for lithium batteries, Nature 394 (1998) 456-458.

[89] D. Lin, W. Liu, Y. Liu, H. R. Lee, P.-C. Hsu, K. Liu, Y. Cui, High ionic conductivity of composite solid polymer electrolyte via in situ synthesis of monodispersed SiO_2 nanospheres in poly (ethylene oxide), Nano Lett. 16 (2016) 459-465.

[90] S. Chen, K. Wen, J. Fan, Y. Bando, D. Golberg, Progress and future prospects of high-voltage and high-safety electrolytes in advanced lithium batteries: from liquid to solid electrolytes, J. Mater. Chem. A 6 (2018) 11631-11663.

[91] P.A.R.D. Jayathilaka, M.A.K.L. Dissanayake, I Albinsson, B.-E Mellander, Effect of nano-porous Al_2O_3 on thermal, dielectric and transport properties of the $(PEO)_9$ LiTFSI polymer electrolyte system, Electrochim. Acta 47 (2002) 3257-3268.

[92] K. Zhu, Y. Liu, J. Liu, A fast charging/discharging all-solid-state lithium ion battery based on PEO-MIL-53(Al)-LiTFSI thin film electrolyte, RSC Adv. 4 (2014) 42278-42284.

[93] W. Wang, E. Yi, A. J. Fici, R. M. Laine, J. Kieffer, Lithium ion conducting poly(ethylene oxide)-based solid electrolytes containing active or passive ceramic nanoparticles, J. Phys. Chem. C 121 (2017) 2563-2573.

[94] A. Gutiérrez-Pardo, Pitillas A. I. Martinez, L. Otaegui, M. Schneider, A. Roters, A. Llordés, F. Aguesse, L. Buannic, Will the competitive future of solid state Li metal batteries rely on a ceramic or a composite electrolyte?, Sustain. Energ. Fuels 2 (2018) 2325-2334.

[95] Y. Zhao, Z. Huang, S. Chen, B. Chen, J. Yang, Q. Zhang, F. Ding, Y. Chen, X. Xu, A promising PEO/LAGP hybrid electrolyte prepared by a simple method for all-solid-

state lithium batteries, Solid State Ionics 295 (2016) 65-71.

[96] J.-H. Choi, C.-H. Lee, J.-H. Yu, C.-H. Doh, S.-M. Lee, Enhancement of ionic conductivity of composite membranes for all-solid-state lithium rechargeable batteries incorporating tetragonal $Li_7La_3Zr_2O_{12}$ into a polyethylene oxide matrix, J. Power Sources 274 (2015) 458-463.

[97] W. Zha, F. Chen, D. Yang, Q. Shen, L. Zhang, High-performance $Li_{6.4}La_3Zr_{1.4}Ta_{0.6}O_{12}$/poly (ethylene oxide)/succinonitrile composite electrolyte for solid-state lithium batteries, J. Power Sources 397 (2018) 87-94.

[98] J. Cao, L. Wang, X. He, M. Fang, J. Gao, J. Li, L. Deng, H. Chen, G. Tian, J. Wang, S. Fan, In situ prepared nano-crystalline TiO_2-poly(methyl methacrylate) hybrid enhanced composite polymer electrolyte for Li-ion batteries, J. Mater. Chem. A 1 (2013) 5955-5961.

[99] K. Fu, Y. Gong, J. Dai, A. Gong, X. Han, Y. Yao, C. Wang, Y. Wang, Y. Chen, C. Yan, Y. Li, E. D. Wachsman, L. Hu, Flexible, solid-state, ion-conducting membrane with 3D garnet nanofiber networks for lithium batteries, Proc. Natl. Acad. Sci. 113 (2016) 7094-7099.

[100] T. Yang, J. Zheng, Q. Cheng, Y.-Y. Hu, C. K. Chan, Composite polymer electrolytes with $Li_7La_3Zr_2O_{12}$ garnet-type nanowires as ceramic fillers: Mechanism of conductivity enhancement and role of doping and morphology, ACS Appl. Mater. Interfaces 9 (2017) 21773-21780.

[101] M. Jing, H. Yang, C. Han, F. Chen, L. Zhang, X. Hu, F. Tu, X. Shen, Synergistic enhancement effects of LLZO fibers and interfacial modification for polymer solid electrolyte on the ambient-temperature electrochemical performances of solid-state battery, J. Electrochem. Soc. 166 (2019) A3019-A3027.

[102] W. Liu, S. W. Lee, D. Lin, F. Shi, S. Wang, A. D. Sendek, Y. Cui, Enhancing

ionic conductivity in composite polymer electrolytes with well-aligned ceramic nanowires, Nat. Energy 2 (2017) 17035.

[103] S. Gomari, M. Esfandeh, I. Ghasemi, All-solid-state flexible nanocomposite polymer electrolytes based on poly(ethylene oxide): Lithium perchlorate using functionalized graphene, Solid State Ionics 303 (2017) 37-46.

[104] M. Yuan, J. Erdman, C. Tang, H. Ardebili, High performance solid polymer electrolyte with graphene oxide nanosheets, RSC Adv. 4 (2014) 59637-59642.

[105] Z. Li, W.-X. Sha, X. Guo, Three-dimensional garnet framework-reinforced solid composite electrolytes with high lithium-ion conductivity and excellent stability, ACS Appl. Mater. Inter. 11 (2019) 26920-26927.

[106] X. Zhang, J. Xie, F. Shi, D. Lin, Y. Liu, W. Liu, A. Pei, Y. Gong, H. Wang, K. Liu, Y. Xiang, Y. Cui, Vertically aligned and continuous nanoscale ceramic-polymer interfaces in composite solid polymer electrolytes for enhanced ionic conductivity, Nano Lett. 18 (2018) 3829-3838.

[107] C. Hu, Y. Shen, M. Shen, X. Liu, H. Chen, C. Liu, T. Kang, F. Jin, L. Li, J. Li, Y. Li, N. Zhao, X. Guo, W. Lu, B. Hu, L. Chen, Superionic conductors via bulk interfacial conduction, J. Am. Chem. Soc. 142 (2020) 18035-18041.

[108] P. Pal, A. Ghosh, Influence of TiO_2 nano-particles on charge carrier transport and cell performance of PMMA-$LiClO_4$ based nano-composite electrolytes, Electrochim. Acta 260 (2018) 157-167.

[109] W. Liu, L. Meng, X. Liu, L. Gao, X. Wang, J. Kang, J. Ju, N. Deng, B. Cheng, W. Kang, 3D spiny AlF_3/Mullite heterostructure nanofiber as solid-state polymer electrolyte fillers with enhanced ionic conductivity and improved interfacial compatibility, J. Energy Chem. 76 (2023) 503-515.

[110] Q. Wang, W.-L. Song, L.-Z. Fan, Y. Song, Flexible, high-voltage, and free-

standing composite polymer electrolyte membrane based on triethylene glycol diacetate-2-propenoic acid butyl ester copolymer for lithium-ion batteries, J. Membrane Sci. 492 (2015) 490-496.

[111] K. Karthik, R. Murugan, Lithium garnet based free-standing solid polymer composite membrane for rechargeable lithium battery, J. Solid State Electr. 22 (2018) 2989-2998.

[112] S. H.-S. Cheng, K.-Q. He, Y. Liu, J.-W. Zha, M. Kamruzzaman, R. L.-W. Ma, Z.-M. Dang, R. K. Y. Li, C. Y. Chung, Electrochemical performance of all-solid-state lithium batteries using inorganic lithium garnets particulate reinforced PEO/$LiClO_4$ electrolyte, Electrochim. Acta 253 (2017) 430-438.

[113] X. Zhang, T. Liu, S. Zhang, X. Huang, B. Xu, Y. Lin, B. Xu, L. Li, C.-W. Nan, Y. Shen, Synergistic coupling between $Li_{6.75}La_3Zr_{1.75}Ta_{0.25}O_{12}$ and poly(vinylidene fluoride) induces high ionic conductivity, mechanical strength, and thermal stability of solid composite electrolytes, J. Am. Chem. Soc. 139 (2017) 13779-13785.

[114] Y. Zhao, C. Wu, G. Peng, X. Chen, X. Yao, Y. Bai, F. Wu, S. Chen, X. Xu, A new solid polymer electrolyte incorporating $Li_{10}GeP_2S_{12}$ into a polyethylene oxide matrix for all-solid-state lithium batteries, J. Power Sources 301 (2016) 47-53.

[115] P. Zhang, L. C. Yang, L. L. Li, M. L. Ding, Y. P. Wu, R. Holze, Enhanced electrochemical and mechanical properties of P(VDF-HFP)-based composite polymer electrolytes with SiO_2 nanowires, J. Membrane Sci. 379 (2011) 80-85.

[116] W. Liu, N. Liu, J. Sun, P.-C. Hsu, Y. Li, H.-W. Lee, Y. Cui, Ionic conductivity enhancement of polymer electrolytes with ceramic nanowire fillers, Nano Lett. 15 (2015) 2740-2745.

[117] P. Zhu, C. Yan, M. Dirican, J. Zhu, J. Zang, R. K. Selvan, C.-C. Chung, H. Jia, Y. Li, Y. Kiyak, N. Wu, X. Zhang, $Li_{0.33}La_{0.557}TiO_3$ ceramic nanofiber-enhanced

polyethylene oxide-based composite polymer electrolytes for all-solid-state lithium batteries, J. Mater. Chem. A 6 (2018) 4279-4285.

[118] R. Fan, C. Liu, K. He, S. H.-S. Cheng, D. Chen, C. Liao, R. K. Y. Li, J. Tang, Z. Lu, Versatile strategy for realizing flexible room-temperature all-solid-state battery through a synergistic combination of salt affluent PEO and $Li_{6.75}La_3Zr_{1.75}Ta_{0.25}O_{12}$ nanofibers, ACS Appl. Mater. Interfaces 12 (2020) 7222-7231.

[119] L. Chen, W. Li, L.-Z. Fan, C.-W. Nan, Q. Zhang, Intercalated electrolyte with high transference number for dendrite-free solid-state lithium batteries, Adv. Funct. Mater. 29 (2019) 1901047.

[120] Y. Sun, F. Jin, J. Li, B. Liu, X. Chen, H. Dong, Y. Mao, W. Gu, J. Xu, Y. Shen, X. Wu, L. Chen, Composite solid electrolyte for solid-state lithium batteries workable at room temperature, ACS Appl. Energy Mater. 3 (2020) 12127-12133.

[121] S. Xia, B. Yang, H. Zhang, J. Yang, W. Liu, S. Zheng, Ultrathin layered double hydroxide nanosheets enabling composite polymer electrolyte for all-solid-state lithium batteries at room temperature, Adv. Funct. Mater. 31 (2021) 2101168.

[122] Z. Sun, Y. Li, S. Zhang, L. Shi, H. Wu, H. Bu, S. Ding, g-C_3N_4 nanosheets enhanced solid polymer electrolytes with excellent electrochemical performance, mechanical properties, and thermal stability, J. Mater. Chem. A 7 (2019) 11069-11076.

[123] L. Gao, S. Luo, J. Li, B. Cheng, W. Kang, N. Deng, Core-shell structure nanofibers-ceramic nanowires based composite electrolytes with high Li transference number for high-performance all-solid-state lithium metal batteries, Energy Storage Mater. 43 (2021) 266-274.

[124] L. Gao, J. Li, J. Ju, L. Wang, J. Yan, B. Cheng, W. Kang, N. Deng, Y. Li, Designing of root-soil-like polyethylene oxide-based composite electrolyte for dendrite-free and long-cycling all-solid-state lithium metal batteries, Chem. Eng. J. 389

(2020) 124478.

[125] L. Liu, J. Lyu, J. Mo, H. Yan, L. Xu, P. Peng, J. Li, B. Jiang, L. Chu, M. Li, Comprehensively-upgraded polymer electrolytes by multifunctional aramid nanofibers for stable all-solid-state Li-ion batteries, Nano Energy 69 (2020) 104398.

[126] L. Chen, Y. Li, S.-P. Li, L.-Z. Fan, C.-W. Nan, J. B. Goodenough, PEO/garnet composite electrolytes for solid-state lithium batteries: From "ceramic-in-polymer" to "polymer-in-ceramic", Nano Energy 46 (2018) 176-184.

[127] Y. Wang, J. Ju, S. Dong, Y. Yan, F. Jiang, L. Cui, Q. Wang, X. Han, G. Cui, Facile design of sulfide-based all solid-state lithium metal battery: In situ polymerization within self-supported porous argyrodite skeleton, Adv. Funct. Mater. 31 (2021) 2101523.

[128] J.-H. Shin, W. A. Henderson, S. Passerini, PEO-based polymer electrolytes with ionic liquids and their use in lithium metal-polymer electrolyte batteries, J. Electrochem. Soc. 152 (2005) A978-A983.

[129] E. Simonetti, M. Carewska, G. Maresca, M. De Francesco, G. B. Appetecchi, Highly conductive, ionic liquid-based polymer electrolytes, J. Electrohem. Soc. 164 (2017) A6213-A6219.

[130] F. Gonzalez, P. Tiembla, N. Garcia, O. Garcia-Calvo, E. Fedeli, A. Kvasha, I. Urdampilleta, High performance polymer/ionic liquid thermoplastic solid electrolyte prepared by solvent free processing for solid state lithium metal batteries, Membranes 8 (2018) 55-65.

[131] H. Wang, N. Imanishi, A. Hiramo, Y. Takeda, O. Yamamoto, Electrochemical properties of the polyethylene oxide-$Li(CF_3SO_2)_2N$ and ionic liquid composite electrolyte, J. Power Sources 219 (2012) 22-28.

[132] P. G. Bruce, A. R. West, The A-C conductivity of polycrystalline LISICON,

$Li_{2+2x}Zn_{1-x}GeO_4$, and a model for intergranular constriction resistances, J. Solid State Chemistry 130 (1983) 662-669.

[133] S. Liu, H. Wang, N. Imanishi, T. Zhang, A. Hirano, Y. Takeda, O. Yamamoto, J. Yang, Effect of co-doping nano-silica filler and N-methyl-N-propylpiperidinium bis(trifluoromethanesulfonyl)imide into polymer electrolyte on Li dendrite formation in Li/poly(ethylene oxide)-$Li(CF_3SO_2)_2N$/Li, J. Power Sources 196 (2011) 7681-7686.

[134] S. Das, A. Ghosh, Charge carrier relaxation in different plasticized PEO/PVDF-HFP blend solid polymer electrolytes, J. Phys. Chem. B 121 (2017) 5422-5432.

[135] B. Jinisha, K. M. Anilkumar, M. Manoj, V. S. Pradeep, S. Jayalekshmi, Development of a novel type of solid polymer electrolyte for solid state lithium battery applications based on lithium enriched poly (ethylene oxide) (PEO)/poly (vinyl pyrrolidone) (PVP) blend polymer, Electrochim. Acta 235 (2017) 210-222.

[136] F. Wu, T. Feng, Y. Bai, C. Wu, L. Ye, Z. Feng, Preparation and characterization of solid polymer electrolytes based on PHEMO and PVDF-HFP, Solid State Ionics 180 (2009) 677-680.

[137] X.-Y. Yu, M. Xiao, S.-J. Wang, Q.-Q. Zhao, Y.-Z. Meng, Fabrication and characterization of PEO/PPC polymer electrolyte for lithium-ion battery, J. Appl. Polym. Sci. 115 (2010) 2718-2722.

[138] R. Khurana, J. L. Schaefer, L. A. Archer, G. W. Coates, Suppression of lithium dendrite growth using cross-linked polyethylene/poly (ethylene oxide) electrolytes: a new approach for practical lithium-metal polymer batteries, J. Am. Chem. Soc. 136 (2014) 7395-7402.

[139] G. M. Stone, S. A. Mullin, A. A. Teran, D. T. Hallinan, A. M. Minor, A. Hexemer, N. P. Balsara, Resolution of the modulus versus adhesion dilemma in solid polymer electrolytes for rechargeable lithium metal batteries, J. Electrochem. Soc. 159 (2011)

A222-A227.

[140] R.A. Zoppi, C.M.N.P. Fonseca, Marco-A. D. Paoli, S.P. Nunes, Solid electrolytes based on poly (amide 6-b-ethylene oxide), Solid State Ionics 91 (1996) 123-130.

[141] Q. Yang, N. Deng, J. Chen, B. Cheng, W. Kang, The recent research progress and prospect of gel polymer electrolytes in lithium-sulfur batteries, Chem. Eng. J. 413 (2020) 127427.

[142] Y.-G. Cho, C. Hwang, D. S. Cheong, Y.-S. Kim, H.-K. Song, Gel/solid polymer electrolytes characterized by in situ gelation or polymerization for electrochemical energy systems, Adv. Mater. 31 (2019) 1804909.

[143] W.-P. Wang, J. Zhang, J. Chou, Y.-X. Yin, Y. You, S. Xin, Y.-G. Guo, Solidifying cathode electrolyte interface for lithium-sulfur batteries, Adv. Energy Mater. 11 (2021) 2000791.

[144] Y. Zhao, Y. Zhang, Z. Bakenov, P. Chen, Electrochemical performance of lithium gel polymer battery with nanostructured sulfur/carbon composite cathode, Solid State Ionics 234 (2013) 40-45.

[145] J.-W. Choi, J.-K. Kim, G. Cheruvally, J.-H. Ahn, H.-J. Ahn, K.-W. Kim, Rechargeable lithium/sulfur battery with suitable mixed liquid electrolytes, Electrochim. Acta 52 (2007) 2075-2082.

[146] P.-K. Singh, B. Bhattacharya, R.-K. Nagarale, Effect of nano-TiO_2 dispersion on PEO polymer electrolyte property, J Appl. Polym. Sci. 118 (2010) 2976-2980.

[147] N.S. Mohamed, A.K. Arof, Investigation of electrical and electrochemical properties of PVDF-based polymer electrolytes, J. Power Sources 132 (2004) 229-234.

[148] W. Huang, Z. Zhu, L. Wang, S. Wang, H. Li, Z. Tao, J. Shi, L. Guan, J. Chen, Quasi-solid-state rechargeable lithium-ion batteries with a calix[4]quinone cathode and gel polymer electrolyte, Angew Chem. Int. Ed. 52 (2013) 9162-9168.

[149] Y. Zhu, S. Xiao, Y. Shi, Y. Yang, Y. Hou, Y. Wu, A composite gel polymer electrolyte with high performance based on poly(vinylidene fluoride) and polyborate for lithium ion batteries, Adv. Energy Mater. 4 (2014) 1300647.

[150] M. Liu, D. Zhou, Y.-B. He, Y. Fu, X. Qin, C. Miao, H. Du, B. Li, Q.-H. Yang, Z. Lin, T.S. Zhao, F. Kang, Novel gel polymer electrolyte for high-performance lithium-sulfur batteries, Nano Energy 22 (2016) 278-289.

[151] S.-J. Tan, J. Yue, Y.-F. Tian, Q. Ma, J. Wan, Y. Xiao, J. Zhang, Y.-X. Yin, R. Wen, S. Xin, Y.-G. Guo, In-situ encapsulating flameretardant phosphate into robust polymer matrix for safe and stable quasi-solid-state lithium metal batteries, Energy Storage Mater. 39 (2021) 186-193.

[152] J. B. Goodenough, Y. Kim, Challenges for rechargeable Li batteries, Chem. Mater. 22 (2010) 587-603.

[153] X. Chen, J. Xie, X. Zhao, T. Zhu, Electrochemical compatibility of solid-state electrolytes with cathodes and anodes for all-solid-state lithium batteries: a review, Adv. Energy Sustain. Res. 2 (2021) 2000101.

[154] C. F. N. Marchiori, R. P. Carvalho, M. Ebadi, D. Brandell, C. M. Araujo, Understanding the electrochemical stability window of polymer electrolytes in solid-state batteries from atomic-scale modeling: the role of Li-ion salts, Chem. Mater. 32 (2020) 7237-7246.

[155] J. Kasnatscheew, B. Streipert, S. Röser, R. Wagner, I. C. Laskovic, M. Winter, Determining oxidative stability of battery electrolytes: validity of common electrochemical stability window (ESW) data and alternative strategies, Phys. Chem. Chem. Phys. 19 (2017) 16078-16086.

[156] R. Ye, M. Ihrig, E. Figgemeier, D. Fattakhova-Rohlfing, M. Finsterbusch, Aqueous processing of $LiCoO_2$-$Li_{6.6}La_3Zr_{1.6}Ta_{0.4}O_{12}$ composite cathode for high-

capacity solid-state lithium batteries, ACS Sustainable Chem. Eng. (2023).

[157] M. Y. Solangi, U. Aftab, M. Ishaque, A. Bhutto, A. Nafady, Z. H. Ibupoto, Polyvinyl fibers as outperform candidature in the solid polymer electrolytes, J. Ind. Text. 51 (2022) 6983S-6995S.

[158] T. Eriksson, A. Mace, Y. Manabe, M. Yoshizawa-Fujita, Y. Inokuma, D. Brandell, J. Mindemark, Polyketones as host materials for solid polymer electrolytes, J. Electrochem. Soc. 167 (2020) 070537.

CHAPTER 2 A poly(ether block amide) based solid polymer electrolyte for solid-state lithium metal batteries

2.1. Introduction

Li-ion batteries (LIBs) are recognized as the most widely used electrochemical devices for energy storage and electric vehicle development[1-4]. With the rapid development of electrified society, huge progress has been made in almost each component of the batteries[5-8]. However, as the main deficiencies of LIBs, energy density and safety are still need to be tackled[9,10]. Continued growth in demand for high-energy-density LIBs urges the utilization of Li metal anode (LMA) owing to its high theoretical specific capacity (3680 mAh g^{-1}) and low reduction potential (−3.04 V vs standard hydrogen electrode)[11]. However, in this case, during the Li plating and stripping process, Li dendrite is always formed to deteriorate interface and cause battery short-circuiting[12-16]. Therefore, more understanding the Li dendrite growth process and promoting uniform Li plating are vital for application of Li metal batteries (LMBs).

Application of solid-state electrolytes (SSEs) is a promising solution for the aforementioned concerns[17-19]. To date, various SSE materials have been investigated for LMBs[20,21], which can be mainly divided into three categories: inorganic solid electrolytes[22-24], solid polymer electrolytes (SPEs)[25-29], and their hybrids[30,31]. In addition, gel polymer electrolyte (GPE) is considered a fourth class of SSEs that combines the high ionic conductivity of liquid electrolytes with the high mechanical strength of polymer electrolytes[32]. The inorganic SSEs with high ionic conductivity are generally too brittle to process into ultrathin slices (<100 μm), which greatly restricts their practical applications, especially in electrical vehicles. The SPEs as the alternative have the advantages of high flexibility, light weight, and low cost.

However, they always have moderate ionic conductivity and soft intrinsic properties, which hinders their use in ASSLMBs[33,34]. Especially, a series of problems could be originated from Li dendrites when they are combined with LMA. Polyethylene oxide (PEO), polyacrylonitrile (PAN), and poly(vinylidenefluoride) (PVDF) based electrolytes are the representatives of SPEs[35-37], by which the Li dendrite issue has not been well solved so that the battery cycle stability and capacity retention properties are still not satisfied. Considering the effects of electrolyte module and surface tension on Li deposition kinetics, Newman and Monroe[38] predicted that Li dendrite growth could be well suppressed when those SPEs with a high shear modulus (G'>7 GPa) are used. To achieve it, hybrid electrolytes have been extensively studied due to their ability to simultaneously improve the ionic conductivity and shear modulus of SPEs[39-47]. In this case, continuous fast Li-ion conduction pathways can be formed by blending PEO with some fillers such as those three-dimensional (3D) garnet frameworks. As such, the enhanced Li-ion conductivity (e.g., 1.2×10^{-4} S cm^{-1} at 30 °C), excellent thermal, mechanical, and electrochemical stabilities can be achieved[39]. It is reported that the hybrid electrolytes fabricated by blending electrospun $Li_7La_3Zr_2O_{12}$ (LLZO) fibers and $Li_{6.25}Ga_{0.25}La_3Zr_2O_{12}$ (Ga-LLZO) nanoparticles with PEO exhibited enhanced Li-ion conductivities of 1.59×10^{-4} S cm^{-1} and 7.2×10^{-5} S cm^{-1} at ambient temperature, respectively[40,43]. While, the cross-linked SPEs are also found to have enhanced ionic conductivity with the suppressing ability to the Li dendrite growth[48-51]. For example, the cross-linked polyethylene (PE)/PEO electrolytes even with low-modulus ($G'\approx1.0\times10^5$ Pa at 90 °C) also exhibited excellent Li dendrite suppression ability with a high ionic conductivity (>1.0×10^{-4} S cm^{-1} at 25 °C)[48]. Thus, the high modulus is not essential for suppressing Li dendrites. Although considerable progresses have been achieved in improving Li-ion conductivity as well as full cell performance,

for the hybrid and cross-linked electrolytes, the manufacturing process is always too complex. Especially, even so, the Li dendrite growth phenomenon still exists [16]. While, the less satisfactory Li-ion conductivity and high operating temperature still hinder their application. As a solution, block copolymer based electrolytes are also considered[52-57]. For instance, it is found that by using polystyrene-block-polyethylene oxide (SEO) block copolymer electrolytes, excellent Li dendrite suppression ability is demonstrated[52]. Thus, the block copolymer based electrolytes with excellent mechanical property and abundant special chemical groups could be also promising candidates for the ASSLMBs.

In this study, a block copolymer named as PEBA 2533 and LiTFSI are used to fabricate novel SPEs and then, Li/PEBA 2533-20% LiTFSI/$LiFePO_4$ ASSLMBs are assembled and tested. As a result, an excellent battery performance with high-capacity retention and a long-cycle life is realized. In addition, charge distributions of ether group and amide group in PEBA 2533 are calculated, which indicates that the amide group has stronger electron donating ability. Moreover, the effect of extra electrons on $TFSI^-$ anions is also investigated. Based on the calculated results, it is inferred that an SEI with enriched LiF should be formed for the rapid Li^+ transfer and Li dendrite suppression.

2.2 Experimental section

2.2.1 Preparation of electrolytes

PEBA 2533 was purchased from Arkema Inc., France. LiTFSI (>99.0%) and super dehydrated N, N-dimethylacetamide (DMAc) (99.5%) was purchased from Wako, Japan. All chemicals were used as received without further purification. Cathode foil and Li metal foil were purchased from Hohsen Corp., Japan and Honjo Chemical Corp. (diameter: 12 mm, thickness: 100 μm), respectively.

PEBA 2533 based SPE was fabricated through a casting method. Firstly, PEBA 2533 and LiTFSI were weighted in a mass ratio of 4:1 and dissolved in DMAc. Then, the resulting solution was placed in an oven at 60 °C for 5 h to remove the generated bubbles in the solution. Thereafter, it was casted on a polytetrafluoroethylene (PTFE) plate followed with a standing period of 2 h before the vacuum drying at 80 °C for 24 h. Finally, the SPE containing 20wt% LiTFSI was punched into a circle-shape sheet with a diameter of 12 mm for battery assembling. Thickness of the SPE was adjusted by an applicator. All these procedures were operated inside an Argon gas filled glove box (Miwa, Japan), where H_2O and O_2 concentration levels were maintained below 0.1 ppm. For a more intuitive understanding of this electrolyte, the schematic of preparation process is shown in Figure 2.1.

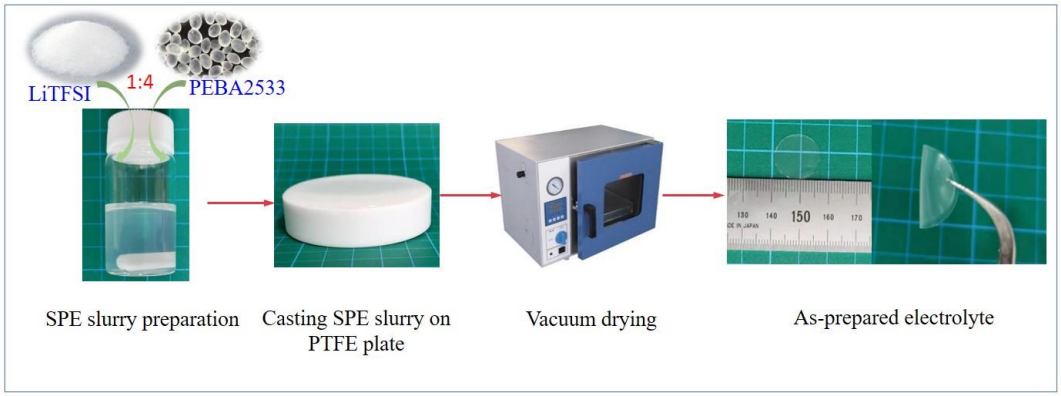

Figure 2.1 Preparation process of PEBA electrolyte and battery assembly procedures.

2.2.2 Characterizations

Morphologies and elemental ratios of the prepared SPEs were examined using a scanning electron microscopy (SEM, Hitachi SU8010) system equipped with a Horiba scientific energy dispersive spectrometer (EDS). Crystal structures of SPEs were determined by an X-ray diffraction machine (XRD, Rigaku Smart Lab X-Ray Diffractometer) using a Cu-Kα (λ=1.5405 Å) radiation source in a 2θ range of 10-90°.

Thermo gravimetric analysis (TGA) curves of SPEs were obtained under N_2 atmosphere by a TGA instrument (DTG-60H) with a heating rate of 10 °C min^{-1} from 25 to 800 °C. Fourier transform infrared spectrum (FT-IR) (FT/IR-4200, JASCO, Japan) spectra of LiTFSI, PEBA2533 and SPEs were analyzed in the range of 500-4000 cm^{-1}.

2.2.3 Electrode preparation and battery assembly

$LiFePO_4$ (Toshima Manufacturing Co. Ltd.), Super P (Alfa Aesar), and PVDF (MTI Co. Ltd.) as the cathode material, conductive material and binders respectively were weighed in a mass ratio of 8:1:1 and blended with a certain amount of N-methyl-2-pyrrolidone (Wako) to get a homogenous slurry. Thereafter, the slurry was coated on an aluminum current collector (10 μm thickness), and dried in a vacuum oven at 100 ℃ for 12 h. Finally, the cathode plate was punched into a circle shape with a diameter of 12 mm.

For the cell assembly, the obtained SPE circle plate with a diameter of 12 mm was sandwiched between the prepared $LiFePO_4$ based cathode (diameter: 12 mm) and a Li foil (diameter: 12 mm). Then, they were placed into a CR2025-type coin cell and pressed with a pressure of 750 psi. The assembled coin cell was measured with an SD8 data testing system (Hokuto Denko Corporation Co., Ltd. Japan). In this study, all the ASSLMBs were assembled without using a separator or additional liquid electrolyte in the Ar-filled glove box as indicated above.

2.2.4 Electrochemical characterizations

Simultaneously, the cell with the stainless steel blocking electrodes was also assembled to test the ionic conductivity of electrolyte at temperatures ranged from 25 to 60 °C on a Princeton electrochemical station VersaSTAT 4 by using the electrochemical impedance spectroscopy (EIS) technique with an AC amplitude of 5

mV in the frequency range of 1 MHz-0.1 Hz. Herein, the ionic conductivity σ was calculated by the following equation S1:

$$\sigma = \frac{R}{L \cdot S} \qquad (S1)$$

where R represents the obtained resistance measured by the EIS technique, L is the thickness of electrolyte, and S stands for the electrolyte effective area.

Based on the ionic conductivity data at different temperatures, the activation energy (Ea) of the electrolyte was obtained from the Arrhenius Eq. S2:

$$\sigma = \mathrm{A}\exp\left(\frac{-Ea}{K_B T}\right) \qquad (S2)$$

where A is a pre-exponential factor, T is the absolute temperature, and k_B is the Boltzmann constant.

Li-ion transference number (t_{Li+}) of the electrolyte was measured in a symmetric Li/SPE/Li cell with a DC polarization voltage of 10 mV associated with the AC impedance measurement, and then calculated by the following equation S3, where the initial (I_0) and steady (I_{ss}) currents were obtained from the DC polarization test. R_0 and R_{ss} were obtained from the AC impedance measurements with a frequency range between 1 MHz and 0.01 Hz.

$$t_{Li+} = \frac{I_{ss}(\Delta v - I_0 R_0)}{I_0(\Delta v - I_{SS} R_{SS})} \qquad (S3)$$

where ΔV is the voltage polarization applied, I_{ss} and R_{ss} are the steady current and resistance, respectively, I_0 and R_0 are the initial current and resistance, respectively.

Linear sweep voltammetry (LSV) measurement was used to evaluate the electrochemical stability window of the SPE in a potential range from 3.0 to 6.0 V at a scanning rate of 1 mV s^{-1} with a stainless steel working electrode and a Li metal sheet as the reference and counter electrodes, respectively.

The performance of ASSLMB assembled with the $LiFePO_4$ as the cathode and Li

metal as the anode was evaluated at a voltage range of 2.5~4.0 V with a charge-discharge rate of 0.5 C at 60 °C.

2.2.5 DFT calculation

The amide group and ether group models were constructed by connecting two amide 12 molecules and two ethylene oxide molecules, respectively, at first. Then, geometry optimization was conducted to get the reasonable structure of these two models with the Dmol3 module included in the Accelrys Material Studio software package. In addition, $TFSI^-$ model was also constructed and optimized with the same method.

For comparing electronegativity of amide group and ether group, charge distributions of them were calculated with the Dmol3 module included in the Accelrys Material Studio software package, in which the charge distribution was partitioned by the Hirshfeld method. Additionally, in order to demonstrate the activation of $TFSI^-$ by electrons, the bond lengths of $TFSI^-$ and $TFSI^-+e^-$ were also calculated with the Dmol3 module. It should be noted that $TFSI^-+e^-$ refers to $TFSI^-$ with an additional e^- applied to it during the calculation procedure.

2.3. Results and discission

As a popular elastomer, PEBA 2533 comprises a regular chain of rigid polyamide, in which nylon12 (PA12), as the hard segment, is interspaced with flexible polyether, and poly-(tetramethylene glycol) (PTMG) serves as the soft segment[58]. Unique mechanical properties derived from the combination of soft and hard segments could make it one of the options for inhibiting Li dendrite growth when used as the SPE material. Figures 2.2(A) and (B) show the cross-section and surface morphologies of the as-prepared PEBA 2533 based SPE (PEBA 2533-20% LiTFSI electrolyte), respectively. One can see that it has a very dense structure without any defects and displays a smooth surface.

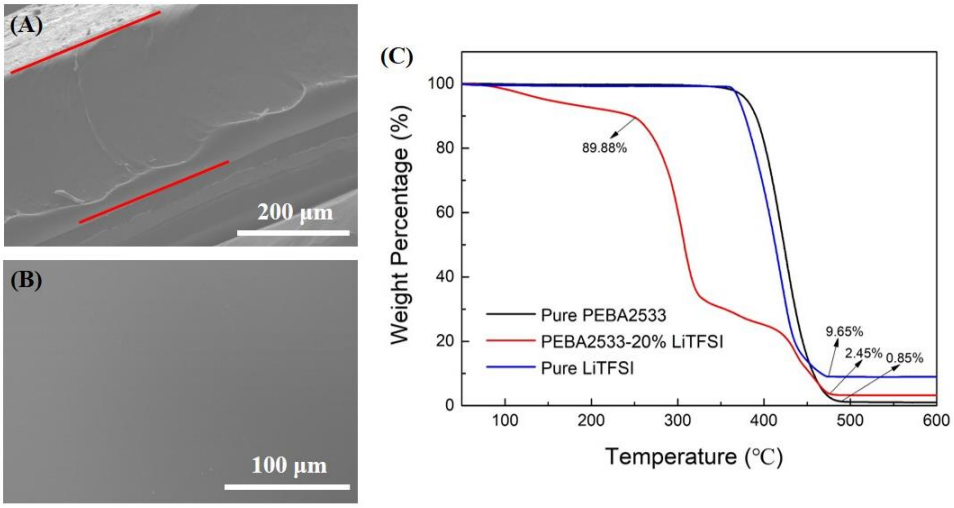

Figure 2.2 (A) Cross-section and (B) surface SEM images of PEBA 2533-20% LiTFSI electrolyte; (C) TGA curves of PEBA 2533, LiTFSI, and PEBA 2533-20% LiTFSI SPE.

Thermal behavior was evaluated by the TGA technique. As shown in Figure 2.2(C), both pure PEBA 2533 and LiTFSI maintain stable at a temperature below 360 °C, and almost completely decomposed at 475 °C with a total weight loss of 99.15% and 90.35% respectively. In comparison, the PEBA 2533-20% LiTFSI SPE has a weight loss of 10.12% below 250 °C, which can be contributed to the residue of solvent. With the further increase of temperature, the PEBA 2533 based SPE begins to decompose and leave a 2.45% residue after 475 °C. It demonstrates that the thermal stability of PEBA 2533 is weakened by the addition of LiTFSI. Nevertheless, it should be noted that the thermal stability at a temperature below 250 °C of the SPE still meets the requirements of ASSLMBs.

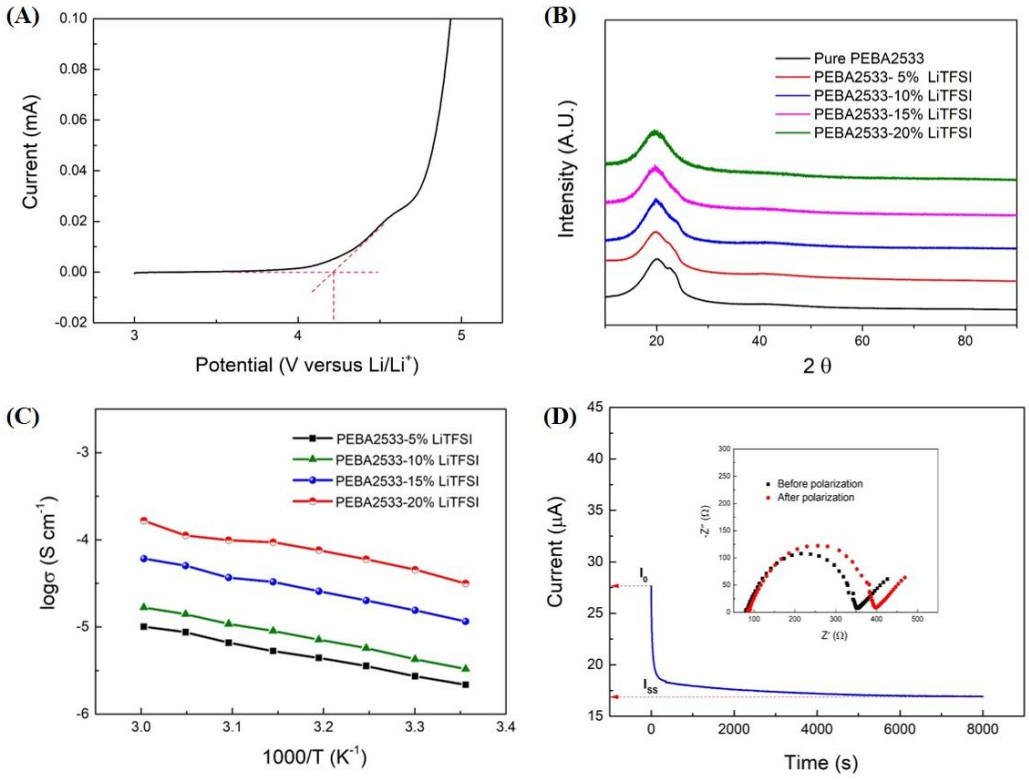

Figure 2.3 (A) LSV curve of the prepared PEBA 2533-20wt% LiTFSI SPE with a electrochemical stable window in a potential range of 3.0-6.0 V; (B) XRD patterns of the pure PEBA 2533 and SPE samples; (C) Ionic conductivities of SPEs vs. temperature in the range of 25-60; (D) DC polarization curve for Li/PEBA 2533-20wt% LiTFSI/Li cell under a polarization voltage of 10 mV (The inset shows the EISs before and after the polarization).

Ideally, the SPEs should be highly ionic conductive, mechanically strong, nonvolatile, non-flammable and chemically/electrochemically stable within the battery operation window. Herein, the electrochemical window is closely related to the choice of cathode material. Figure 2.3(A) shows LSV of the PEBA 2533-20% LiTFSI SPE. One can see that the SPE begins to decompose until ~4.2 V with a current of 4.7 μA, indicating its good electrochemical stability at this voltage window, which is suitable for the ASSLMBs. It should be pointed out that the voltage corresponding to the intersection of the two tangent lines in Figure 2.3(A) is considered to be the decomposition voltage

of the electrolyte. Additionally, the LSV curves of SPEs with 10wt%, 15wt%, and 20wt% LiTFSI content were also compared and shown in Figure 2.4. It is easy to find that the electrochemical stability of SPEs increase with the decrease of LiTFSI content. It is mostly caused by the mechanical strength differences of SPEs, which can result in interface contact difference and further change the current signals. Thus, the electrochemical stability of PEBA 2533-20% LiTFSI SPE is more credible.

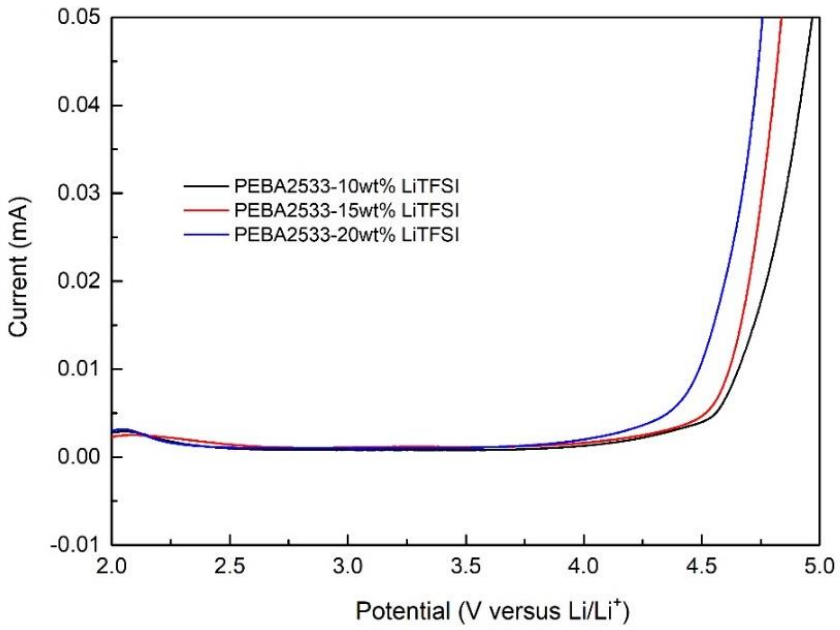

Figure 2.4 LSV curves of the prepared SPEs with a electrochemical stable window in a potential range of 2.0-5.0 V.

Figure 2.3(B) shows XRD patterns of the pure PEBA 2533 and SPE samples, in which the peaks at 2θ near 24° and 20° correspond to the (110) and (020) reflections of PTMG crystalline phase. The small peak at 2θ near 21° could be attributed to the PA12 crystalline reflection. However, it should be noted that it is close to the maximum of the amorphous halo of the glassy phase so that it is hard to be distinguished clearly[59]. From the peak at 2θ near 24°, the effect of LiTFSI content on polymer crystallization

behavior can be observed. One can see that the peak intensity decreases gradually with the increase of LiTFSI content, indicating an increase in amorphous regions, which are available for Li ion migration. It also suggests an interaction between LiTFSI and abundant functional groups inside PEBA 2533. The FT-IR spectra of the SPEs are displayed in Figure 2.5, which reveal characteristic peaks corresponding to PEBA2533 for all of the SPEs. The peak at 3299 cm^{-1} is attributed to the amide -N-H stretching vibration, while the band at 1735 cm^{-1} is assigned to the -C=O stretching vibration of the carboxylic acid [60]. The absorption peak at 1639 cm^{-1} is attributed to the out-of-plane H-N-C=O vibration of the amide, and the peak at 1111 cm^{-1} is ascribed to the polyether C-O-C stretching vibration, while the band at 1367 cm^{-1} is associated with the amide C-N stretching mode [61]. The absorption peaks at 1639 cm^{-1} and 1367 cm^{-1} were blue and red shifted respectively with the increase of LiTFSI content. Additionally, The FT-IR spectra of LiTFSI is also displayed in Figure 2.5, the peak at 1062 cm^{-1} is attributed to the S-N-S asymmetric stretching mode, while the band at 1201 cm^{-1} is assigned to the -CF_3 symmetric stretching mode[62]. The absorption peaks at 1201 cm^{-1} was blue shifted. Therefore, the interaction between amide group and LiTFSI is proved.

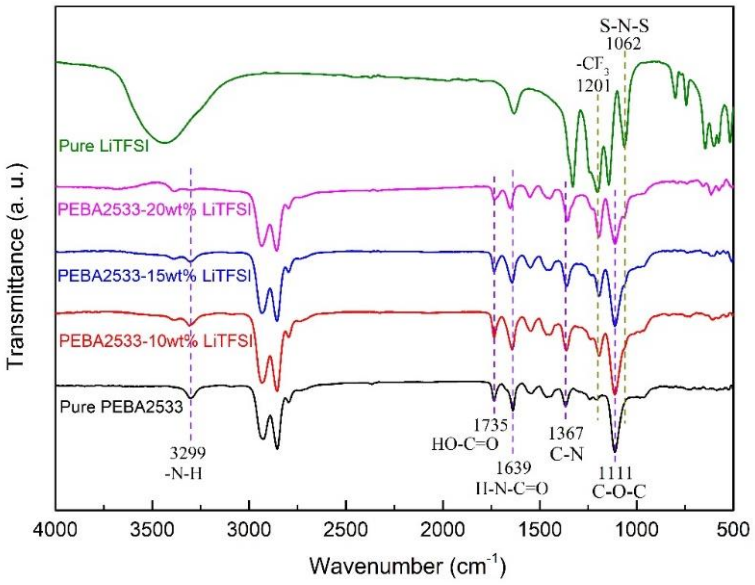

Figure 2.5 Fourier transform infrared spectra of pure LiTFSI, pure PEBA 2533 and SPEs.

Figure 2.3(C) shows ionic conductivities of the as-prepared various SPEs including PEBA 2533-5wt% LiTFSI, PEBA 2533-10wt% LiTFSI, PEBA 2533-15wt% LiTFSI, and PEBA 2533-20wt% LiTFSI ones tested at a temperature range of 25-60 °C. Herein, the PEBA 2533-20wt% LiTFSI SPE exhibits ionic conductivities of 3.16×10^{-5} S cm^{-1} at 25℃ and 1.66×10^{-4} S cm^{-1} at 60 ℃, which are comparable to the traditional PEO/LiTFSI electrolyte (4.17×10^{-5} S cm^{-1} at 25 ℃)[46]. While, it should be noted that the ionic conductivity of PEBA based SPE can be enhanced with the increase of LiTFSI content while the Li dendrite suppression problem should be balanced. The mechanical strength of electrolyte decreases with the increase of LiTFSI content, which weaks the ability of Li dendrite suppression, and makes the coin cell easy to be short circuit because of ultrothin electrolyte under assembly pressure. Considering the limitations of experimental conditions and the convenience of cell assembly, in the following study, the PEBA 2533-20wt% LiTFSI SPE was chosen. Herein, the activation energy (Ea) of it is only ca. 0.158 eV, indicating the easiness of Li ion migration in this SPE.

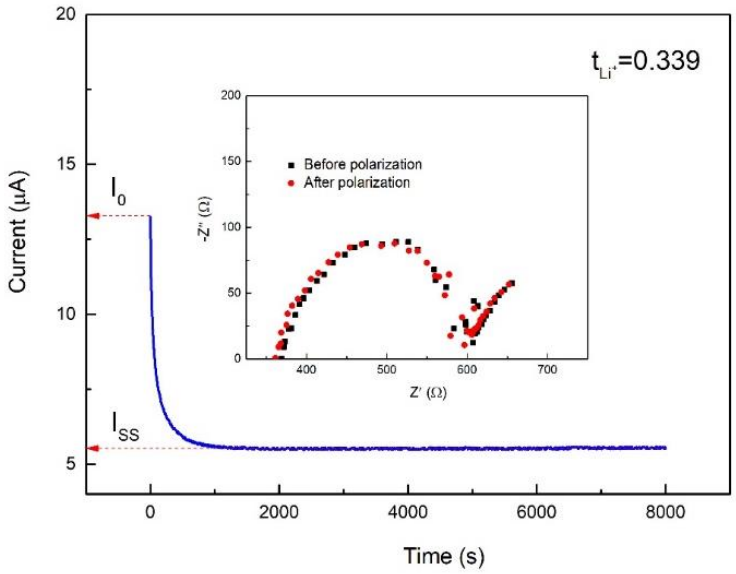

Figure 2.6 DC polarization curve for Li/PEBA 2533-10wt% LiTFSI/Li cell under a polarization voltage of 10 mV (The inset shows the EISs before and after the polarization).

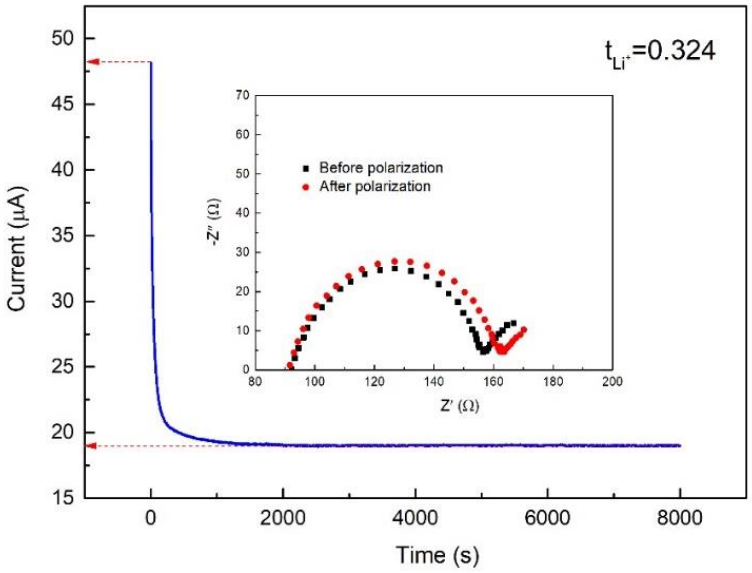

Figure 2.7 DC polarization curve for Li/PEBA 2533-15wt% LiTFSI/Li cell under a polarization voltage of 10 mV (The inset shows the EISs before and after the polarization).

Generally, the SPE should be also a dual-ion conductor, by which the Li ion and its counter anion can both easily move in it, causing a low t_{Li+}. In order to evaluate the contribution of Li ions to the ionic conductivity of the PEBA 2533-20wt% LiTFSI SPE, a steady-state current method was adopted to determine the t_{Li+} based on a symmetrical Li/SPE/Li cell. As shown in Figure 2.3(D), the initial current before the polarization and the steady current after the polarization are 27.65 and 16.91 μA, respectively, with a DC voltage of 10 mV. While, the resistance increases from 261.89 to 299.22 Ω after the polarization. Therefore, the t_{Li+} of PEBA 2533-20wt% LiTFSI SPE can be calculated to be 0.303, which is higher than that of the traditional PEO/LiTFSI SPE(~0.21). Such a high t_{Li+} could also enable dendrite-free Li deposition[63]. In addition, t_{Li+} of PEBA 2533-10wt% LiTFSI (0.339) and PEBA 2533-15wt% LiTFSI (0.324) were also calculated and shown in Figure 2.6 and Figure 2.7. With the decrease of LiTFSI content, the t_{Li+} of SPEs increase slightly. It may be caused by the stronger limitation of $TFSI^-$ by the polymer matrix with the decrease of LiTFSI content.

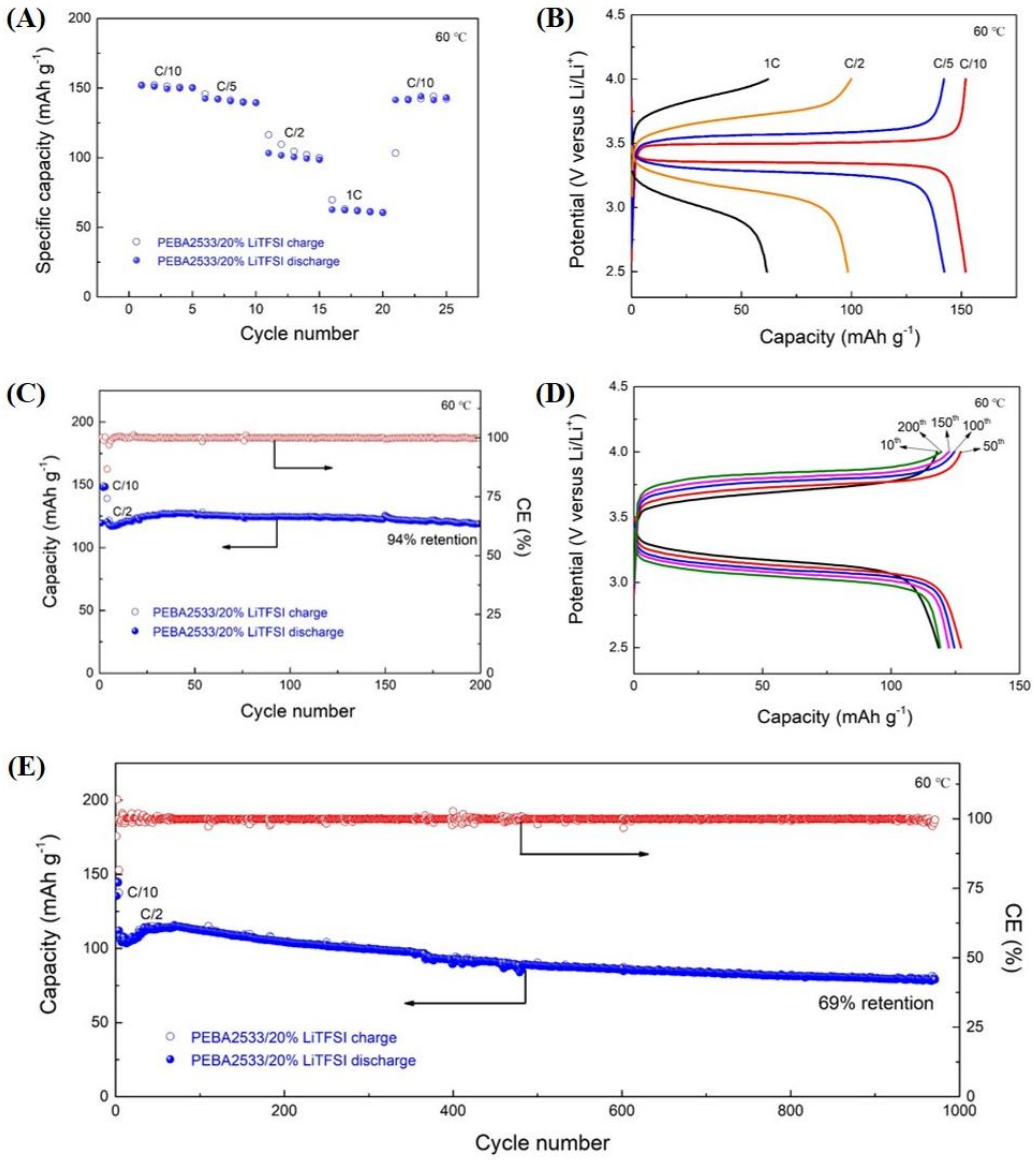

Figure 2.8 (A) Rate performance and (B) charge-discharge voltage profiles of the Li/PEBA 2533-20wt% LiTFSI/$LiFePO_4$ full cell at different current densities; (C) cycling performance and (D) charge-discharge voltage profiles of the Li/PEBA 2533-20wt% LiTFSI/$LiFePO_4$ full cell (a real capacity: 0.15 mAh cm^{-2}); (E) Long-term cycling performance of Li/PEBA 2533-20wt% LiTFSI/$LiFePO_4$ full cell.

Along with the improvement of the ionic conductivity of SPEs, it should consider the interface compatibility in the ASSLMBs [64-67]. To verify the practicality of PEBA based SPEs in ASSLMBs, the PEBA 2533-20wt% LiTFSI SPE was also used to

assemble the cell with $LiFePO_4$ as the cathode material. As shown in Figure 2.8(A), the cell offers high discharge capacities of 151.9, 142.4, 103.2 and 62.6 mAh g^{-1} at rates of 0.1, 0.2, 0.5 and 1 C, respectively. Meanwhile, with the cycling rate decreasing from 1 to 0.1 C, the discharge capacity is recovered to 143.1 mAh g^{-1} (94.2% of the initial discharge capacity), proving that the PEBA 2533-20wt% LiTFSI SPE is stable during the charge-discharge process at different current densities. While, Figure 2.8(B) shows the charge-discharge voltage profiles of Li/SPE/$LiFePO_4$ cell tested at 60 ℃. It can be clearly observed that the potential plateau during the charging process rises with the increase of charge-discharge rate, indicating that the insufficient ionic conductivity occurs with the increase of current density, and the charge-discharge capacity is decreased to a great extent.

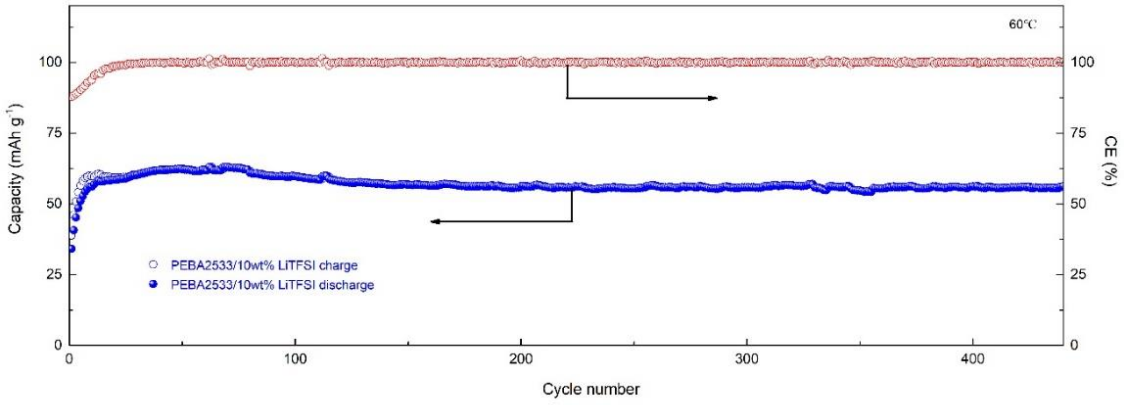

Figure 2.9 Cycling performance of the Li/PEBA 2533-10wt% LiTFSI/$LiFePO_4$ full cell at the rate of 0.5 C (areal capacity: 0.15 mAh cm^{-2}).

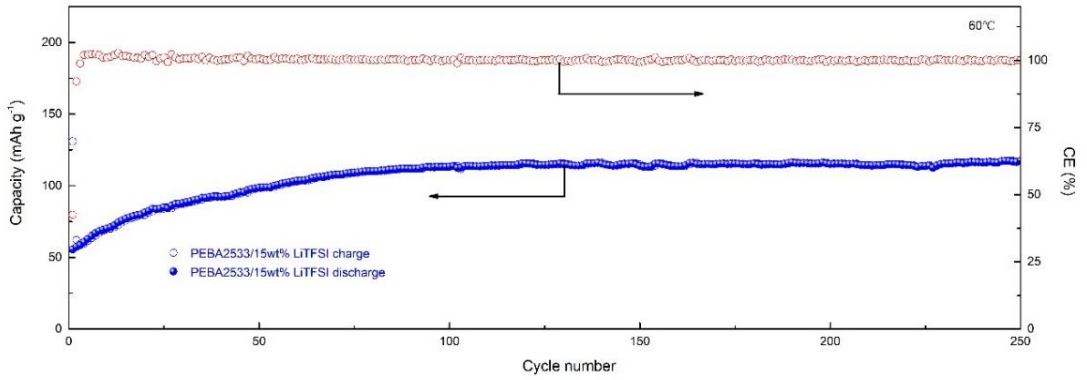

Figure 2.10 Cycling performance of the Li/PEBA 2533-15wt% LiTFSI/$LiFePO_4$ full cell at the rate of 0.5 C (areal capacity: 0.15 mAh cm^{-2}).

Figure 2.8(C) shows the performance of the Li/SPE/$LiFePO_4$ cell assembled with the as-prepared PEBA 2533-20wt% LiTFSI SPE. One can see that this cell possesses a high specific capacity of 149.4 mAh g^{-1} at the rate of 0.1 C and 60 ℃. While, it also shows very stable cycling for 200 cycles and remains 94% of its maximum capacity (127.4 mAh g^{-1}) at the rate of 0.5 C and 60 ℃ with a high average coulomb efficiency (CE) of 99.92%. Such an excellent cycling performance of the battery reveals that the PEBA based SPE possesses unique Li dendrite suppression properties. That is, by application of it, both of the dead-Li layer and continuous growth of SEI can be avoided to some extent since they are usually considered to be the main reasons for the attenuation of specific capacity[16]. In addition, the performances of the Li/SPE/$LiFePO_4$ cells assembled with the as-prepared PEBA 2533-10wt% LiTFSI and PEBA 2533-15wt% LiTFSI SPEs were also tested and shown in Figure 2.9 and Figure 2.10 respectively. Both of them exhibit excellent cycling stability without even capacity fading. It should be point out that as the LiTFSI content is reduced to 15wt%, the specific capacity decreased slightly. However, as the LiTFSI content is reduced to 10wt%, the specific capacity decreased obviously due to the decrease of ionic conductivity. While, the

mechanical strength of SPEs related to LiTFSI content also make a great difference on the interface contact and further affect the performance of battery. Figure 2.8(D) shows the voltage profiles of the as-prepared ASSLMB at the 10^{th}, 50^{th}, 100^{th}, and 200^{th} cycles, which reveals that the polarization phenomenon occurs during the cycling process, which should be the main reason for the slight decline of charge-discharge capacity. Actually, if the charge-discharge cut-off voltage is widened, the attenuation of specific capacity will be even more slightly. It also indicates that the Li-ion migration resistance could be increased during the charge-discharge process. As shown in the early stage of charge-discharge process, the voltage increases rapidly and then keep stable. Thus, it can be considered that the SEI layer could be not punctured but damaged, which will be analyzed in details in the following. Additionally, in order to evaluate long-term cycling stability of PEBA based SPE, another Li/SPE/$LiFePO_4$ cell was assembled and tested at the rate of 0.5 C and 60 °C. As shown in Figure 2.8(E), the cell cycles maintain stably for almost 1000 cycles with an average CE of 99.83%, and 69% of its maximum capacity (115.3 mAh g^{-1}) is retained after the 1000 cycles, indicating that the PEBA 2533-20wt% LiTFSI SPE possesses excellent chemical stability and mechanical resilience. Li et al.[68] designed self-assembled monolayers with polar carboxyl groups linked to aluminum oxide-coated separator and proved that the chemical groups with strong dipole moments can offer excess electrons to accelerate the degradation dynamics of carbon-fluorine bond cleavage in LiTFSI. As such, the SEI with enriched LiF could be generated to suppress dendritic Li growth. Similarly, the PEBA based electrolytes with abundant amide groups could also accelerate the degradation dynamics of carbon-fluorine bond cleavage in LiTFSI, which should also increase the LiF content in the SEI layer for the further suppressing the growth of Li dendrite. In order to demonstrate it, electronegativity of amide and ether group were calculated by

density functional theory (DFT). Herein, for demonstrating the activation of TFSI- by electrons, the bond lengths of $TFSI^-$ and $TFSI^-+e^-$ were also calculated with the Dmol3 module.

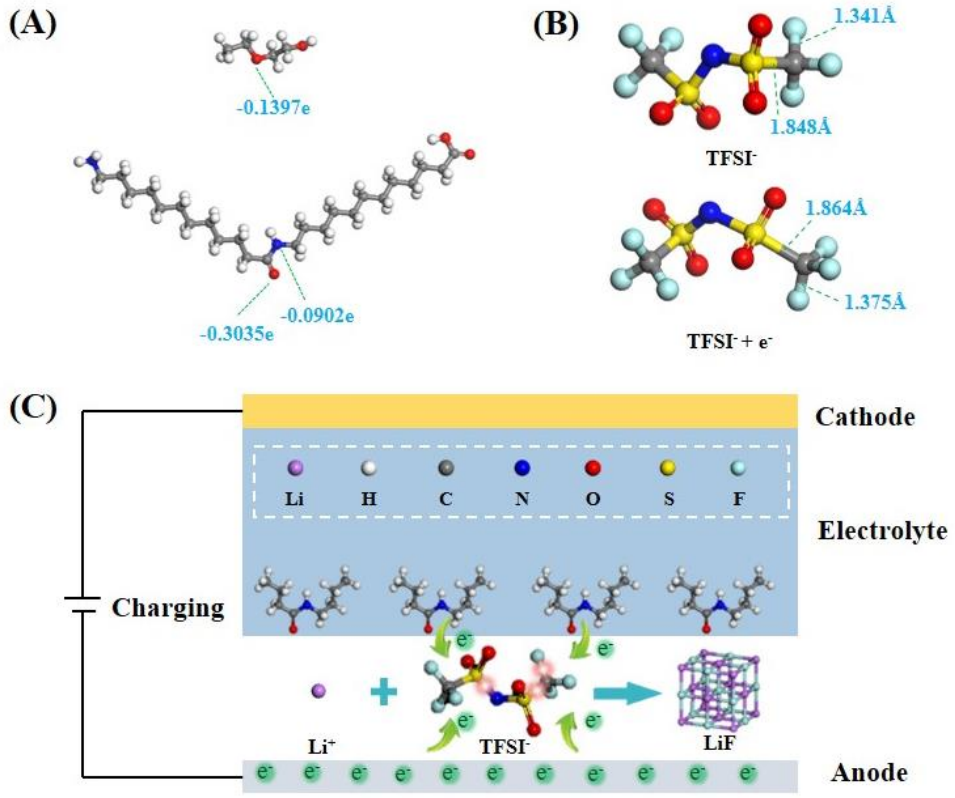

Figure 2.11 (A) Charge distributions of ether and amide group; (B) effect of extra electrons on the bond length of $TFSI^-$; (C) schematic diagram of SEI with enriched LiF.

Based on the calculations with Dmol 3 module by Hirshfeld method, as shown in Figure 2.11(A), the charge of ether oxygen is -0.1397 |e|. However, the charge of amide oxygen is -0.3035 |e|, which is higher than the ether oxygen. It demonstrates that the amide group has stronger electron donating ability. In order to evaluate the effect of electrons on $TFSI^-$, the lengths of chemical bonds were calculated for $TFSI^-$ and $TFSI^-+e^-$. As shown in Figure 2.11(B), the lengths of C-F and S-C bonds are 1.341 and 1.848 Å, respectively, for the $TFSI^-$ anion. However, when an extra electron is endowed to $TFSI^-$, the lengths of C-F and S-C bonds are changed to 1.375 and 1.864 Å, respectively,

proving that the $TFSI^-$ can be activated by extra electrons. Based on these results, a mechanism is proposed as shown Figure 2.11(C), in which $TFSI^-$ is activated with the attack of electrons from both the amide groups and the Li anode during the charging process. Due to the carbon-fluorine bond cleavage in LiTFSI, the generation of LiF could result in formation of the LiF enriched SEI layer with strong Li dendrites suppression ability, which is expected to improve battery performance with a higher capacity retention and a longer cycle life.

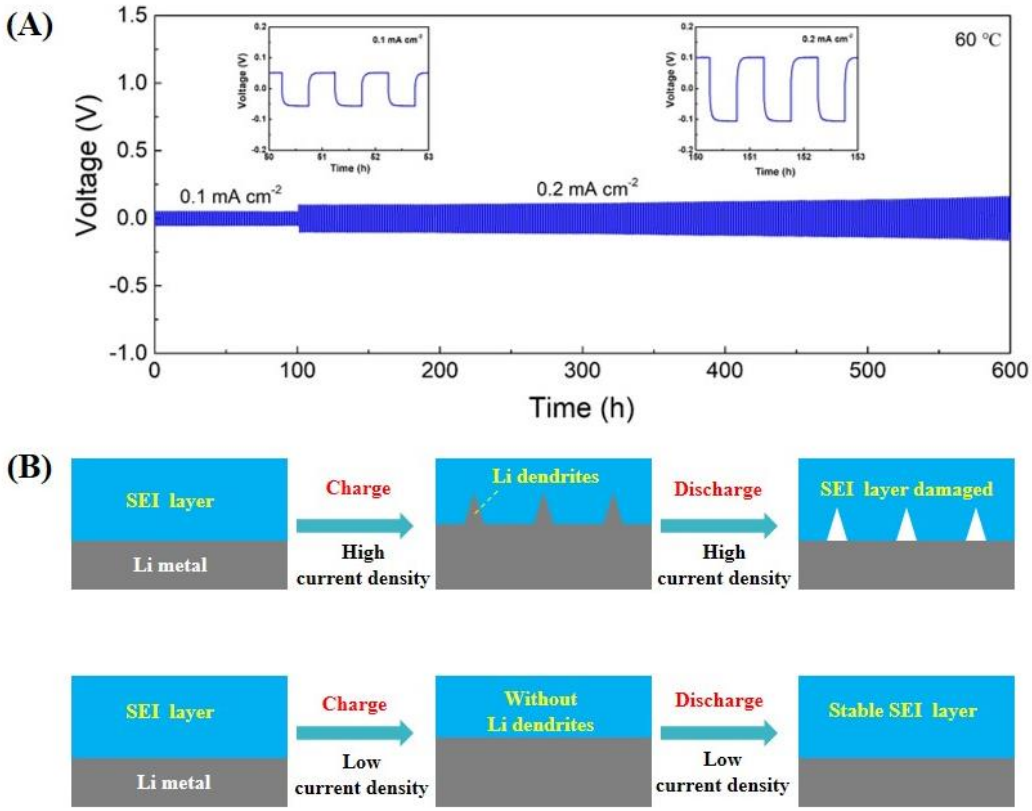

Figure 2.12 (A) Galvanostatic cycling curves of the Li/PEBA 2533-20wt% LiTFSI/Li symmetric cells at different current densities; (B) Schematic diagram of SEI destruction process.

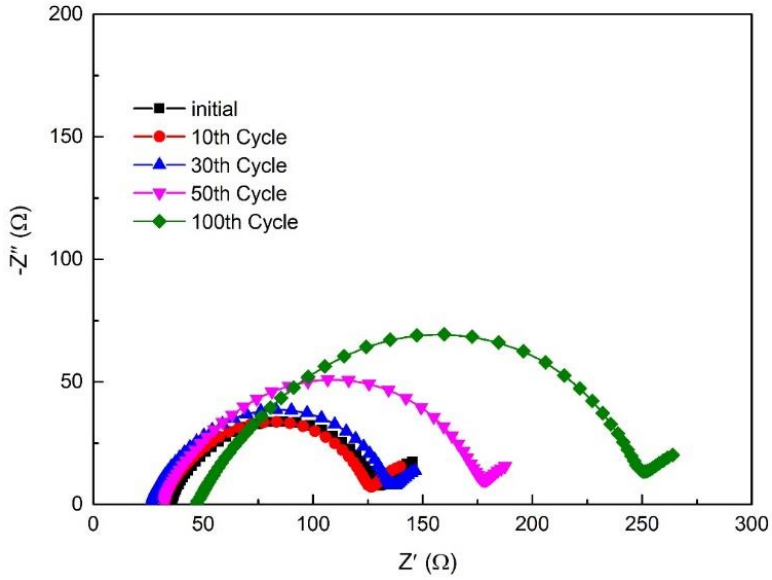

Figure 2.13 EIS plots of Li-Li symmetry battery by employing PEBA2533-20wt% LiTFSI as electrolyte.

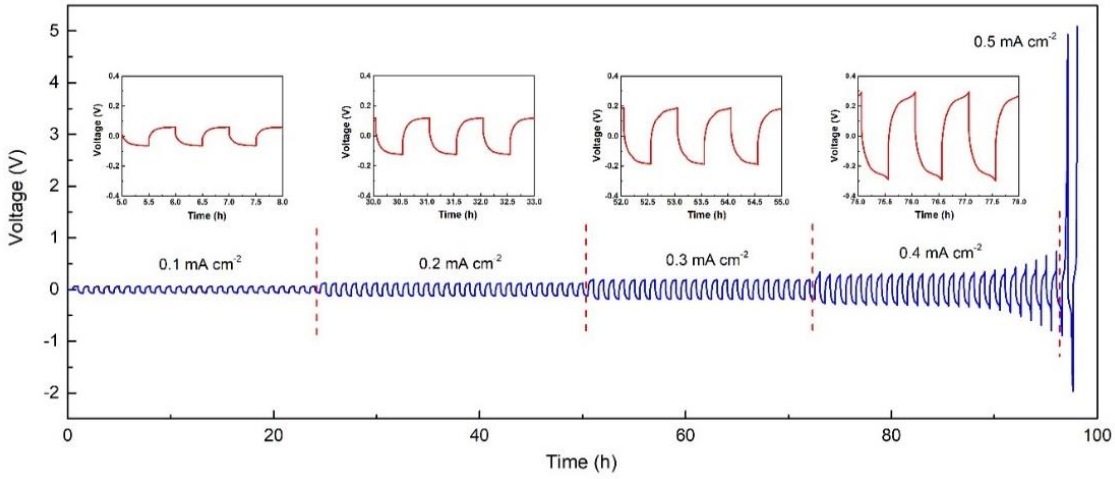

Figure 2.14 Galvanostatic cycling curves of the Li/PEBA 2533-20wt% LiTFSI/Li symmetric cells at different current densities.

However, there are still some issues existed from a full battery point of view. As illustrated in Figure 2.8(D), the voltage polarization is getting worse during the cycling process. To better understand anode interface behavior, a symmetrical Li/SPE/Li cell

was assembled and tested. Figure 2.12(A) shows the voltage profile of the cell cycled at current densities of 0.1 mA cm^{-2} and 0.2 mA cm^{-2}, respectively. One can see that the symmetrical cell shows outstanding cycling stability for more than 600 h without short circuiting. During the first 100 cycles, it shows excellent Li dendrite suppression property at a current density of 0.1 mA cm^{-2}. However, continuous voltage polarization occurs at the current density of 0.2 mA cm^{-2}, which is consistent with the voltage polarization phenomenon observed in Figure 2.8(D). It confirms that the interface between Li metal and SPE should be damaged gradually during the cycling process. Additionally, EIS of a symmetrical Li/SPE/Li cell is also tested at the current density of 0.2 mA cm^{-2} and shown in Figure 2.13. Increased impedance is observed obviously, which corresponds to the deterioration of interface contact with the increase of cycle numbers. However, it is critical to gain insight into the causes of interface deterioration and thus, the situation of SEI layer as a key factor in determining battery performance is worth studying. According to the aforementioned analyses, an SEI damage mechanism accounting for the voltage polarization is proposed as illustrated in Figure 2.12(B). Herein, at a low current density, the SEI layer always maintain excellent Li dendrite suppression performance since the SEI layer can keep stable during the cycling at this condition. In contrast, the SEI layer always cannot hinder the growth of Li dendrites at a high current density, and it will be damaged during the cycling process. As such, a resulting rough surface could be formed at the same charge-discharge rate in this case. That is the reason why the voltage polarizations appear in both Figures 2.8(D) and 2.12(A). Additionally, critical current density (CCD) as a main factor for assessing Li dendrite suppression ability is also measured and shown in Figure 2.14. But, the symmetric cell failed before the CCD value since the protection voltage is triggered. As we know, under the condition of constant time, the amount of lithium stripping will

increase with the increase of current density. It means that new Li metal stripping happened in the latter part of higher current density, which corresponding to smaller contact area between Li metal and electrolyte, and further result in an rapid increase of voltage. However, It reveals that the CCD value is higher than 0.4 mA cm^{-2} at least. To sum up, improving interface contact and cycling at limited current density should be two effective solutions for battery performance improving.

2.4 Conclusions

In summary, the PEBA based SPEs with LiTFSI as the Li salt was successfully fabricated through a solution casting method. Thereafter, the PEBA 2533-20% LiTFSI with an ionic conductivity of 3.0×10^{-5} S cm^{-1} at 25 ℃ was adopted to assemble the ASSLMBs with the $LiFePO_4$ cathode. Electrochemical performance tests of Li/SPE/$LiFePO_4$ cell showed that the battery remained 94% of its maximum capacity (127.5 mAh g^{-1}) at the rate of 0.5 C and 60 ℃ after 200 cycles. However, the voltage polarization was getting worse during the cycling process. Based on the calculations, it is found that the amide group in the PEBA has stronger electron donating ability than the ether group. Moreover, the effect of extra electrons on $TFSI^-$ anions was also investigated, and it is proved that $TFSI^-$ anion can be activated with the existence of extra electrons by comparing the bond lengths of $TFSI^-$ and $TFSI^-+e^-$. As such, a mechanism was proposed, in which $TFSI^-$ can be activated with the attack of electrons from both the amide groups and the Li anode during the charging process with the generation of LiF enriched SEI layer. In addition, the voltage polarization was also observed in a symmetrical Li/SSE/Li cell at the current density of 0.2 mA cm^{-2}. Thus, an SEI damage mechanism accounting for the voltage polarization was also proposed. It is considered that improving interface contact and cycling at limited current density should be two effective solutions for battery performance improving.

References

[1] M. Armand, J.-M. Tarascon, Building better batteries, Nature, 451 (2008) 652-657.

[2] M. S. Whittingham, Lithium batteries and cathode materials, Chem. Rev., 104 (2004) 4271-4302.

[3] J. B. Goodenough, K.-S. Park, The Li-ion rechargeable battery: a perspective, J. Am. Chem. Soc., 135 (2013) 1167-1176.

[4] Y. Sun, N. Liu, Y. Cui, Promises and challenges of nanomaterials for lithium-based rechargeable batteries, Nat. Energy, 1 (2016) 1-12.

[5] K. Xu, Electrolytes and interphases in Li-ion batteries and beyond, Chem. Rev., 114 (2014) 11503-11618.

[6] L. Suo, O. Borodin, T. Gao, M. Olguin, J. Ho, X. Fan, C. Luo, C. Wang, K. Xu, "Water-in-salt" electrolyte enables high-voltage aqueous lithium-ion chemistries, Science, 350 (2015) 938-943.

[7] G. Tan, R. Xu, Z. Xing, Y. Yuan, J. Lu, J. Wen, C. Liu, L. Ma, C. Zhan, Q. Liu, T. Wu, Z. Jian, R. Shahbazian-Yassar, Y. Ren, D. J. Miller, L. A. Curtiss, X. Ji, K. Amine, Burning lithium in CS_2 for high-performing compact Li_2S-graphene nanocapsules for Li-S batteries. Nat. Energy, 2 (2017) 1-10.

[8] Y.-K. Sun, S.-T. Myung, B.-C. Park, J. Prakash, I. Belharouak, K. Amine, High-energy cathode material for long-life and safe lithium batteries, Nat. Mater., 8 (2009) 320-324.

[9] X. Shen, Y. Li, T. Qian, J. Liu, J. Zhou, C. Yan and J. B. Goodenough, Lithium anode stable in air for low-cost fabrication of a dendrite-free lithium battery, Nat. Commun., 10 (2019) 1-9.

[10] A. M. Hafez, Y. Jiao, J. Shi, Y. Ma, D. Cao, Y. Liu, H. Zhu, Stable metal anode enabled by porous lithium foam with superior ion accessibility, Adv. Mater., 30 (2018)

1802156.

[11] J.-M. Tarascon, M. Armand, Issues and challenges facing rechargeable lithium batteries, Nature, 414 (2001) 359-367.

[12] D. Lin, Y. Liu, Y. Cui, Reviving the lithium metal anode for high-energy batteries, Nat. Nanotechnol., 12 (2017) 194-206.

[13] Y. Lu, Z. Tu, L. A. Archer, Stable lithium electrodeposition in liquid and nanoporous solid electrolytes, Nat. Mater., 13 (2014) 961-969.

[14] Q. Zheng, L. Ma, R. Khurana, L. A. Archer, G. W. Coates, Structure-property study of cross-linked hydrocarbon/poly(ethylene oxide) electrolytes with superior conductivity and dendrite resistance, Chem. Sci., 7 (2016) 6832-6838.

[15] X. Ji, D.-Y. Liu, D. G. Prendiville, Y. Zhang, X. Liu, G. D. Stucky, Spatially heterogeneous carbon-fiber papers as surface dendrite-free current collectors for lithium deposition, Nano Today, 7 (2012) 10-20.

[16] K.-H. Chen, K. N. Wood, E. Kazyak, W. S. LePage, A. L. Davis, A. J. Sanchez, N. P. Dasgupta, Dead lithium: mass transport effects on voltage, capacity, and failure of lithium metal anodes. J. Mater. Chem. A, 5 (2017) 11671-11681.

[17] J. C. Bachman, S. Muy, A. Grimaud, H.-H. Chang, N. Pour, S. F. Lux, O. Paschos, F. Maglia, S. Lupart, P. Lamp, L. Giordano, S.-H. Yang, Inorganic solid-state electrolytes for lithium batteries: mechanisms and properties governing ion conduction, Chem. Rev., 116 (2016) 140-162.

[18] T. F. Miller, Z.-G. Wang, G. W. Coates, N. P. Balsara, Designing polymer electrolytes for safe and high capacity rechargeable lithium batteries, Acc. Chem. Res., 50 (2017) 590-593.

[19] A. Manthiram, X. Yu, S. Wang, Lithium battery chemistries enabled by solid-state electrolytes, Nat. Rev. Mater., 2 (2017) 16103.

[20] Y. Wang, W. D. Richards, S. P. Ong, L. J. Miara, J. C. Kim, Y. Mo, G. Ceder, Design principles for solid-state lithium superionic conductors, Nat. Mater., 14 (2015) 1026-1031.

[21] L. Fan, S. Wei, S. Li, Q. Li, Y. Lu, Recent progress of the solid-state electrolytes for high-energy metal-based batteries, Adv. Energy Mater., 8 (2018) 1702657.

[22] X. Han, Y. Gong, K. Fu, X. He, G. T. Hitz, J. Dai, A. Pearse, B. Liu, H. Wang, G. Rubloff, Y. Mo, V. Thangadurai, E. D. Wachsman, L. Hu, Negating interfacial impedance in garnet-based solid-state Li metal batteries, Nat. Mater., 16 (2017) 572-579.

[23] F. Han, T. Gao, Y. Zhu, K. J. Gaskell, C. Wang, A battery made from a single material, Adv. Mater., 27 (2015) 3473-3483.

[24] Y. Kato, S. Hori, T. Saito, K. Suzuki, M. Hirayama, A. Mitsui, M. Yonemura, H. Iba, R. Kanno, High-power all-solid-state batteries using sulfide superionic conductors, Nat. Energy, 1 (2016) 16030.

[25] A. M. Christie, S. J. Lilley, E. Staunton, Y. G. Andreev, P. G. Bruce, Increasing the conductivity of crystalline polymer electrolytes, Nature 433 (2005) 50-53.

[26] J. Zhang, J. Zhao, L. Yue, Q. Wang, J. Chai, Z. Liu, X. Zhou, H. Li, Y. Guo, G. Cui, L. Chen, Safety-reinforced poly(propylene carbonate)-based all-solidstate polymer electrolyte for ambient-temperature solid polymer lithium batteries, Adv. Energy Mater., 5 (2015) 1501082.

[27] Y. Li, Z. Fu, S. Lu, X. Sun, X. Zhang, L. Weng, Polymer nanofibers framework composite solid electrolyte with lithium dendrite suppression for long life all-solid-state lithium metal battery, Chem. Eng. J., 440 (2022) 135816.

[28] Y. Li, Z. Sun, L. Shi, S. Lu, Z. Sun, Y. Shi, H. Wu, Y. Zhang, S. Ding, Poly (ionic liquid)-polyethylene oxide semi-interpenetrating polymer network solid electrolyte for

safe lithium metal batteries. Chem. Eng. J., 375 (2019) 121925.

[29] Y. Li, Z. Sun, D. Liu, S. Lu, F. Li, G. Gao, M. Zhu, M. Li, Y. Zhang, H. Bu, Z. Jia, S. Ding, Bacterial cellulose composite solid polymer electrolyte with high tensile strength and lithium dendrite inhibition for long life battery. Energy Environ. Mater., 4 (2021) 434-443.

[30] D. Lin, W. Liu, Y. Liu, H. R. Lee, P.-C. Hsu, K. Liu, Y. Cui, High ionic conductivity of composite solid polymer electrolyte via in situ synthesis of monodispersed SiO_2 nanospheres in poly(ethylene oxide), Nano Lett., 16 (2016) 459-465.

[31] W. Liu, S. W. Lee, D. Lin, F. Shi, S. Wang, A. D. Sendek, Y. Cui, Enhancing ionic conductivity in composite polymer electrolytes with well-aligned ceramic nanowires, Nat. Energy, 2 (2017) 17035.

[32] W. Ren, C. Ding, X. Fu, Y. Huang, Advanced gel polymer electrolytes for safe and durable lithium metal batteries: Challenges, strategies, and perspectives. Energy Stor. Mater., 34 (2021), 515-535.

[33] K. J. Harry, D. T. Hallinan, D. Y. Parkinson, A. A. MacDowell, N. P. Balsara, Detection of subsurface structures underneath dendrites formed on cycled lithium metal electrodes, Nat. Mater., 13 (2014) 69-73.

[34] Z. Xue, D. He, X. Xie, Poly(ethylene oxide)-based electrolytes for lithium-ion batteries, J. Mater. Chem. A, 3 (2015) 19218-19253.

[35] D. Golodnitsky, E. Livshits, E. Peled, Highly conductive oriented PEO-based polymer electrolytes, Macromol. Symp., 203 (2003) 27-46.

[36] F. Yuan, H.-Z. Chen, H.-Y. Yang, H.-Y. Li, M. Wang, PAN-PEO solid polymer electrolytes with high ionic conductivity, Mater. Chem. Phys., 89 (2005) 390-394.

[37] A.K. Arof, M.F. Aziz, M.M. Noor, M.A. Careem, L.R.A.K. Bandara, C.A. Thotawatthage, W.N.S. Rupasinghe, M.A.K.L. Dissanayake, Efficiency enhancement

by mixed cation effect in dyesensitized solar cells with a PVdF based gel polymer electrolyte, Int. J. Hydro. Energy, 39 (2014) 2929-2935.

[38] C. Monroe, J. Newman, The impact of elastic deformation on deposition kinetics at lithium/polymer interfaces, J. Electrochem. Soc., 152 (2005) A396-A404.

[39] Z. Li, W.-X. Sha, X. Guo, Three-dimensional garnet framework-reinforced solid composite electrolytes with high lithium-ion conductivity and excellent stability, ACS Appl. Mater. Interfaces, 11 (2019) 26920-26927.

[40] Z. Li, H.-M. Huang, J.-K. Zhu, J.-F. Wu, H. Yang, L. Wei, X. Guo, Ionic conduction in composite polymer electrolytes: case of PEO: Ga-LLZO composites, ACS Appl. Mater. Interfaces, 11 (2018) 784-791.

[41] Z. Li, X. Guo, Integrated interface between composite electrolyte and cathode with low resistance enables ultra-long cycle-lifetime in solid-state lithium-metal batteries, Sci. China Chem., 64 (2021) 673-680.

[42] F. Chen, D. Yang, W. Zha, B. Zhu, Y. Zhang, J. Li, Y. Gu, Q. Shen, L. Zhang, D. R. Sadoway, Solid polymer electrolytes incorporating cubic $Li_7La_3Zr_2O_{12}$ for all-solid-state lithium rechargeable batteries, Electrochim. Acta, 258 (2017) 1106-1114.

[43] M. Jing, H. Yang, C. Han, F. Chen, L. Zhang, X. Hu, F. Tu, X. Shen, Synergistic enhancement effects of LLZO fibers and interfacial modification for polymer solid electrolyte on the ambient-temperature electrochemical performances of solid-state battery, J. Electrochem. Soc., 166 (2019) A3019-A3027.

[44] J. Za J. M. pez del Amo, M. J. Cordill, F. Aguesse, L. Buannic, A. Llordés, Garnet-polymer composite electrolytes: new insights on local Li-ion dynamics and electrodeposition stability with li metal anodes, ACS Appl. Energy Mater., 2 (2019) 1734-1746.

[45] F. Croce, L. Persi, B. Scrosati, F. Serraino-Fiory, E. Plichta, M.A. Hendrickson,

Role of the ceramic fillers in enhancing the transport properties of composite polymer electrolytes, Electrochim. Acta, 46 (2001) 2457-2461.

[46] P.A.R.D. Jayathilaka, M.A.K.L. Dissanayake, I. Albinsson, B.-E. Mellander, Effect of nano-porous Al_2O_3 on thermal, dielectric and transport properties of the $(PEO)_9$LiTFSI polymer electrolyte system, Electrochim. Acta, 47 (2002) 3257-3268.

[47] Z. Xie, Z. Wu, X. An, A. Yoshida, Z. Wang, X. Hao, A. Abudula, G. Guo, Bifunctional ionic liquid and conducting ceramic co-assisted solid polymer electrolyte membrane for quasi-solid-state lithium metal batteries, J. Membrane Sci., 586 (2019) 122-129.

[48] R. Khurana, J. L. Schaefer, L. A. Archer, G. W. Coates, Suppression of lithium dendrite growth using cross-linked polyethylene/poly(ethylene oxide) electrolytes: a new approach for practical lithium-metal polymer batteries, J. Am. Chem. Soc., 136 (2014) 7395-7402.

[49] Q. Lu, Y.-B. He, Q. Yu, B. Li, Y. V. Kaneti, Y. Yao, F. Kang, Q.-H. Yang, Dendrite-free, high-rate, long-life lithium metal batteries with a 3D cross-linked network polymer electrolyte, Adv. Mater., 29 (2017) 1604460.

[50] Q. Zheng, L. Ma, R. Khurana, L. A. Archer, G. W. Coates, Structure-property study of cross-linked hydrocarbon/poly(ethylene oxide) electrolytes with superior conductivity and dendrite resistance, Chem. Sci., 7 (2016) 6832-6838.

[51] T.-C. Wang, C.-Y. Tsai, Y.-L. Liu, Solid polymer electrolytes based on cross-linked polybenzoxazine possessing poly (ethylene oxide) segments enhancing cycling performance of lithium metal batteries, ACS Sustain. Chem. Eng., 9 (2021) 6274-6283.

[52] G. M. Stone, S. A. Mullin, A. A. Teran, D. T. Hallinan, A. M. Minor, N. P. Balsara, Resolution of the modulus versus adhesion dilemma in solid polymer electrolytes for rechargeable lithium metal batteries, J. Electrochem. Soc., 159 (2011) A222-A227.

[53] R. A. Zoppi, C. M. N. P. Fonseca, M.-A. De Paoli, S. P. Nunes, Solid electrolytes based on poly (amide 6-b-ethylene oxide), Solid State Ionics, 91 (1996) 123-130.

[54] R. A. Zoppi, C. M. N. P. Fonseca, M.-A. De Paoli, S. P. Nunes, Hybrid electrolytes of poly (ethylene oxide) copolymers/$LiClO_4$/SiO_2: thermal analysis, mechanical properties and chemometric study of ionic conductivity, Acta Polym., 48 (1997) 193-198.

[55] N. S. Schauser, K. J. Harry, D. Y. Parkinson, H. Watanabe, N. P. Balsara, Lithium dendrite growth in glassy and rubbery nanostructured block copolymer electrolytes, J. Electrochem. Soc., 162 (2015) A398-A405.

[56] T. N. T. Phan, S. Issa, D. Gigmes, Poly (ethylene oxide)-based block copolymer electrolytes for lithium metal batteries, Polymer. Int., 68 (2019) 7-13.

[57] S. Chakraborty, G. K. Sethi, L. Frenck, A. S. Ho, I. Villaluenga, H. Wantanabe, N. P. Balsara, Effect of yield stress on stability of block copolymer electrolytes against lithium metal electrodes, ACS Appl. Energy Mater., 5 (2022) 852-861.

[58] E. Tocci, A. Gugliuzza, L. D. Lorenzo, M. Macchione, G. D. Luca, E. Drioli, Transport properties of a co-poly(amide-12-b-ethylene oxide) membrane: a comparative study between experimental and molecular modelling results, J. Membr. Sci., 323 (2008) 316-327.

[59] E. Okoroafor, J. Rault, Cryodilation of thermoplastic PEBA elastomers, J. Polym. Sci. B Polym. Phys., 29 (1991) 1427-1436.

[60] A. Ghadimi, T. Mohammadi, N. Kasiri, A novel chemical surface modification for the fabrication of PEBA/SiO_2 nanocomposite membranes to separate CO_2 from syngas and natural gas streams, Ind. Eng. Chem. Res., 53 (2014) 17476-17486.

[61] A. Ghadimi, M. Amirilargani, T. Mohammadi, N. Kasiri, B. Sadatnia, Preparation of alloyed poly (ether block amide)/poly (ethylene glycol diacrylate) membranes for

separation of CO_2/H_2 (syngas application). J. Membr. Sci., 458 (2014) 14-26.

[62] S. M. Mohd Razalli, S. I. Y. Sheikh Mohd Saaid, A. M. Marwan Ali, O. H. Hassan, M. Z. A. Yahya, Cellulose acetate-lithium bis (trifluoromethanesulfonyl) imide solid polymer electrolyte: ATR-FTIR and ionic conductivity behavior. Functional Materials Letters, 8 (2015) 1540017.

[63] C.-Z. Zhao, X.-Q. Zhang, X.-B. Cheng, Q. Zhang, An anion-immobilized composite electrolyte for dendrite-free lithium metal anodes, P. Natl Acad. Sci., 114 (2017) 11069-11074.

[64] Z. Gao, H. Sun, L. Fu, F. Ye, Y. Zhang, W. Luo, Y. Huang, Promises, challenges, and recent progress of pnorganic solid-state electrolytes for all-solid-state lithium batteries, Adv. Mater., 30 (2018) 1705702.

[65] Y. Lu, L. Li, Q. Zhang, Z. Niu, J. Chen, Electrolyte and interface engineering for solid-state sodium batteries, Joule, 2 (2018) 1747-1770.

[66] J. Ma, B. Chen, L. Wang, G. Cui, Progress and prospect on failure mechanisms of solid-state lithium batteries, J. Power Sources, 392 (2018) 94-115.

[67] Y. Shen, Y. Zhang, S. Han, J. Wang, Z. Peng, L. Chen, Unlocking the energy capabilities of lithium metal electrode with solid-state electrolytes, Joule, 2 (2018) 1674-1689.

[68] Y. Liu, X. Tao, Y. Wang, C. Jiang, C. Ma, O. Sheng, G. Lu, X. Lou, Self-assembled monolayers direct a LiF-rich interphase toward long-life lithium metal batteries, Science, 375 (2022) 739-745.

CHAPTER 3 Effect of nano Al_2O_3 addition on cycling performance of poly(ether block amide) based solid-state lithium metal batteries

3.1 Introduction

Realizing of electrochemical energy storage with high energy density, high security and low cost has received increasing attention in both research and industrial fields [1-4]. With their rapid application in electrical vehicles and portable electronic machines, lithium-ion batteries (LIBs) are still not catching up to the expectations either in security or energy density [5-8]. Therefore, it is urgent to develop the next-generation advanced-batteries [9]. Li metal is commonly considered as an alternative anode material because of its highly theoretical capacity (3860 $mAh \cdot g^{-1}$) and low reduction potential (-3.04 V versus the standard hydrogen electrode (SHE)) [10-14]. However, Li metal anode (LMA) has poor cyclability in liquid electrolytes due to its high reactivity and rapid dendrite growth during the charging and discharging process [15-21]. Additionally, those liquid electrolytes with flammable organics may incur serious safety issue [22,23]. Therefore, various solid-state electrolytes (SSEs) such as solid sulfide electrolytes [24-29], solid oxide electrolytes [30-34] and solid-state polymer electrolytes (SPEs) [35-40] have received extensive researches.

Solid-state-electrolytes with increased chemical stability and Li dendrite suppression ability potentially offer a solution to those issues existed in the LIBs containing liquid-electrolytes [41]. Nevertheless, some unresolved issues primarily including chemical degradation, mechanical fracture and loss-of-contact still hinder the application of all solid-state lithium metal batteries (ASSLMBs) [42]. Unlike brittle inorganic electrolytes, SPEs are more economical, easier to manufacture, and more highly flexible

to fit the battery shape. However, in the application of SPEs-based ASSLMBs, there are at least three main issues, i.e., (1) limited ionic conductivity restricted by the low mobility of polymer segments at room temperature (RT); (2) uncontrolled Li dendrite growth during the plating and stripping process; (3) contact degradation between the SPE and electrodes due to the volume variation. All these issues are still needed to be addressed.

In recent years, enormous works have been conducted to address these issues. For example, to obtain SPEs with high ionic conductivity, various polymers such as poly(ethylene oxide) (PEO), poly(methyl methacrylate) (PMMA), polyacrylonitrile (PAN), and poly(vinylidenefluoride) (PVDF) have been used [43-45]. Among them, PEO-based electrolytes with low ion conductivities (10^{-6}-10^{-8} S cm^{-1}) at room temperature have received the most attention due to the effective interaction between ether oxygens and cations by using it [46-48]. While, the addition of nano-inorganic particles as the solid plasticizer has been proved to suitably decrease the crystallinity of PEO, thereby promoting the ion conductivity [49]. In addition, it is also found that the doping of some inorganic solid electrolytes with high ion conductivity can improve the ionic conductivity of those PEO-based electrolytes [50]. For example, by adopting $Li_7La_3Zr_2O_{12}$ (LLZO) as the filler, the Li-ion conductivity of PEO-based electrolyte can be enhanced to 5.5×10^{-4} S cm^{-1} at 30 °C with improved electrochemical, mechanical and thermal stability [51]. However, the uncontrollable Li dendrite growth and other problems, especially, the generation of "dead Li" and voids on LMA during the charging and discharging process, are still the obstacle for the application of PEO-based SPEs in ASSLMBs [52-56]. Several models such as heterogeneous nucleation model, surface nucleating and diffusion model and space-charge model have been constructed to study the effect of initial nucleation of Li metal on the deposition behavior for the growth of

Li dendrites, and considerable efforts have been dedicated to realizing the uniform plating and stripping of LMA [57-60]. For example, three-dimensional (3D) current collector with submicron skeleton and porous structure was adopted for Li dendrite growth suppression and a high coulomb efficiency (CE) at a reasonable current density was achieved [61]. While, construction of an artificial protection layer as another effective solution for Li dendrite suppression has been also extensively studied. It is proved that by using various fillers such as metal oxides [62], nitrides [63], sulfides [64], and metal fluorides [65] to enhance artificial solid-electrolyte interphase (SEI) can effectively suppress Li dendrites. However, neither the 3D current collector nor the artificial SEIs can support the ultra-long cycling of ASSLMBs due to the mechanically fragile property of SEIs under vigorous volume changes during the charging and discharging process [66]. In addition, it is difficult to ensure the stability and uniformity of SEIs at a nanoscale in mass production. Apart from the Li anode side, loss of contact between SPEs and cathode side is another key factor in battery cycling degradation. With the increase of cycle number, the polarization caused by contact loss always becomes more and more serious [40]. Thus, the robust interfacial contact should be one of the key factors to achieve ultra-long cycling life of SPEs-based ASSLMBs.

In this study, Al_2O_3 nanoparticles (~50 nm) were adopted with lithium (Li) bis-(trifluoromethanesulfonyl)imide (LiTFSI) salt as the filler to fabricate poly(ether block amide) (PEBA)-based SPEs for ASSLMBs. Based on the preliminary experiments, a Li/PEBA 2533-20wt% LiTFSI-3wt% Al_2O_3/ $LiFePO_4$ ASSLMB was assembled and tested, which exhibited a high-capacity retention ability and a long-cycle life. While, a Li/PEBA 2533-20wt% LiTFSI-3wt% Al_2O_3/Li symmetry cell was also fabricated, which showed excellent stability at 0.1, 0.2, and 0.3 mA cm^{-2} during the plating and stripping process. Based on X-ray photoelectron spectroscope (XPS) analysis, a self-

aggregation layer (SAL) of polyamide 12 (PA12) of PEBA 253 was discovered, which should contribute to promoting the formation of lithium fluoride (LiF) enriched SEI layer, accounting for the excellent battery performance. Moreover, the effect of Al_2O_3 nanoparticle addition amount on the battery performance was also investigated. In addition, it is found that the slight capacity degradation should be attributed to the contact loss between the SPE and cathode.

3.2 Experimental section

3.2.1 SPE preparation

PEBA 2533 was provided from Arkema Inc., France. LiTFSI (>99.0%), Al_2O_3 nanoparticles, N, N-dimethylacetamide (DMAc, dehydrated, 99.5%), and N-methyl-2-pyrrolidone (>99.0%) were purchased from Wako, Japan and used directly. Li metal disk (12 mm in diameter with a thickness of 100 μm) was provided from Hohsen Corp., Japan. $LiFePO_4$ (Toshima Manufacturing Co. Ltd., Japan), Super P (Alfa Aesar, USA), and PVDF (MTI Co. Ltd. Japan) were also used as received.

PEBA 2533-based SPE was prepared via a casting method. Briefly, PEBA 2533 and LiTFSI were dissolved in DMAc with a mass ratio of 4:1 at first and then, Al_2O_3 nanoparticles were added and stirred. After the above slurry was heated at 60 °C for 2 hours for the removal of those generated bubbles, it was casted on a polytetrafluoroethylene (PTFE) plate. Thereafter, the slurry-casted plate was dried in a vacuum oven at 70 °C for 36 hours. Finally, the dried SPE film was punched into several circle-shape sheets (12 mm in diameter) and their thicknesses were adjusted using an applicator. While, pure PEBA2533 film was prepared through the same procedure. The above operations were performed in an Argon glove box (Miwa, Japan), in which the concentrations of moisture and oxygen were lower than 0.1 ppm.

3.2.2 Characterizations of samples

Morphology of the sample was characterized by a scanning electron microscopy (SEM, Hitachi SU8010). Crystalline structure was determined by a Rigaku Smart Lab X-Ray Diffractometer (XRD, Japan). Thermo gravimetric analysis (TGA) was performed in a nitrogen gas flow with a DTG-60H machine (Shimadzu, Japan). Fourier transform infrared (FT-IR) spectrum in the range of 500-4000 cm^{-1} was obtained on a JASCO FT/IR-4200 (Japan) equipment. Surface compositions were measured by an X-ray photoelectron spectroscope (XPS, XI 250 ESCALAB system) with 200 W monochromatized Al Kα radiation as the X-ray source, and the atom ratio of C, N and O on the surface of pure PEBA 2533 was evaluated by fitting the XPS spectra using a CasaXPS software.

3.2.3 Electrode and battery fabrications

$LiFePO_4$, Super P and PVDF with a mass ratio of 8:1:1 were mixed with N-methyl-2-pyrrolidone under stirring until a homogenous slurry was obtained. Then, it was casted on an aluminum current collector, and vacuum-dried at 80 ℃ for 24 hours. Afterwards, the dried sheet was punched into several circle-shape ones (12 mm in diameter, areal capacity: 0.15 mAh cm^{-2}).

To fabricate battery cell, the prepared circle-shape SPE was sandwiched between the Li sheet and the $LiFePO_4$-based cathode sheet, and then put into a CR2032-type coin cell, which was pressed under a 750 psi pressure. Herein, all the full batteries were assembled with the PTFE side of SPE in contact with the Li sheet. The performance of this coin cell was evaluated with a battery testing machine (SD8, Hokuto Denko Co. Ltd., Japan). Herein, neither separator nor additional liquid electrolyte was used in the battery cell.

3.2.4 Electrochemical performance test

Ionic conductivity (σ) of the obtained SPE was measured by assembling of a cell with stainless steel (SS) blocking electrodes at a temperature range of 25-60 °C. Electrochemical impedance spectroscopy (EIS) was determined on an electrochemical station (VersaSTAT 4, Princeton, USA) in frequencies ranged from 10^6 Hz to 0.1 Hz (AC amplitude: 10 mV). Herein, the σ was calculated by Eq. 1:

$$\sigma = L/(R \cdot S) \qquad (1)$$

where, L (cm) is the electrolyte thickness, R (Ω) the resistance measured, and S (cm^2) the effective area of SPE.

Activation energy (Ea) of the SPE was evaluated by Eq. 2:

$$\sigma(T) = Aexp[-Ea/(K_B T)] \qquad (2)$$

where A is the pre-exponential parameter, T Kalvin temperature, and k_B Boltzmann constant.

Li-ion transference number (t_{Li+}) in the SPE was analyzed with the AC impedance method by using a symmetric Li/SPE/Li cell with a DC polarization voltage of 10 mV. Herein, Eq. 3 was used, in which the initial (I_0) and steady (I_{ss}) currents were determined by the DC polarization measurement. R_0 and R_{ss} were determined via the AC impedance measurement (10^6 Hz-0.01 Hz, AC amplitude: 10 mV).

$$t_{Li+} = [I_{ss}(\Delta v - I_0 R_0)]/[I_0(\Delta v - I_{SS} R_{SS})] \qquad (3)$$

Electrochemical stability of the prepared SPE was evaluated by using Linear sweep voltammetry (LSV) analysis in a potential range of 2.0-6.0 V at 1 mV s^{-1}, in which a Li foil and a SS sheet served as the reference and counter electrodes, respectively.

For the ASSLMB with $LiFePO_4$-based cathode and LMA, the performance was examined at voltages ranged from 2.5 to 4.0 V with a charging/discharging current density of 0.1 mA cm^{-2} at 60 °C.

3.3 Results and discussion

3.3.1 Morphologies and crystallinity of SPE

PEBA 2533 contains a rigid polyamide chain with flexible polyethers, in which poly-(tetramethylene glycol) (PTMG) and PA12 are the soft and hard segments respectively [67]. These two segments endow the PEBA 2533 to have unique mechanical property. In this study, it is expected to use it as the SPE matrix for the improvement of CE of ASSLMBs. As shown in Figure 3.1(A), the prepared PEBA 2533-20wt% LiTFSI-3wt% Al_2O_3 SPE has a smooth surface, in which no agglomerated Al_2O_3 nanoparticles are observed. Meanwhile, uniform and dense cross-section morphology (Figure 3.1(B)) is also achieved.

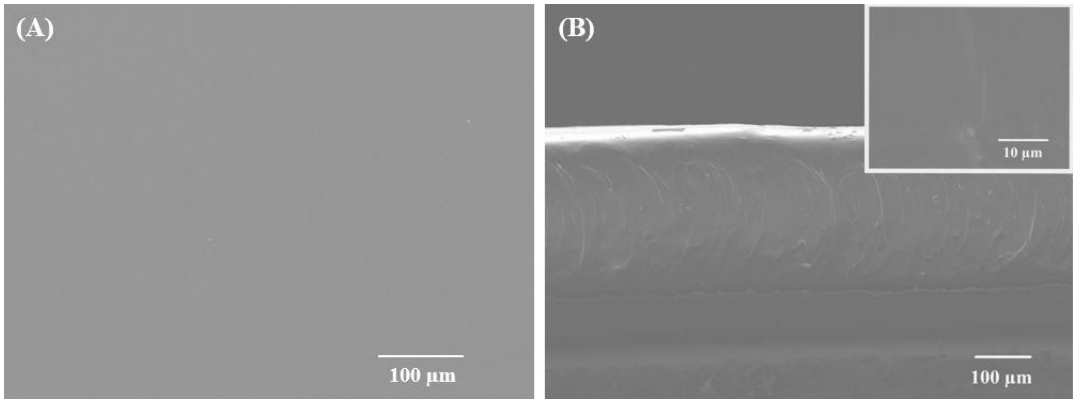

Figure 3.1 (A) Surface and (B) cross-section SEM images of PEBA 2533-20wt% LiTFSI-3wt% Al_2O_3 SPE.

Figure 3.2(A) displays XRD profiles of Al_2O_3 nanoparticles, pure PEBA 2533 and PEBA 2533-3wt% Al_2O_3, in which the peaks corresponding to Al_2O_3 can be observed in the XRD pattern of PEBA 2533-3wt% Al_2O_3. In order to understand the effect of Al_2O_3 nanoparticle addition on the crystalline property of PEBA 2533, the XRD patterns of pure PEBA 2533 and PEBA 2533-3wt% Al_2O_3 are carefully compared. On the XRD pattern of pure PEBA 2533, the characteristic peaks at 2θ near 20° and 24° are the reflections of (110) and (020) planes of crystalline PTMG phase whereas a weak

peak at 2θ near 21° corresponds to the reflection of crystalline PA12. Nevertheless, it is worth noting that the reflection of crystalline PA12 is very close to the maximal amorphous halo of glassy phase so that it is not so easy to be observed [68]. Therefore, the influence of Al_2O_3 nanoparticle addition on the crystalline change of PEBA 2533 could be distinguished by observation of the peak variation at 2θ near 24°. As shown in Figure 3.2(A), the intensity of this peak is not obviously decreased after the addition of Al_2O_3 nanoparticles, suggesting that no more amorphous phases have been generated in this case.

3.3.2 Thermal stability and FT-IR characterizations

Figure 3.2(B) shows thermal stability change after the addition of Al_2O_3 nanoparticles and/or LiTFSI salt. It can be seen that either LiTFSI salt or pure PEBA 2533 keep stable when the temperature is increased to ~370 °C, but they are almost decomposed completely as the temperature is increased to 475 °C. In contrast, the starting temperature for the decomposition of PEBA 2533-20% LiTFSI SPE is about 260 °C. It should be noted that there is negligible loss of mass before 260 °C, revealing that no solvent residue exists inside the SPE. As the temperature is further increased, the decomposition occurs and finally ends at 475 °C, revealing that LiTFSI addition can weaken PEBA 2533`s thermal stability. Thermal behaviors of SPEs with various Al_2O_3 contents were also investigated. It is observed that the decomposition temperature (~240 °C) decreases with the increase of Al_2O_3 content, demonstrating that the addition of Al_2O_3 nanoparticles can reduce the thermal stability of PEBA 2533-based SPEs. This should be attributed to the enhanced dispersion of polymer segments in the presence of Al_2O_3 nanoparticles. However, it is worth noting that the thermal stability at ~240 °C of the present SPEs still meets the requirements of ASSLMBs.

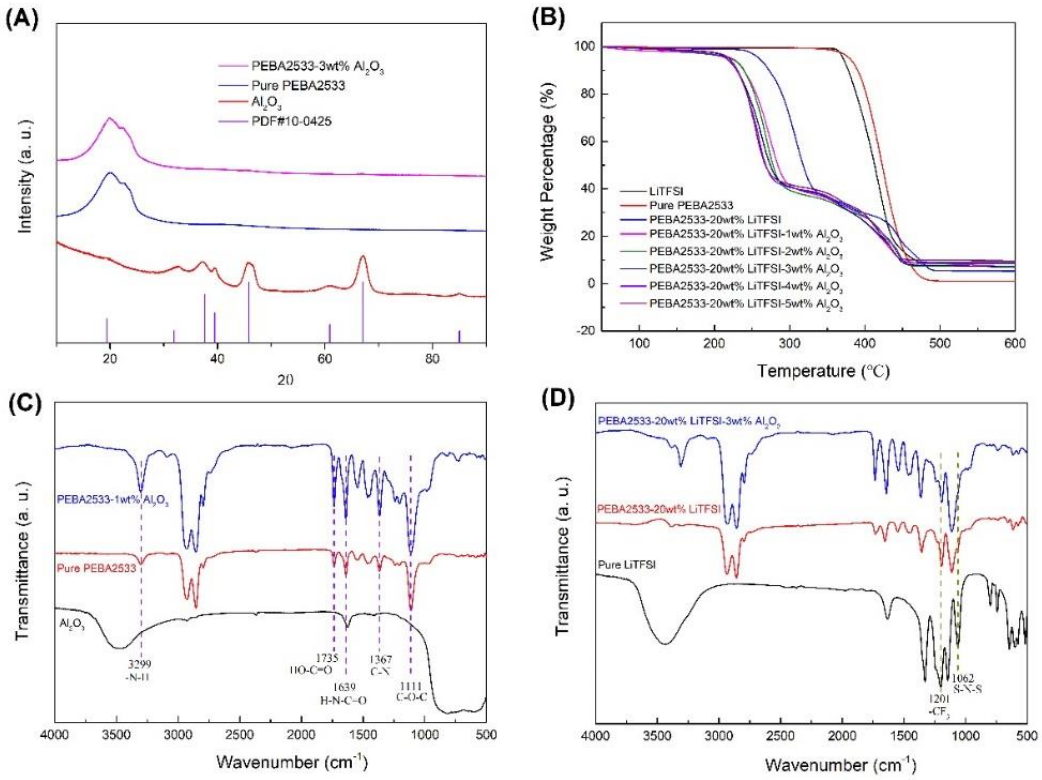

Figure 3.2 (A) XRD patterns of Al_2O_3 nanoparticles, pure PEBA 2533 and PEBA 2533-3wt% Al_2O_3; (B) TGA curves of PEBA 2533, LiTFSI, and SPE samples; (C) FT-IR spectra of Al_2O_3 nanoparticles, pure PEBA2533, and PEBA 2533-1wt% Al_2O_3; (D) FT-IR spectra of pure LiTFSI, PEBA 2533-20wt% LiTFSI and PEBA 2533-20wt% LiTFSI-3wt% Al_2O_3.

As shown in Figure 3.2(C), the peaks at 1735 and 3299 cm^{-1} are attributed to the -C=O and the stretching vibrations of -N-H of the amide, respectively [69]. The absorption peaks at 1111 and 1639 cm^{-1} are assigned to the stretching vibration of C-O-C of polyether and the out-of-plane vibration of H-N-C=O, respectively. The peak at 1367 cm^{-1} corresponds to the stretching mode of amide C-N [70]. Compared with the absorption peaks of pure PEBA 2533, for the PEBA 2533-1wt% Al_2O_3, all these absorption peaks have no shift. Figure 3.2(D) shows the FT-IR spectrum of LiTFSI, in which the peaks at 1062 and 1201 cm^{-1} are assigned to the asymmetric stretching mode of S- N-S and the symmetric stretching mode of -CF_3, respectively [71]. One can see

that there is no shift for the absorption peaks of LiTFSI in the SPE. Therefore, the addition of Al_2O_3 nanoparticles has no great effect on the changing of FT-IR spectra of either PEBA 2533 or LiTFSI. That is why no obvious crystallinity variation can be observed in Figure 3.2(A) after the addition of Al_2O_3 nanoparticles.

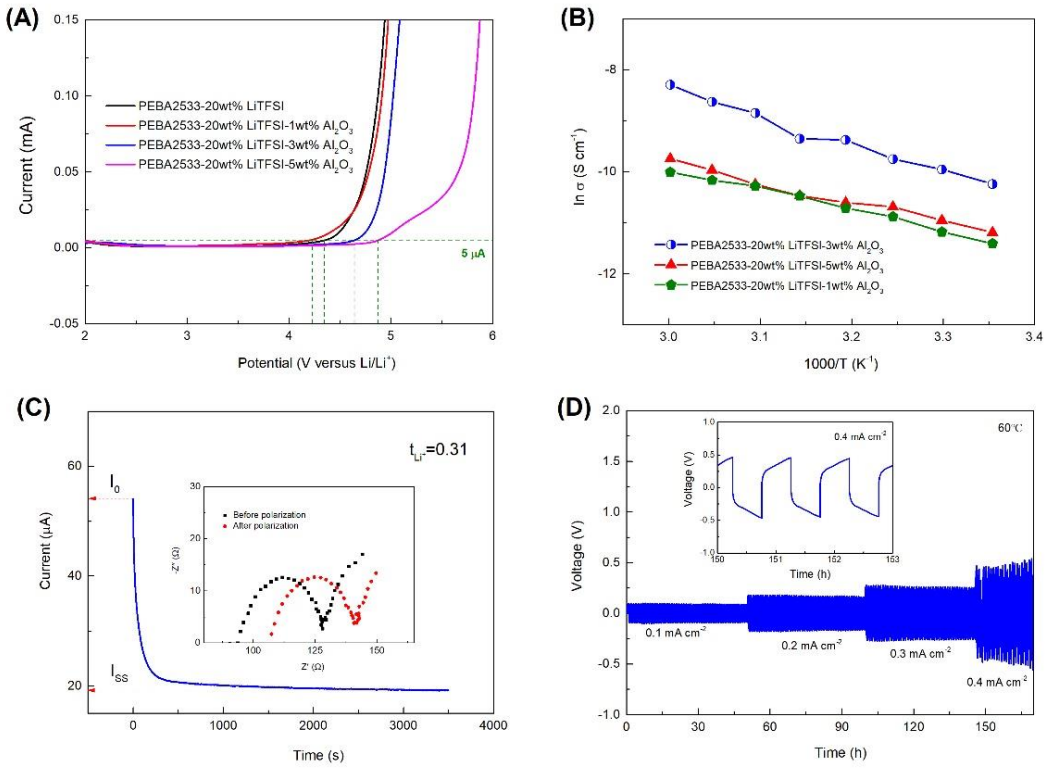

Figure 3.3 (A) LSV curves of the prepared various; (B) Ionic conductivities of SPEs vs. temperature; (C) DC polarization curve for Li/PEBA 2533-20wt% LiTFSI-3wt% Al_2O_3/Li cell under a polarization voltage of 10 mV (The inset shows the EISs before and after the polarization); (D) Galvanostatic cycling curves of the Li/PEBA 2533-20wt% LiTFSI-3wt% Al_2O_3/Li symmetric cell at different current densities.

3.3.3 Electrochemical stability window and ionic conductivity

For an ideal SPE, it should have strong mechanical strength, high ionic conductivity and electrochemical stability within the operation window. Figure 3.3(A) shows LSV

curves of the SPEs with 0, 1, 3 and 5wt% Al_2O_3 nanoparticles respectively. One can see that the decomposition of both SPEs without and with 1 wt% of Al_2O_3 nanoparticles begins at ~4.2 V, suggesting that they have excellent electrochemical stability, which should fit to the $LiFePO_4$ cathode. Herein, the decomposition voltage of a SPE can be determined at a current of above 5 μA. While, with the increase in the addition amount of Al_2O_3 nanoparticles, the electrochemical stability increases, which should be resulted from the increase in the mechanical strength since it can change the interface contact resistance and further decrease the current intensity. According to the FT-IR analysis, since the addition of Al_2O_3 nanoparticles has no great effect on the changing of FT-IR spectra of either PEBA 2533 or LiTFSI, the electrochemical stability of SPE should have no significant change. Thus, the mechanical strength of SPE should be the main reason for the electrochemical stability increasing.

Figure 3.3(B) displays ionic conductivities of the fabricated PEBA 2533-20wt% LiTFSI-based SPEs with three different addition amounts of Al_2O_3 nanoparticles measured at different temperatures ranged from 25 to 60 °C. One can see that the SPE with 3wt% Al_2O_3 nanoparticles shows ionic conductivities of 3.57×10^{-5} and 2.5×10^{-4} S cm^{-1} at 25 and 60 ℃, respectively, which are comparable to those of the SPEs without Al_2O_3 nanoparticles (e.g., 3.0×10^{-5} S cm^{-1} at 25 ℃) [40]. In addition, the ion conductivity is also compared with the data reported in other works (Table 3.1), which shows that the present SPE possesses a moderate ion conductivity.

Table 3.1 Ionic conductivities of SPEs with various active fillers

Polymer matrix	Additive	Ion conductivity (S cm^{-1})	Temperature (℃)	Ref.
PEO	40wt% LLZTO particles	1.1×10^{-5}	25	[72]
PEO	70wt% LGPS particles	2.2×10^{-4}	25	[73]
PEO	15wt% AlF_3 nanofibers	1.58×10^{-4}	30	[74]
PAN	15wt% LLTO particles	3.2×10^{-5}	25	[75]
PAN	5wt% LLZO nanowires	1.31×10^{-4}	20	[76]
PVDF	10wt% LLZTO particles	5.0×10^{-4}	25	[77]
PEBA 2533	3wt% Al_2O_3 particles	3.57×10^{-5}	25	This work

Herein, it is worth noting that the ionic conductivity increases with the increase in Al_2O_3 content from 1 to 3wt% and then decreases with the further increase from 3 to 5wt%, and the Ea of SPE with 3wt% Al_2O_3 nanoparticles is only ca. 0.47 eV. Considering that no more amorphous phases have been generated after the addition of Al_2O_3, the slight increase of ionic conductivity should be attributed to the plasticization of polymer by the addition of nanoparticles. More precisely, the added Al_2O_3 nanoparticles work as the plasticizer for PA 12 segment but have opposite effect on PTMG segment. Herein, it should be noted that the addition of LiTFSI has decreased the crystallinity of PTMG [40]. Thus, addition of Al_2O_3 particles can not decrease the crystallinity of PTMG segment further, and otherwise it will hinder the mobility of PTMG segment. That is why the ionic conductivity increases with the increase in Al_2O_3 content from 1 to 3 wt% and then decreases with the further increase from 3 to 5wt%.

3.3.4 Li^+ ion transference number and cycle stability

The t_{Li+} of PEBA 2533-20wt% LiTFSI-3wt% Al_2O_3 SPE was measured using a Li/SPE/Li cell. As displayed in Figure 3.3(C), as the DC voltage is 10 mV, the initial and steady currents before and after the polarization are 54.11 and 19.21 μA,

respectively. Meanwhile, after the polarization, it can be seen that the resistance is increased to 35.39 Ω from 34.26 Ω. As such, the calculated t_{Li+} of this SPE is 0.31, which is even the same as that of SPE without Al_2O_3 nanoparticles (0.303). This result is consistent with the FT-IR analysis, that is, the addition of Al_2O_3 nanoparticles has no great effect on the changing of FT-IR spectra of either PEBA 2533 or LiTFSI.

The Li symmetrical cell was also used to explore the anode interface behavior during the depositing-stripping process. Figure 3.3(D) displays the battery voltage profile cycled at different current densities, i.e., 0.1, 0.2, 0.3 and 0.4 mA cm^{-2}. Obviously, the symmetrical cell can cycle stably for about 50 h without short circuiting at various current densities, demonstrating the stable interface. In addition, the decrease of cycle voltage with the increase of cycle number reveals that the interface contact can be improved after the cycling. While, in contrast to the decrease of voltage at the current densities from 0.1 to 0.3 mA cm^{-2}, a continuous voltage polarization takes place at 0.4 mA cm^{-2}, suggesting that the interfaces between the electrode and electrolyte should be gradually damaged during the cycling. Even though, the Li/SPE/Li cell with the SPE containing 3wt% Al_2O_3 nanoparticles has an improved performance compared with that without Al_2O_3 nanoparticle addition, in which the voltage polarization happens at 0.2 mA cm^{-2} [40]. Considering the deteriorating interface contact with the possible following with the short-circuit of the cell, the value of 0.4 mA cm^{-2} can be thought as the critical current density (CCD) of SPE with 3wt% Al_2O_3 content.

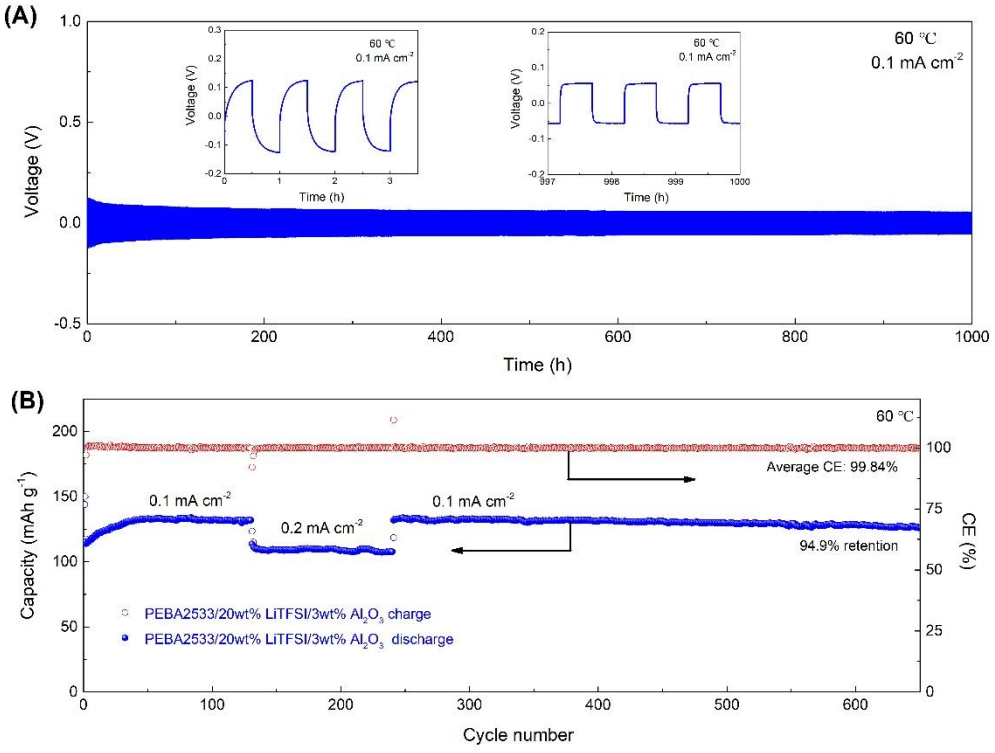

Figure 3.4 (A) Galvanostatic cycling curve of the Li/PEBA 2533-20wt% LiTFSI-3wt% Al_2O_3/Li symmetrical cell at 0.1 mA cm^{-2} and 60 ℃; (B) Long-term cycling performances of Li/PEBA 2533-20wt% LiTFSI-3wt% Al_2O_3/$LiFePO_4$ full cell at different current densities and 60 ℃.

Generally, excellent plating and stripping performance of Li/SPE/Li cell is necessary for the running of ASSLMBs. Thus, the stability of Li/SPE/Li cell with PEBA 2533-20wt% LiTFSI-3wt% Al_2O_3 SPE was tested at 0.1 mA cm^{-2}. As displayed in Figure 3.4(A), the voltage platform decreases from 0.125 V at the first cycle to 0.056 V at the 1000^{th} cycle. It is consistent with the aforementioned analyses of electrochemical stability and surface morphology of electrolyte. In addition, the Arc-shaped voltage profiles of the cycles at beginning and the final are also compared and shown in the inset of Figure 3.4(A). It also reveals that the interface resistance of the Li symmetrical cell decreases gradually with the increase of cycle number. Additionally, it should be noted that a higher current density was not adopted for the testing of cycling stability

since the protection voltage is easy to be triggered at the first several cycles. Herein, the excellent cycling stability of the Li symmetrical cell with the SPE containing 3wt% Al_2O_3 is demonstrated at 0.1 mA cm^{-2} and 60 ℃, but similar performance is also expected at 0.2 and 0.3 mA cm^{-2} if considering the result shown in Figure 3.3(D).

However, the performance of ASSLMB is always affected by numerous factors. Herein, excellent plating and stripping performance of Li/SPE/Li cell is only one of the necessary conditions for the running of ASSLMBs. Thus, to further evaluate the performance of ASSLMBs using the present SPE, a Li/PEBA 2533-20wt% LiTFSI-3wt% Al_2O_3/$LiFePO_4$ cell was also fabricated and its performance was evaluated at 60 ℃. As displayed in Figure 3.4(B), the cell exhibits large discharge capacities of 133.9 and 111.4 mAh g^{-1} at 0.1 and 0.2 mA cm^{-2}, respectively. While, with the decreasing of current density from 0.2 to 0.1 mA cm^{-2}, the recovery of discharge capacity to 133.7 mAh g^{-1} (99.85% of the initial discharge capacity) occurs, identifying that this SPE can maintain stably during the charging and discharging processes at various current densities. When the cell continues to cycle at 0.1 mA cm^{-2}, which remains stably during the cycling for 650 cycles and maintains 94.9% of its maximal capacity (133.9 mAh g^{-1}) at 60 ℃ with a high average CE of 99.84%.

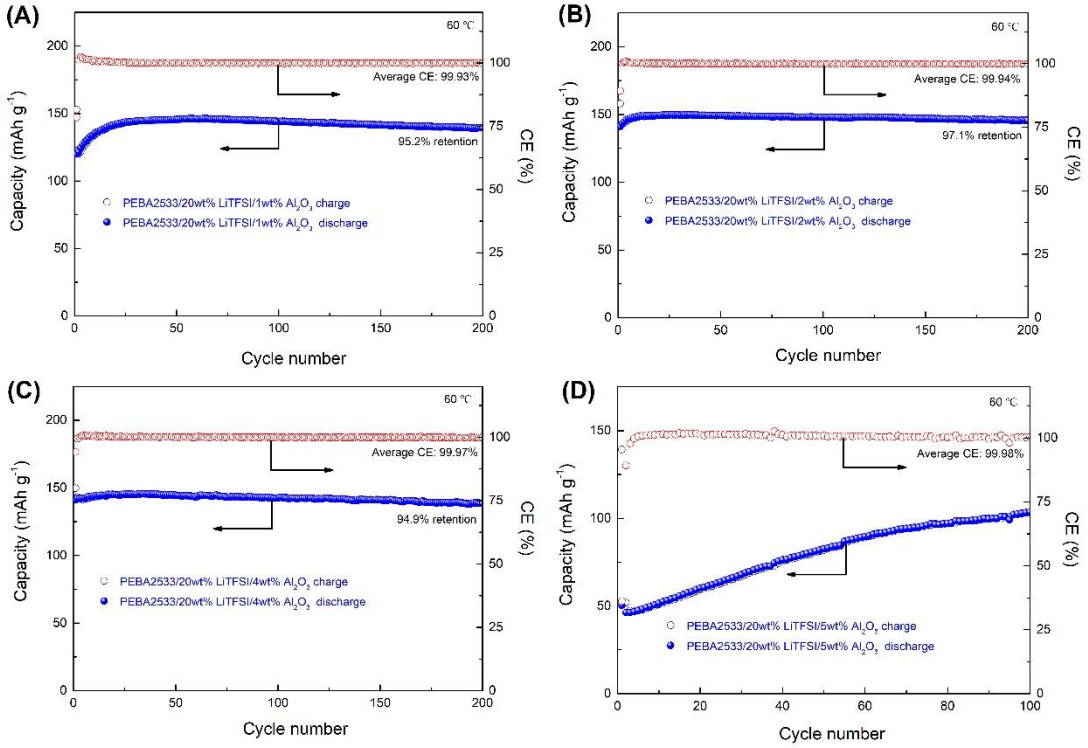

Figure 3.5 Cycling performances of Li/SPE/ $LiFePO_4$ full cells with (A) PEBA 2533-20wt% LiTFSI-1wt% Al_2O_3, (B) PEBA 2533-20wt% LiTFSI-2wt% Al_2O_3, (C) PEBA 2533-20wt% LiTFSI-4wt% Al_2O_3 and (D) PEBA 2533-20wt% LiTFSI-5wt% Al_2O_3 SPEs at 60 ℃ with the current density of 0.1 mA cm^{-2}.

Additionally, cycling performances of the ASSLMBs assembled with PEBA 2533-20wt% LiTFSI-1wt% Al_2O_3, PEBA 2533-20wt% LiTFSI-2wt% Al_2O_3, PEBA 2533-20wt% LiTFSI-4wt% Al_2O_3, and PEBA 2533-20wt% LiTFSI-5wt% Al_2O_3 SPEs were all evaluated at 60 ℃ with 0.1 mA cm^{-2} (Figure 3.5). It is found that all the batteries demonstrate excellent performance. After further comparation, the batteries assembled with PEBA 2533-20wt% LiTFSI-2wt% Al_2O_3 and PEBA 2533-20wt% LiTFSI-3wt% Al_2O_3 possess higher capacity retentions than others. It proves that the mechanical strength of SPEs with 2wt% and 3wt% Al_2O_3 nanoparticle additions are more suitable for the formation of good cathode structure. Additionally, the continuous increase of specific capacity shown in Figure 3.5(D) proves that the SPE with 5wt% Al_2O_3 addition

is difficult to immerse into cathode structure so that its performance becomes worse, which is consistent with the LSV result. While, the voltage profile of Li/PEBA 2533-20wt% LiTFSI-3wt% Al_2O_3/$LiFePO_4$ battery was also analyzed. As shown in Figure 3.6, the voltage plateau increases with the increasing of cycle number in the charging process, suggesting that the resistance increases with the proceeding of this process. However, it should be noted that the resistance is decreased for the Li/SPE/Li cell with the increasing of cycle number (Figure 3.4(A)). Therefore, the increase of potential plateau in the Li/SPE/$LiFePO_4$ cell should be attributed to the degradation of interface between SPE and cathode, and the disruption of the electron conducting network under the volume change condition is another possible reason. Comparing with our previous work (200 cycles, 94% retention) [40], the Li/SPE/$LiFePO_4$ battery with the 3wt% Al_2O_3 dopped SPE shows obviously improved capacity retention as well as cycle life. Therefore, the performance of ASSLMB can be improved further by adjusting the mechanical strength of SPEs or enhancing the robustness of cathode structure.

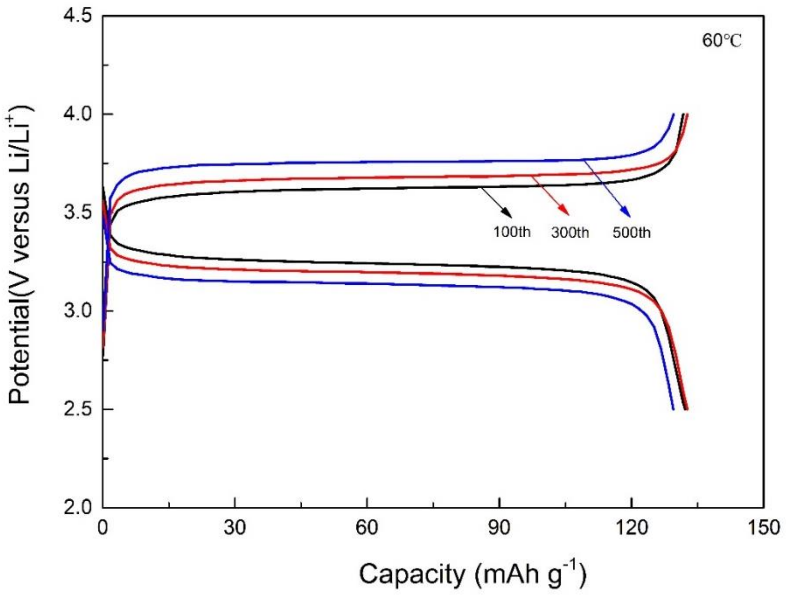

Figure 3.6 Charge-discharge voltage profiles of the Li/PEBA 2533-20wt% LiTFSI-3wt% Al_2O_3/ $LiFePO_4$ full cell (areal capacity: 0.15 mAh cm^{-2}).

3.3.5 Mechanism analysis of dendrite suppression

The PEBA 2533-based SPE with Al_2O_3 additive also possesses unique Li dendrite suppression property, which avoids the specific capacity attenuation greatly. In general, it is difficult to explore the causes of stable cycling of an ASSLMB. In our previous work [40], it is demonstrated that the amide group could activate $TFSI^-$ anions and

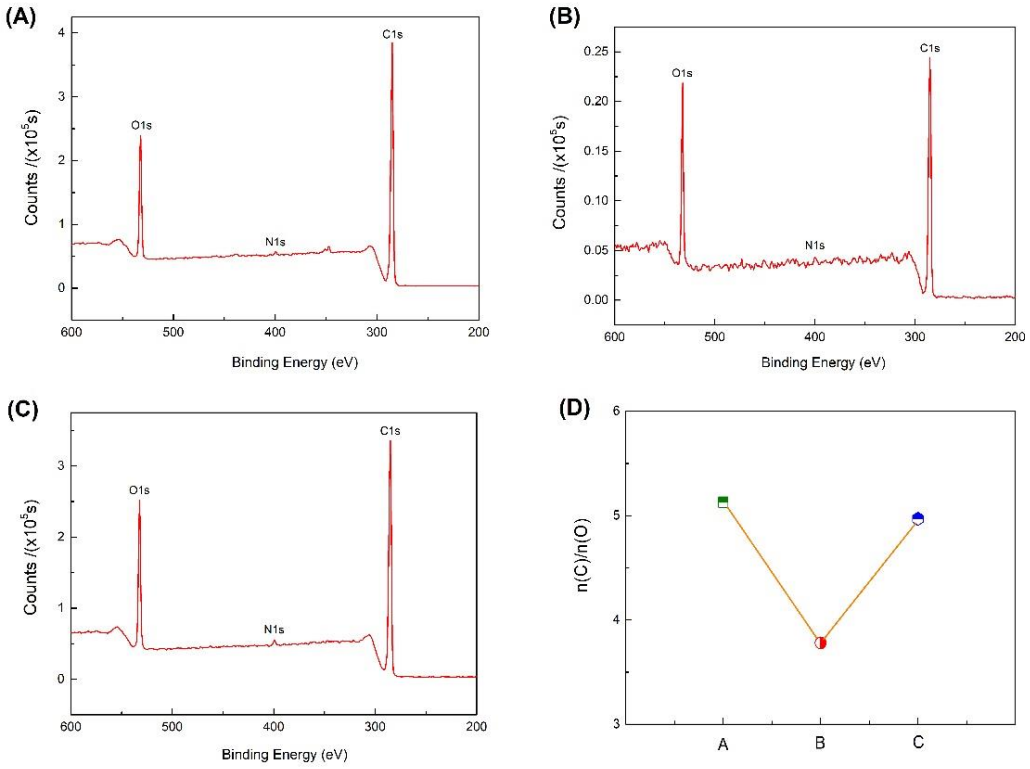

Figure 3.7 XPS survey spectra of (A) surface contacted with PTFE plate, (B) Cross section and (C) surface contacted with air of pure PEBA 2533; (D) Ratios of carbon to oxygen of two surfaces and the membrane cross section (A: the surface contacted with PTFE plate; B: cross section; C: the surface contacted with air).

further enrich LiF additive content in the SEI layer, which endows the full-cell with enhanced cyclability. However, PEBA 2533 is composed of 20 wt% of PA 12 and 80 wt% of PTMO [78]. It means that the available amide groups for $TFSI^-$ anion activation should be in a low ratio and distribute randomly on the interface between SPE and LMA,

which could not effectively contribute to the formation of uniform LiF enriched SEI layer. Thus, in order to further understand the excellent Li dendrite suppression ability of PEBA 2533-based SPEs, in this study, the difference of amide group contents on the surface of and inside the pure PEBA 2533 membrane was characterized by XPS analysis. Herein, the pure PEBA 2533 was used in order to avoid the effects of Li salt and Al_2O_3 nanoparticles. Figures 3.7(A) and (C) show the XPS survey spectra of the surface contacted with a PTFE plate and the surface contacted with air, respectively, and Figure 3.7(B) shows the XPS survey spectrum of the cross section of PEBA 2533 membrane. A summary of the ratios of carbon to oxygen is shown in Figure 3.7(D). One can see that both the surface contacted with the PTFE plate and the surface contacted with air have higher carbon to oxygen ratios than that of the cross section, directly demonstrating that the PA12 segment of PEBA 2533 with a higher carbon to oxygen ratio rather than the PTMO segment should be accumulated on the surface of PEBA 2533 membrane. It can infer that this SAL of PA12 composed of abundant amide groups on the surface of SPE should contribute to promoting the robustness of LiF enriched SEI layer so that PEBA 2533-based SPEs exhibits excellent Li dendrite suppression ability.

3.4 Conclusions

In this study, the PEBA 2533-based SPE with LiTFSI as the Li salt and Al_2O_3 nanoparticles as the solid plasticizer was prepared via a casting method. It is found that the obtained SPE with 3wt% Al_2O_3 dopped had an ionic conductivity of 3.57×10^{-5} S cm^{-1} at 25 ℃. When it was applied to fabricate ASSLMBs with the $LiFePO_4$ based cathode, the obtained optimal Li/SPE/$LiFePO_4$ cell remained 94.9% of its maximal capacity (133.9 mAh g^{-1}) at 60 ℃ with 0.1 mA cm^{-2} even after 650 cycles and the CE was also as high as 99.84%. In addition, the fabricated Li/ PEBA 2533-20% LiTFSI-

3wt% Al_2O_3/Li symmetrical cell also showed excellent cycling stability (1000 h). By comparing the voltage profiles of Li symmetrical battery and the full battery, it is found that the interface contact degradation should be the cause of voltage polarization. In addition, by XPS characterizations, SAL of PA12 was discovered, which should contribute to promoting the robustness of LiF enriched SEI layer so that PEBA 2533-based SPEs exhibit excellent Li dendrite suppression ability. Thus, the PEBA based SPEs have potential for the application of it in ASSLMBs.

References

[1] J. Liu, Z. Bao, Y. Cui, E. J. Dufek, J. B. Goodenough, P. Khalifah, Q. Li, B. Y. Liaw, P. Liu, A. Manthiram, Y. S. Meng, V. R. Subramanian, M. F. Toney, V. V. Viswanathan, M. S. Whittingham, J. Xiao, W. Xu, J. Yang, X.-Q. Yang, J.-G. Zhang, Pathways for practical high-energy long-cycling lithium metal batteries, Nat. Energy 4 (2019) 180-186.

[2] P. Albertus, S. Babinec, S. Litzelman, A. Newman, Status and challenges in enabling the lithium metal electrode for high-energy and low-cost rechargeable batteries, Nat. Energy 3 (2018) 16-21.

[3] C.P. Grey, J.M. Tarascon, Sustainability and in situ monitoring in battery development, Nat. Mater. 16 (2016) 45-56.

[4] J. Luo, C. Wang, H. Wang, X. Hu, E. Matios, X. Lu, W. Zhang, X. Tao, W. Li, Pillared mxene with ultralarge interlayer spacing as a stable matrix for high performance sodium metal anodes, Adv. Funct. Mater. 29 (2018) 1805946.

[5] T. Placke, R. Kloepsch, S. Dühnen, M. Winter, Lithium ion, lithium metal, and alternative rechargeable battery technologies: the odyssey for high energy density, J. Solid State Electrochem. 21 (2017) 1939-1964.

[6] C. Jin, J. Nai, O. Sheng, H. Yuan, W. Zhang, X. Tao, X. W. Lou, Biomass-based materials for green lithium secondary batteries, Energy Environ. Sci. 14 (2021) 1326-1379.

[7] W. Fu, E. Zhao, Z. Sun, X. Ren, A. Magasinski, G. Yushin, Iron fluoride-carbon nanocomposite nanofibers as free-standing cathodes for high-energy lithium batteries, Adv. Funct. Mater. 28 (2018) 1801711.

[8] W. Liu, Y. Jiang, N. Wang, W. Fu, Recent progress in flame retardant technology of battery: A review, Resour. Chem. Mater. 2 (2023) 80-99.

[9] O. Sheng, J. Zheng, Z. Ju, C. Jin, Y. Wang, M. Chen, J. Nai, T. Liu, W. Zhang, Y. Liu, X. Tao, In situ construction of a LiF-enriched interface for stable all-solid-state batteries and its origin revealed by Cryo-TEM, Adv. Mater. 32 (2020) 2000223.

[10] C. Fang, J. Li, M. Zhang, Y. Zhang, F. Yang, J. Z. Lee, M.-H. Lee, J. Alvarado, M. A. Schroeder, Y. Yang, B. Lu, N. Williams, M. Ceja, L. Yang, M. Cai, J. Gu, K. Xu, X. Wang, Y. S. Meng, Quantifying inactive lithium in lithium metal batteries, Nature 572 (2019) 511-515.

[11] C. Jin, O. Sheng, M. Chen, Z. Ju, G. Lu, T. Liu, J. Nai, Y. Liu, Y. Wang, X. Tao, Armed lithium metal anodes with functional skeletons, Mater. Today Nano 13 (2021) 100103.

[12] X. Tao, J. Wang, Z. Ying, Q. Cai, G. Zheng, Y. Gan, H. Huang, Y. Xia, C. Liang, W. Zhang, Yi Cui, Strong sulfur binding with conducting magnéli-phase Ti_nO_{2n-1} nanomaterials for improving lithium-sulfur batteries, Nano Lett. 14 (2014) 5288-5294.

[13] X. Tao, J. Wang, C. Liu, H. Wang, H. Yao, G. Zheng, Z. W. Seh, Q. Cai, W. Li, G. Zhou, C. Zu, Y. Cui, Balancing surface adsorption and diffusion of lithium-polysulfides on nonconductive oxides for lithium-sulfur battery design, Nat. Commun. 7 (2016) 1-9.

[14] J. B. Park, C. Choi, S. Yu, K. Y. Chung, D. W. Kim, Interfacial framework via self-discharge mechanism for stable lithium metal anode with superior rate, Adv. Energy Mater. 11 (2021) 2101544.

[15] X.-B. Cheng, R. Zhang, C.-Z. Zhao, F. Wei, J.-G. Zhang, Q. Zhang, A review of solid electrolyte interphases on lithium metal anode, Adv. Sci. 3 (2015) 1500213.

[16] Y. Jie, X. Ren, R. Cao, W. Cai, S. Jiao, Advanced liquid electrolytes for rechargeable Li metal batteries, Adv. Funct. Mater. 30 (2020) 1910777.

[17] J. Cui, T.-G. Zhan, Z.-K. Da, D. Chen, The recent advances in constructing

designed electrode in lithium metal batteries, Chin. Chem. Lett. 28 (2017) 2171-2179.

[18] Y. Sun, N. Liu, Y. Cui, Promises and challenges of nanomaterials for lithium-based rechargeable batteries, Nat Energy 1 (2016) 16071.

[19] M. D. Tikekar, S. Choudhury, Z. Tu, L. A. Archer, Design principles for electrolytes and interfaces for stable lithium-metal batteries, Nat Energy. 1 (2016) 16114.

[20] X.-B. Cheng, C.-Z. Zhao, Y.-X. Yao, H. Liu, Q. Zhang, Recent advances in energy chemistry between solid-state electrolyte and safe lithium-metal anodes, Chem. 5 (2019):74-96.

[21] Q. Wang, C. Yang, J. J. Yang, K. Wu, L. Qi, H. Tang, Z. Zhang, W. Liu, H. Zhou, Stable Li metal anode with protected interface for high-performance Li metal batteries. Energy Storage Mater. 15 (2018) 249-256.

[22] A. Manthiram, X. Yu, S. Wang, Lithium battery chemistries enabled by solid-state electrolytes, Nat. Rev. Mater. 2 (2017) 16103.

[23] K. Xu, Electrolytes and interphases in Li-ion batteries and beyond, Chem. Rev. 114 (2014) 11503-11618.

[24] M. Murayama, N. Sonoyama, A. Yamada, R. Kanno, Material design of new lithium ionic conductor, thio-LISICON, in the Li_2S-P_2S_5 system, Solid State Ionics 170 (2004) 173-180.

[25] T. Ohtomo, F. Mizuno, A. Hayashi, K. Tadanaga, M. Tatsumisago, Electrical and electrochemical properties of Li_2S-P_2S_5-P_2O_5 glass-ceramic electrolytes, J. Power Sources 146 (2005) 715-718.

[26] M. Nagao, H. Kitaura, A. Hayashi, M. Tatsumisago, Characterization of all-solid-state lithium secondary batteries using $Cu_xMo_6S_{8-y}$ electrode and Li_2S-P_2S_5 solid electrolyte, J. Power Sources 189 (2009) 672-675.

[27] M. Nagao, A. Hayashi, M. Tatsumisago, Sulfur-carbon composite electrode for

allsolid-state Li/S battery with Li_2S-P_2S_5 solid electrolyte, Electrochim Acta 56 (2011) 6055-6059.

[28] N. Kamaya, K. Homma, Y. Yamakawa, M. Hirayama, R. Kanno, M. Yonemura, T. Kamiyama, Y. Kato, S. Hama, K. Kawamoto, A. Mitsui, A lithium superionic conductor, Nat. Mater. 10 (2011) 682-686.

[29] F. Mizuno, A. Hayashi, K. Tadanaga, T. Minami, M. Tatsumisago, All-solid-state lithium secondary batteries using Li_2S-SiS_2-Li_4SiO_4 glasses and $Li_2S{\cdot}P_2S_5$ glass ceramics as solid electrolytes, Solid State Ionics 175 (2004) 699-702.

[30] J. B. Goodenough, H.Y-P. Hong, J.A. Kafalas, Fast Na^+-ion transport in skeleton structures, Mater. Res. Bull. 11 (1976) 203-220.

[31] L. Latie, G. Villeneuve, D. Conte, G. Le Flem, Ionic conductivity of oxides with general formula $Li_xLn_{1/3}Nb_{1-x}Ti_xO_3$ (Ln=La, Nd), J. Solid State Chem. 51 (1984) 293-299.

[32] K. K. Fu, Y. Gong, G. T. Hitz, D. W. McOwen, Y. Li, S. Xu, Y. Wen, L. Zhang, C. Wang, G. Pastel, J. Dai, B. Liu, H. Xie, Y. Yao, E. D. Wachsman, L. Hu, Three-dimensional bilayer garnet solid electrolyte based high energy density lithium metal-sulfur batteries, Energy Environ. Sci. 10 (2017) 1568-1575.

[33] R. J. Charles, Some structural and electrical properties of lithium silicate glasses, J. Am. Ceram. Soc. 46 (1963) 235-238.

[34] J. B. Bates, N.J. Dudney, G. R. Gruzalski, R. A. Zuhr, A. Choudhury, C. F. Luck, J. D. Robertson, Electrical properties of amorphous lithium electrolyte thin films, Solid State Ionics 53 (1992) 647-654.

[35] X. Yang, F. Zhang, L. Zhang, T. Zhang, Y. Huang, Y. Chen, A high-performance graphene oxide-doped ion gel as gel polymer electrolyte for all-solid-state supercapacitor applications, Adv. Funct. Mater. 23 (2013) 3353-3360.

[36] J. Zhang, J. Zhao, L. Yue, Q. Wang, J. Chai, Z. Liu, X. Zhou, H. Li, Y. Guo, G. Cui, L. Chen, Safety-reinforced poly(propylene carbonate)-based all-solid-state polymer electrolyte for ambient-temperature solid polymer lithium batteries, Adv. Energy Mater. 5 (2015) 1501082.

[37] X. Ban, W. Zhang, N. Chen, C. Sun, A high-performance and durable poly(ethylene oxide)-based composite solid electrolyte for all solid-state lithium battery, J. Phys. Chem. C 122 (2018) 9852-9858.

[38] U. H. Choi, S. Liang, M. V. O'Reilly, K. I. Winey, J. Runt, R. H. Colby, Influence of solvating plasticizer on ion conduction of polysiloxane single-ion conductors, Macromolecules 47 (2014) 3145-3153.

[39] L. Porcarelli, A. S. Shaplov, M. Salsamendi, J. R. Nair, Y. S. Vygodskii, D. Mecerreyes, C. Gerbaldi, Single-ion block copoly(ionic liquid)s as electrolytes for all-solid state lithium batteries, ACS Appl. Mater. Interfaces 8 (2016) 10350-10359.

[40] C. Liu, Y. He, X. An, N. Kitiphatpiboon, X. Du, X. Hao, A. Abudula, G. Guan, A poly (ether block amide) based solid polymer electrolyte for solid-state lithium metal batteries. J. Colloid Interf. Sci. 630 (2023) 595-603.

[41] M. Pasta, D. Armstrong, Z. L. Brown, J. Bu, M. R. Castell, P. Chen, A. Cocks, S. A. Corr, E. J. Cussen, E. Darnbrough, V. Deshpande, C. Doerrer, M. S. Dyer, H. El-Shinawi, N. Fleck, P. Grant, G. L. Gregory, C. Grovenor, L. J. Hardwick, J. T. S. Irvine, H. J. Lee, G. Li, E. Liberti, I. McClelland, C. Monroe, P. D. Nellist, P. R. Shearing, E. Shoko, W. Song, D. S. Jolly, C. I. Thomas, S. J. Turrell, M. Vestli, C. K. Williams, Y. Zhou, P. G. Bruce, 2020 roadmap on solid-state batteries, J. Phys. Energy 2 (2020) 032008.

[42] M.-C. Pang, K. Yang, R. Brugge, T. Zhang, X. Liu, F. Pan, S. Yang, A. Aguadero, B. Wu, M. Marinescu, H. Wang, G. J. Offer, Interactions are important: Linking multi-

physics mechanisms to the performance and degradation of solid-state batteries, Mater. Today 49 (2021) 145-183.

[43] J. W. Fergus, Ceramic and polymeric solid electrolytes for lithium-ion batteries, J. Power Sources 195 (2010) 4554-4569.

[44] F. Croce, G. B. Appetecchi, L. Persi, B. Scrosati, Nanocomposite polymer electrolytes for lithium batteries, Nature 394 (1998) 456-458.

[45] D. M. Smith, B. Dong, R. W. Marron, M. J. Birnkrant, Y. A. Elabd, L. V. Natarajan, V. P. Tondiglia, T. J. Bunning, C. Y. Li, Tuning ion conducting pathways using holographic polymerization, Nano Lett. 12 (2012) 310-314.

[46] F. M. Gray, Polymer electrolytes, Royal Society of Chemistry, 1997.

[47] B. Scrosati, Applications of electroactive polymers, Springer, 1993.

[48] J. G. Kim, B. Son, S. Mukherjee, N. Schuppert, A. Bates, O. Kwon, M. J. Choi, H. Y. Chung, S. Park, A review of lithium and non-lithium based solid state batteries, J. Power Sources 282 (2015) 299-322.

[49] F. Croce, L. Persi, B. Scrosati, F. Serraino-Fiory, E. Plichta, M. A. Hendrickson, Role of the ceramic fillers in enhancing the transport properties of composite polymer electrolytes. Electrochim. Acta 46 (2001) 2457-2461.

[50] S. Srivastava, J. L. Schaefer, Z. Yang, Z. Tu, L. A. Archer, 25th anniversary article: polymer-particle composites: phase stability and applications in electrochemical energy storage, Adv. Mater. 26 (2014) 201-234.

[51] F. Chen, D. Yang, W. Zha, B. Zhu, Y. Zhang, J. Li, Y. Gu, Q. Shen, L. Zhang, D. R. Sadoway, D. R. Sadoway, Solid polymer electrolytes incorporating cubic $Li_7La_3Zr_2O_{12}$ for all-solid-state lithium rechargeable batteries. Electrochim. Acta, 258 (2017) 1106-1114.

[52] K.-H. Chen, K. N. Wood, E. Kazyak, W. S. LePage, A. L. Davis, A. J. Sanchez, N.

P. Dasgupta, Dead lithium: mass transport effects on voltage, capacity, and failure of lithium metal anodes, J. Mater. Chem. A 5 (2017) 11671-11681.

[53] W. S. LePage, Y. Chen, E. Kazyak, K.-H. Chen, A. J. Sanchez, A. Poli, E. M. Arruda, M. D. Thouless, N. P. Dasgupta, Lithium mechanics: roles of strain rate and temperature and implications for lithium metal batteries, J. Electrochem. Soc. 166 (2019) A89-A97.

[54] Y. Lu, C.-Z. Zhao, H. Yuan, X.-B. Cheng, J.-Q. Huang, Q. Zhang, Critical current density in solid-state lithium metal batteries: mechanism, influences, and strategies, Adv. Funct. Mater. 31 (2021) 1-33.

[55] J. Kasemchainan, S. Zekoll, D. S. Jolly, Z. Ning, G. O. Hartley, J. Marrow, P. G. Bruce, Critical stripping current leads to dendrite formation on plating in lithium anode solid electrolyte cells, Nat. Mater. 18 (2019) 1105-1111.

[56] S. Wenzel, T. Leichtweiss, D. Krüger, J. Sann, J. Janek, Interphase formation on lithium solid electrolytes-An in situ approach to study interfacial reactions by photoelectron spectroscopy, Solid State Ionics 278 (2015) 98-105.

[57] J.-N. Chazalviel, Electrochemical aspects of the generation of ramified metallic electrodeposits, Phys. Rev. A 42 (1990) 7355.

[58] C. Ling, D. Banerjee, M. Matsui, Study of the electrochemical deposition of Mg in the atomic level: Why it prefers the non-dendritic morphology, Electrochim. Acta 76 (2012) 270-274.

[59] D. R. Ely, R. E. García, Heterogeneous nucleation and growth of lithium electrodeposits on negative electrodes, J. Electrochem. Soc. 160 (2013) A662-A668.

[60] R. Xu, X.-B. Cheng, C. Yan, X.-Q. Zhang, Y. Xiao, C.-Z. Zhao, J.-Q. Huang, Q. Zhang, Artificial interphases for highly stable lithium metal anode, Matter 1 (2019) 317-344.

[61] B. Lu, E. Olivera, J. Scharf, M. Chouchane, C. Fang, M. Ceja, L. E. Pangilinan, S. Zheng, A. Dawson, D. Cheng, W. Bao, O. Arcelus, A. A. Franco, X. Li, S. H. Tolbert, Y. S. Meng, Quantitatively designing porous copper current collectors for lithium metal anodes, ACS Appl. Energy Mater. 4 (2021) 6454-6465.

[62] Y. Liu, Y. Wu, J. Zheng, Y. Wang, Z. Ju, G. Lu, O. Sheng, J. Nai, T. Liu, W. Zhang, X. Tao, Silicious nanowires enabled dendrites suppression and flame retardancy for advanced lithium metal anodes, Nano Energy 82 (2021) 105723.

[63] K. Yan, H.-W. Lee, T. Gao, G. Zheng, H. Yao, H. Wang, Z. Lu, Y. Zhou, Z. Liang, Z. Liu, S. Chu, Y. Cui, Ultrathin two-dimensional atomic crystals as stable interfacial layer for improvement of lithium metal anode, Nano Lett. 14 (2014) 6016-6022.

[64] H. Chen, A. Pei, D. Lin, J. Xie, A. Yang, J. Xu, K. Lin, J. Wang, H. Wang, F. Shi, D. Boyle, Y. Cui, Uniform high ionic conducting lithium sulfide protection layer for stable lithium metal anode, Adv. Energy Mater. 9 (2019) 1900858.

[65] J. Tan, J. Matz, P. Dong, J. Shen, M. Ye, A growing appreciation for the role of LiF in the solid electrolyte interphase, Adv. Energy Mater. 11 (2021) 2100046.

[66] H. Shang, Z. Zuo, X. Dong, F. Wang, F. Lu, H. Zheng, K. Li, Y. Li, Efficiently suppressing lithium dendrites on atomic level by ultrafiltration membrane of graphdiyne, Mater. Today Energy 10 (2018) 191-199.

[67] E. Tocci, A. Gugliuzza, L. D. Lorenzo, M. Macchione, G. D. Luca, E. Drioli, Transport properties of a co-poly(amide-12-b-ethylene oxide) membrane: a comparative study between experimental and molecular modelling results, J. Membr. Sci. 323 (2008) 316-327.

[68] E. Okoroafor, J. Rault, Cryodilation of thermoplastic PEBA elastomers, J. Polym. Sci. B Polym. Phys. 29 (1991) 1427-1436.

[69] A. Ghadimi, T. Mohammadi, N. Kasiri, A novel chemical surface modification for

the fabrication of PEBA/SiO_2 nanocomposite membranes to separate CO_2 from syngas and natural gas streams, Ind. Eng. Chem. Res. 53 (2014) 17476-17486.

[70] A. Ghadimi, M. Amirilargani, T. Mohammadi, N. Kasiri, B. Sadatnia, Preparation of alloyed poly (ether block amide)/poly (ethylene glycol diacrylate) membranes for separation of CO_2/H_2 (syngas application), J. Membr. Sci., 458 (2014) 14-26.

[71] S. M. Mohd Razalli, S. I. Y. Sheikh Mohd Saaid, A. M. Marwan Ali, O. H. Hassan, M. Z. A. Yahya, Cellulose acetate-lithium bis (trifluoromethanesulfonyl) imide solid polymer electrolyte: ATR-FTIR and ionic conductivity behavior, Funct. Mater. Lett. 8 (2015) 1540017.

[72] C.-Z. Zhao, X.-Q. Zhang, X.-B. Cheng, R. Zhang, R. Xu, P.-Y. Chen, H.-J. Peng, J.-Q. Huang, Q. Zhang, An anion-immobilized composite electrolyte fordendrite-free lithium metal anodes, Proc. Nati. Acad. Sci. 114 (2017) 11069-11074.

[73] J. Zheng, P. Wang, H. Liu, Y.-Y. Hu, Interface-enabled ion conduction in $Li_{10}GeP_2S_{12}$-poly (ethylene oxide) hybrid electrolytes, ACS Appl. Energy Mater. 2 (2019) 1452-1459.

[74] W. Liu, L. Meng, X. Liu, L. Gao, X. Wang, J. Kang, J. Ju, N. Deng, B. Cheng, W. Kang, 3D spiny AlF_3/Mullite heterostructure nanofiber as solid-state polymer electrolyte fillers with enhanced ionic conductivity and improved interfacial compatibility, J. Energy Chem. 76 (2023) 503-515.

[75] W. Liu, N. Liu, J. Sun, P.-C. Hsu, Y. Li, H.-W. Lee, Y. Cui, Ionic conductivity enhancement of polymer electrolytes with ceramic nanowire fillers, Nano lett. 15 (2015) 2740-2745.

[76] T. Yang, J. Zheng, Q. Cheng, Y.-Y. Hu, C. K. Chan, Composite polymer electrolytes with $Li_7La_3Zr_2O_{12}$ garnet-type nanowires as ceramic fillers: mechanism of conductivity enhancement and role of doping and morphology, ACS appl. Mater. Interfaces 9 (2017)

21773-21780.

[77] X. Zhang, T. Liu, S. Zhang, X. Huang, B. Xu, Y. Lin, B. Xu, L. Li, C.-W. Nan, Y. Shen, Synergistic coupling between $Li_{6.75}La_3Zr_{1.75}Ta_{0.25}O_{12}$ and poly (vinylidene fluoride) induces high ionic conductivity, mechanical strength, and thermal stability of solid composite electrolytes, J. Am. Chem. Soc. 139 (2017) 13779-13785.

[78] M. E. Rezac, T. John, P. H. Pfromm, Effect of copolymer composition on the solubility and diffusivity of water and methanol in a series of polyether amides, J. Appl. Polym. Sci. 65 (1997) 1983-1993.

CHAPTER 4 Performance enhancement of all-solid-state lithium metal batteries by adopting poly(ether block amide) 4033 based electrolyte

4.1 Introduction

All solid-state Li metal batteries (ASSLMBs) are promising in energy storage field and critical for the advent of clean energy era[1,2], in which Li metal with high theoretical capacity (3860 $mAh \cdot g^{-1}$) and low reduction potential (-3.04 V versus the standard hydrogen electrode (SHE)) is used as the anode[3-7]. Development of safe and cheap electrochemical energy storage system has received ever-increasing attention in both research and industrial fields[8-11]. Solid-state polymer electrolyte (SPE) with many advantages, such as light weight, easy processing, excellent flexibility, and low cost is thought as a competitive option among numerous electrolytes after being proposed to use in ASSLMBs by Armand[12]. However, there are still several issues exist to hinder the industrial application of ASSLMBs, such as uncontrolled Li dendrite growth[13-17], contact degradation[18-20], and poor ion conductivity of SPEs[21]. Although enormous researches have been conducted for the improvement of ASSLMBs performance, more efforts are still needed for solving the safety issue and expanding the lifespan by hindering the continuous growth of Li dendrite, especially for the ASSLMBs assembled with the high-loading cathode.

Huang et al. [22] fabricated the poly(ethylene oxide) (PEO)-$Li_{6.4}La_3Zr_{1.4}Ta_{0.6}O_{12}$ (LLZTO)-LiTFSI composite polymer electrolyte (CPE) modified with dopamine to improve the interface contact and used it to assemble the ASSLMBs with $LiFePO_4$ cathode. The result shows that improved cycling performance of cell is realized comparing with the CPE without dopamine. However, it can work for only 50 cycles

with a CE lower than 99.4%. Additionally, the loading amount of $LiFePO_4$ cathode is also low (~1 mg cm^{-2}). Li et al. [23] prepared the PEO based CPE with $Li_{6.25}Ga_{0.25}La_3Zr_2O_{12}$ nanofibers as the fillers, by which a high ionic conductivity (3.2×10^{-4} S cm^{-1}) was realized at room tempreature (RT). Thereafter, $LiFePO_4$ cathode (2 mg cm^{-2}) was adopted to fabricate the ASSLMBs and the interface between CPE and cathode is improved with ionic liquids (IL) based electrolyte. Moreover, the cell delivered a high capacity (158.0 mA h g^{-1}) with significant capacity retention near 90% even after 800 cycles. However, the $LiFePO_4$ loading amount is much lower than the industrial requirement. Therefore, improvement of ASSLMBs cycling performance and clearifying the battery failure mechanism is still urgent until now.

Ye et al. [24] prepared the $LiCoO_2$-$Li_{6.6}La_3Zr_{1.6}Ta_{0.4}O_{12}$ (LCO-LLZTO) composite cathode with a high areal capacity (>3.0 mAh cm^{-2}) through a water-based method, and high specific capacity (~120 mAh g^{-1}) was realized at the current density of 0.05 mA cm^{-2} and 60 °C. However, the specific capacity of the full cell decreased rapidly to lower than 70 mAh g^{-1} in only 11 cycles later, and the mechanism is still unclear. In addition, Ihrig et al. [25] tried to enhance the contact between electrolyte and cathode by infiltration of SPE into $LiFePO_4$-$Li_{1.5}Al_{0.5}Ti_{1.5}(PO_4)_3$ (LFP-LATP) composite cathode (~19.6 mg cm^{-2}). The cycling performance of the full cell assembled with this cathode showed a high specific capacity (>160 mAh g^{-1}) after 8 cycles, which revealed that the cathode and SPE was fully contacted. However, during the first 8 cycles, the contact between cathode and SPE was improved gradually, which demonstrated that the interface should be not perfect at the first cycle. Additionally, the specific capacity began to decrease after 30 cycles, and the mechanism was also still unclear. Based on the aforementioned analysis, there are still many obstacles for the application of ASSLMBs, especially for the high-loading cathode batteries.

In our previous work[26], PEBA 2533 based SPE was prepared with LiTFSI as the Li salt, and the battery assembled with the as-prepared SPE and $LiFePO_4$ cathode (0.15 mAh cm^{-2}) showed long lifespan over 1000 cycles. In addition, excellent cycle stability (94% capacity retention after 200 cycles) and high average CE (99.92%) were realized. However, it should be pointed out that the Li dendrite suppression ability of PEBA based electrolyte is still unknown when the high-loading cathode is adopted. In the present work, PEBA 4033 was adopted as the polymer matrix to combine with LiTFSI for the preparation of SPEs and then, ionic conductivities of SPEs with 20wt%, 30wt%, and 40wt% LiTFSI were tested. Moreover, effects of solvent evaporation temperature on battery performance were investigated based on PEBA 4033 based SPEs.

4.2 Experimental section

4.2.1 SPE fabrication

PEBA 4033 was obtained from Arkema Inc., France. The chemicals used in this study, including LiTFSI (>99.0%), Al_2O_3 nanoparticles, and N, N-dimethylacetamide (DMAc, dehydrated, 99.5%), were purchased from Wako, Japan and employed without further purification. Li metal disks (diameter: 12 mm; thickness: 100 μm) and $LiFePO_4$ cathodes (1.5 mAh cm^{-2}) were provided by Hohsen Corp., Japan.

A PEBA 4033-based SPE was prepared using a casting method. To do so, PEBA 4033 and LiTFSI were dissolved in DMAc (mass ratio of 3:2) at 130°C, and Al_2O_3 nanoparticles were stirred into the solution. The resulting mixture was cast onto a PTFE plate and dried in a vacuum oven (90°C, 24 hours). The dried SPE film was then cut into several circle-shaped sheets (12 mm in diameter). In parallel, a pure PEBA 4033 sample was prepared using the same procedure. Both operations were carried out in an Argon glove box (Miwa, Japan) with less than 0.1 ppm of moisture and oxygen.

4.2.2 Sample characterizations

The sample underwent various analyses using different instruments. Its morphology was examined via SEM (Hitachi SU8010), and its crystalline structure was determined by XRD analysis using a Rigaku Smart Lab instrument (Japan). TGA was also conducted on the sample in a nitrogen gas environment using a DTG-60H machine (Shimadzu, Japan) at a heating rate of 15 °C min^{-1}.

4.2.3 Electrode and battery fabrications

A battery cell was fabricated by sandwiching the circle-shaped SPE between the Li sheet and the cathode sheet, and then placing it into a CR2032-type coin cell that was pressed under a 750 psi pressure. The performance of the coin cell was evaluated using a battery testing machine (SD8, Hokuto Denko Co. Ltd., Japan). It is worth noting that no separator or additional liquid electrolyte was used in the battery cell.

4.2.4 Electrochemical performance test

The SPE's ionic conductivity (σ) was measured by assembling a cell with stainless steel (SS) blocking electrodes in a temperature range of 25-60 °C. Electrochemical impedance spectroscopy (EIS) was then determined on an electrochemical station (VersaSTAT 4, Princeton, USA) using frequencies from 10^6 Hz to 0.1 Hz (AC amplitude: 10 mV). Herein, the σ was calculated by Eq. S1:

$$\sigma = L/(R \cdot S) \qquad (S1)$$

where, L (cm) is the electrolyte thickness, R (Ω) the resistance measured, and S (cm^2) the effective area of SPE.

Activation energy (Ea) of the SPE was evaluated by Eq. S2:

$$\sigma(T) = Aexp[-Ea/(K_B T)] \qquad (S2)$$

where A is the pre-exponential parameter, T Kalvin temperature, and k_B Boltzmann

constant.

The SPE's electrochemical stability was assessed using linear sweep voltammetry (LSV) analysis with a potential range of 2.0-6.0 V and a scan rate of 1 mV s^{-1}. The LSV analysis employed a Li foil as the reference electrode and a stainless steel (SS) sheet as the counter electrode.

The ASSLMBs incorporating $LiFePO_4$ cathode were tested for their performance in the voltage range of 2.5 to 4.0 V at a charging/discharging current density of 0.1 mA cm-2 and 60 °C.

4.3 Results and discussion

4.3.1 Crystallinity of SPE

PEBA 4033 with nylon 12 (PA12) and poly-(tetramethylene glycol) (PTMG) as the hard and soft segments respectively possesses unique mechanical properties[27]. In this study, it is expected to improve the cycling performance of ASSLMBs assembled with high-loading cathode by using PEBA 4033 based SPE.

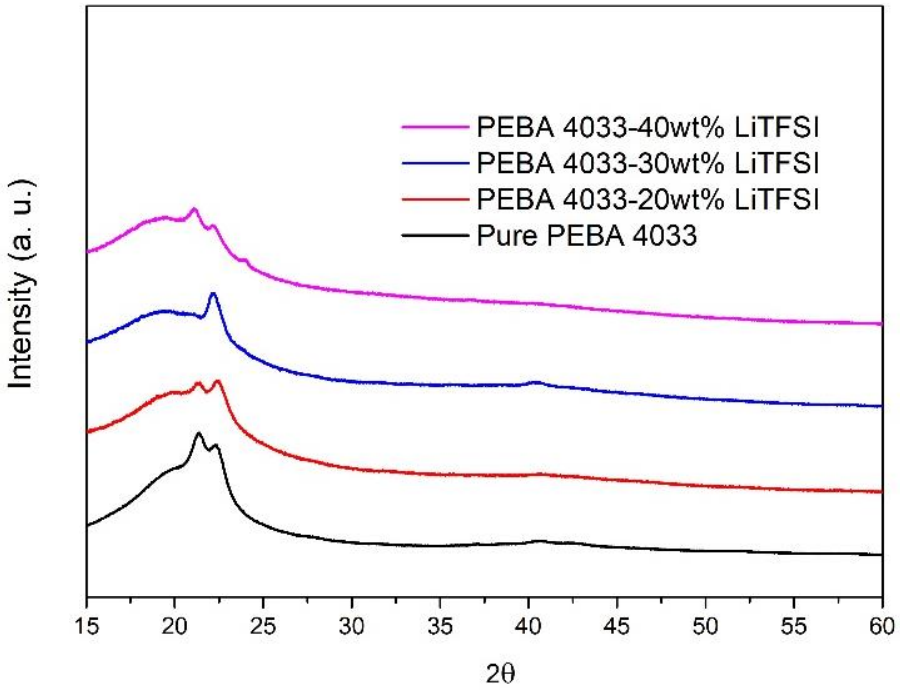

Figure 4.1 XRD patterns of pure PEBA 4033, and SPEs with various LiTFSI contents (solvent evaporation temperature: 90 °C).

As shown in Figure 4.1, the distinct peaks in diffraction pattern of pure PEBA 4033 at angles 2θ of near 21.4° and 22.3° correspond to the α phase and γ phase of PA12 crystal separately[28-30]. In order to investigate the influence of LiTFSI contents, the XRD patterns of SPEs with 20wt% LiTFSI, 30wt% LiTFSI, and 40wt% LiTFSI addition were also tested and compared with that of pure PEBA 4033. It is found that with 20wt% LiTFSI added, both diffraction peaks were weakened. It proves that the crystallinity of PA12 decreases with the addition of LiTFSI. In addition, the relative intensities of diffraction peaks also changed with the increase of LiTFSI content. As shown in Figure 4.1, the peak correspond to α phase nearly disappered with the LiTFSI content increased from 20wt% to 30wt%. It means that the addition of LiTFSI is benefit for the formation of γ phase of PA12 and harmful for the existence of α phase, which should be caused by the interaction between Li ions and amide groups. However, with

the further increase of LiTFSI content to 40wt% content, the opposite phenomenon happened, that is, the diffraction peak of α phase appeared again and the diffraction peak of γ phase decreased obviously. In our opinion, it is caused by the annealing of SPE. In other words, the annealing can promote the conversion of PA12 crystal from γ phase to α phase.

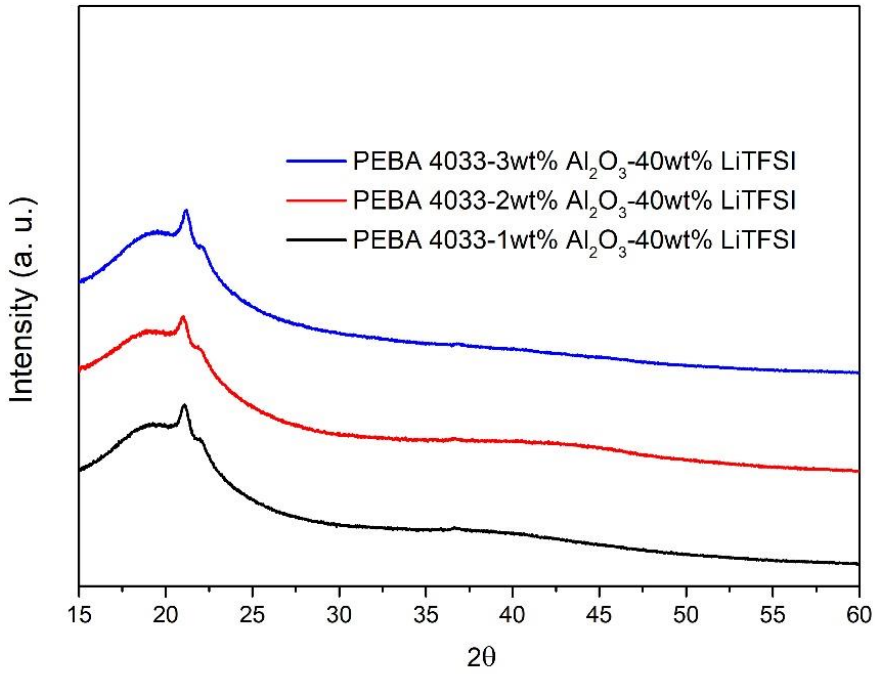

Figure 4.2 XRD patterns of CPEs with 40wt% LiTFSI and various Al_2O_3 contents (solvent evaporation temperature: 95 °C).

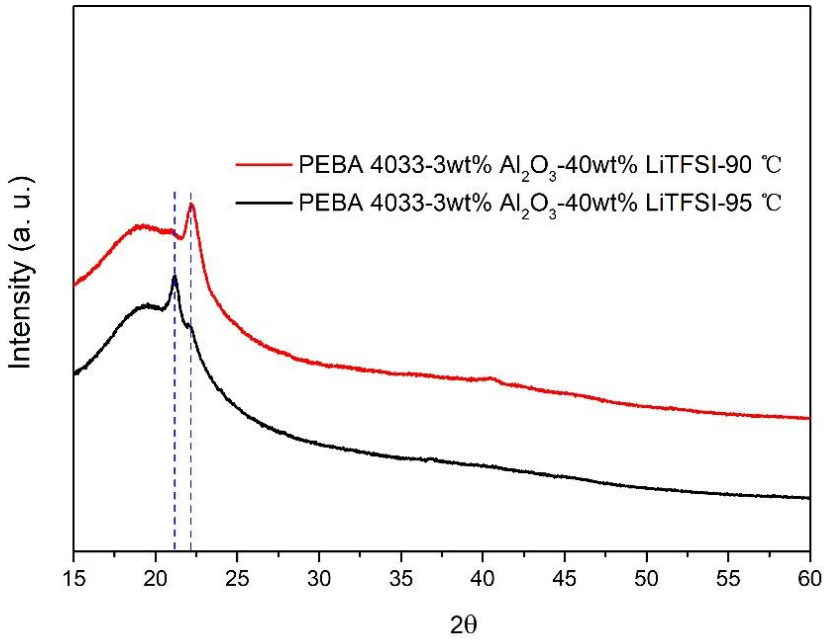

Figure 4.3 XRD patterns of PEBA 4033-3wt% Al_2O_3-40wt% LiTFSI CPE at different solvent evaporation temperatures.

In order to improve the mechanical strength of the SPEs, composite polymer electrolytes (CPEs) with aluminum oxide (Al_2O_3) nanoparticles (~50 nm) were also prepared and characterized. Figure 4.2 displays the XRD patterns of CPEs with 1wt%, 2wt%, and 3wt% Al_2O_3 addition, separately. It can be found that all of them had a significant diffraction peak of α phase and a weaken diffraction peak of γ phase, which should be caused by the high temperature (95 °C) during the solvent evaporation process. The high solvent evaporation temperature can accelerate the rearrangement of PA12 segments and further result in the conversion of crystal phases. To confirm this analysis, PEBA 4033-3wt% Al_2O_3-40wt% LiTFSI CPE was adopted to analyze the effects of solvent evaporation temperature on crystal phases. As shown in Figure 4.3, the diffraction peak of α phase is strong and the diffraction peak of γ phase is weakened with the solvent evaporation temperature at 90 °C. However, opposite phenomenon

happened when the solvent evaporation temperature was increased to 95 °C. It demonstarte that the solvent evaporation temperature has significant effect on the crystal phase of PA12.

4.3.2 Morphologies and thermal stability characterizations

Figure 4.4 shows the surface and cross-section morphologies of PEBA 4033-3wt% Al_2O_3-40wt% LiTFSI. It can be found that the surface of CPE is very smooth (Figure 4.4 (A)), however, the cross-section looks rough with many bumps (Figure 4.4 (B)). Considering the uneven distribution of bumps and the low content of Al_2O_3 nanoparticles, the rough morphology should be not caused by the agglomeration of Al_2O_3 nanoparticles but by the special mechanical strength and the cutting with scissors. In order to prove this analysis, the cross-section morphology of CPE broken by cooling in liquid nitrogen is shown in Figure 4.5, and rough but uniform morphology can be seen.

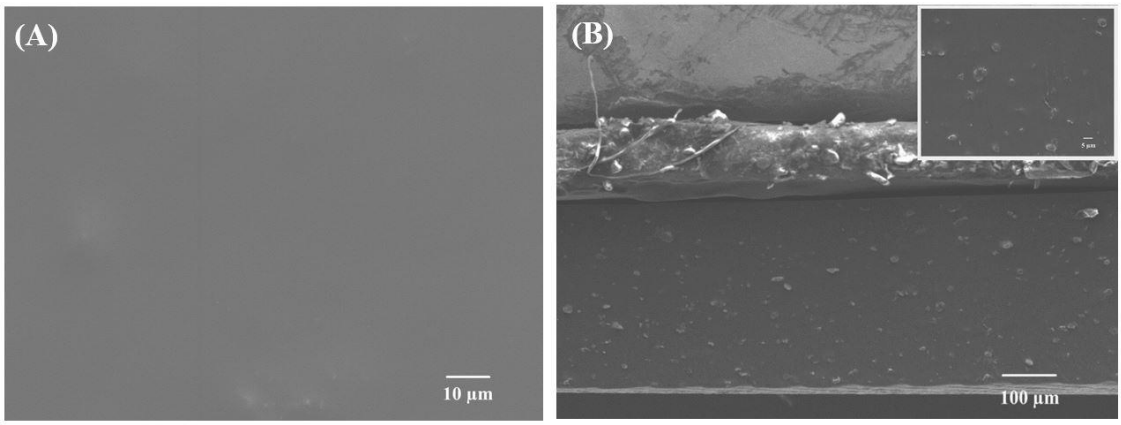

Figure 4.4 (A) Surface SEM images and (B) cross-section image of PEBA 4033-3wt% Al_2O_3-40wt% LiTFSI electrolyte.

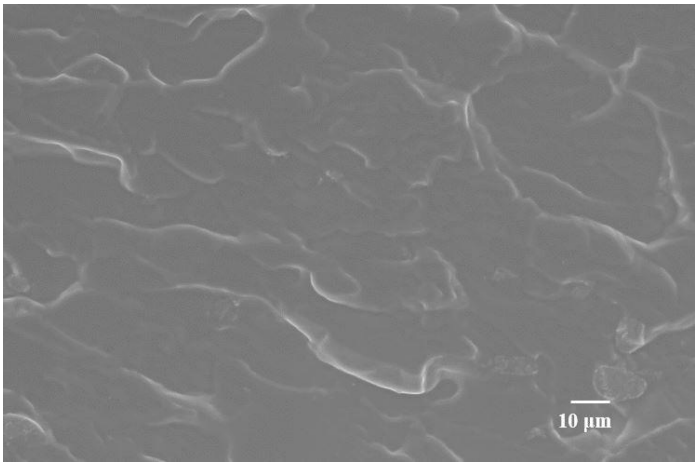

Figure 4.5 Cross-section image of PEBA 4033-3wt% Al_2O_3-40wt% LiTFSI electrolyte.

Figure 4.6 shows the thermal stability change with the increase of LiTFSI content. It can be seen that LiTFSI salt and pure PEBA 4033 start to decompose when the temperature are increased to ~370 °C and ~400 °C respectively, but they are almost decomposed completely as the temperature is increased to 475 and 500 °C. In contrast, the SPEs with various LiTFSI contents start to decompose at the temperature of ~250 °C, and negligible loss of mass is observed before 250 °C, revealing that the addition of LiTFSI has a significant effect on the thermal stability of PEBA 4033 and no solvent residue exists inside the SPE. In addition, the mass loss rate difference of SPEs at the temperature over 250 °C reveals that the LiTFSI content also has great influence on the decomposition kinetics of SPEs. Furthermore, thermal behaviors of CPEs with various Al_2O_3 contents were also investigated based on the PEBA 4033-40wt% LiTFSI SPE. As shown in Figure 4.7, the mass loss ratio of CPEs before 250 °C is much higher than that of PEBA 4033-40wt% LiTFSI SPE. It seems to be due to the adsorption of solvent by Al_2O_3 nanoparticles. However, no obvious differences of mass loss ratio exist between SPEs. Therefore, in our opinion, the enhanced dispersion of polymer segments caused by Al_2O_3 nanoparticles should be the real cause of higher mass loss ratio of CPEs. In addition, effects of solvent evaporation temperature on thermal behaviors of

CPEs were also investigated based on PEBA 4033-3wt% Al_2O_3-40wt% LiTFSI electrolyte. As shown in Figure 4.8, the CPE with a solvent evaporation temperature of 95 °C shows a lower mass loss ratio than the CPEs with the solvent evaporation temperatures of 80 and 90 °C. However, the CPE with a solvent evaporation temperature of 85 °C displays a similar mass loss ratio with the CPE prepared at 95 °C, which can be attributed to the electrolyte solution with a heating history, making the SPE annealing happened even at 85 °C. After annealing, α phase of PA12 is generated and accumulated, which should directly change the complete decomposition temperature from ~450 °C to ~465 °C.

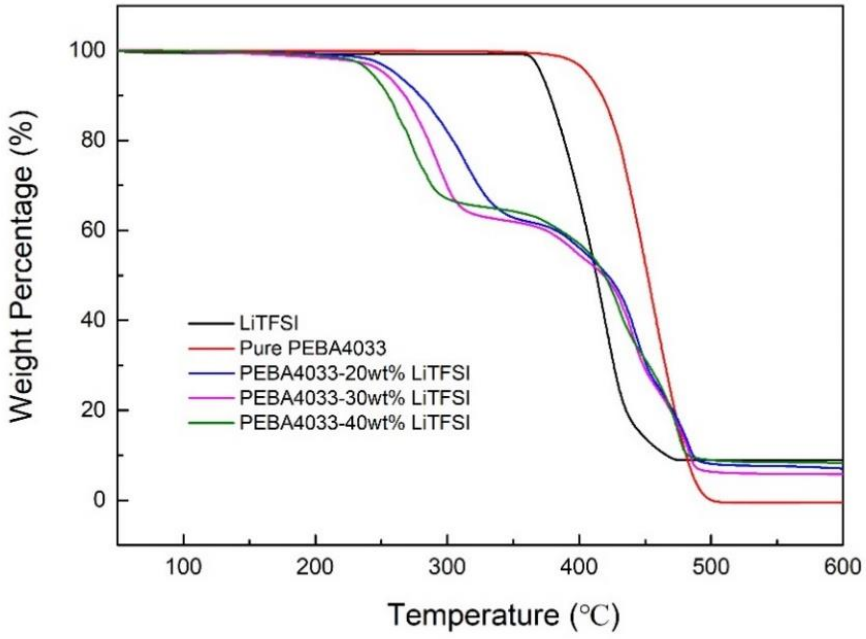

Figure 4.6 TGA curves of PEBA 4033, LiTFSI, and SPE samples (solvent evaporation temperature: 90 °C).

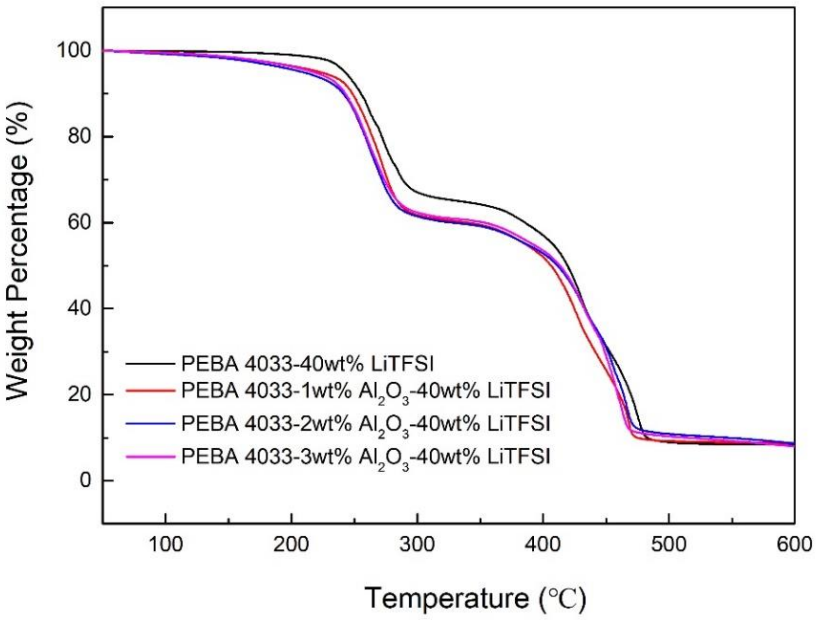

Figure 4.7 TGA curves of PEBA 4033-3wt% Al_2O_3-40wt% LiTFSI and CPE samples (solvent evaporation temperature: 95 °C).

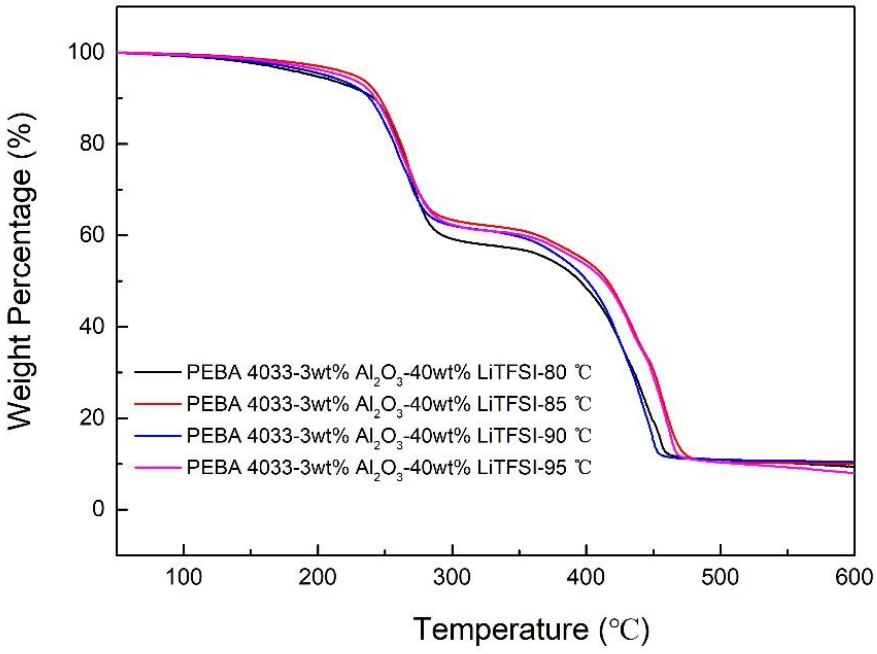

Figure 4.8 TGA curves of CPEs prepared at various solvent evaporation temperatures.

4.3.3 Electrochemical stability window and ionic conductivity

For an ideal ASSLMB with higher power density and energy density, high electrochemical stability which determines adapted electrode materials is critical. Figure 4.9 shows LSV curves of the SPEs with 20, 30 and 40wt% LiTFSI contents respectively. One can see that all the SPEs can keep stable until ~4.5 V, suggesting the excellent electrochemical stability. Thus, most anode materials are optional, such as $LiFePO_4$, $LiCoO_2$, and $LiNi_xMn_yCo_zO_2$. Herein, the decomposition voltage of a SPE can be determined at a current of above 5 μA. In addition, with the increase of LiTFSI content, the electrochemical stability decreases slightly, which should be resulted from the variety of mechanical strength since it can change the interface contact resistance. The electrochemical stability of CPEs were also tested and shown in Figure 4.10. It can be found that the addition of Al_2O_3 nannoparticles has no effect on the electrochemical stability of these CPEs.

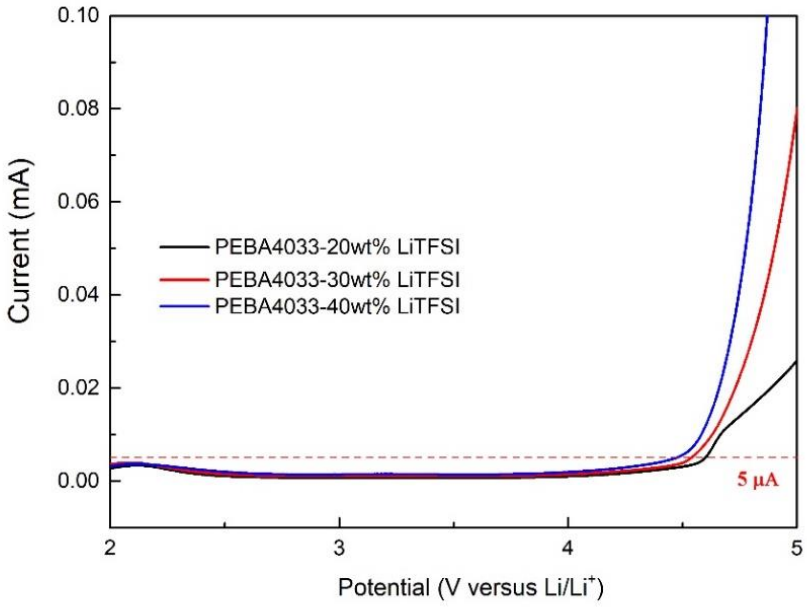

Figure 4.9 LSV curves of the prepared SPEs with various LiTFSI contents (solvent

evaporation temperature: 90 °C).

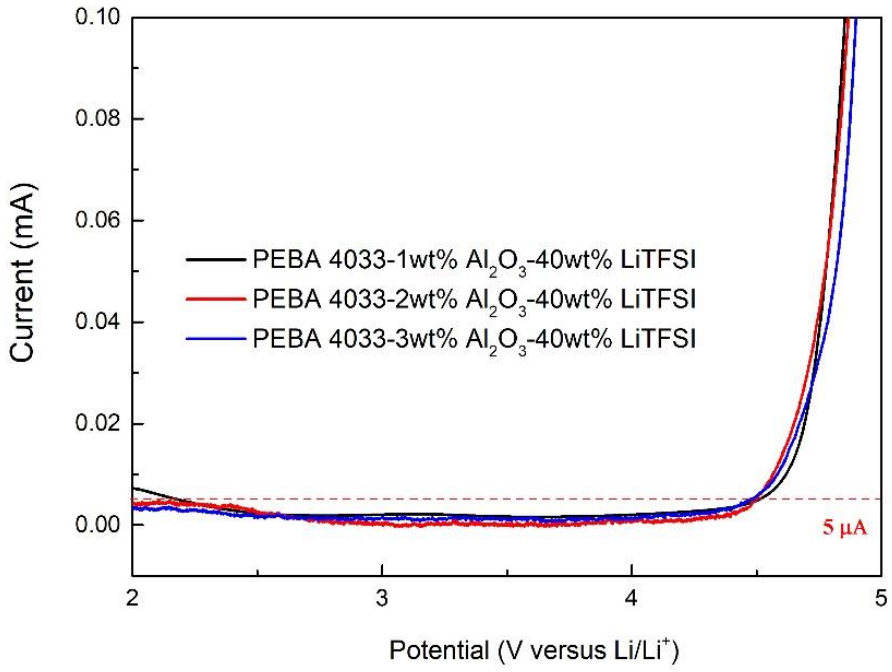

Figure 4.10 LSV curves of the prepared CPEs with various Al_2O_3 nanoparticle contents (solvent evaporation temperature: 95 °C).

Figure 4.11 displays ion conductivities of the PEBA 4033 based SPEs with various LiTFSI contents at different temperatures ranged from 25 to 60 °C. The SPE with 40wt% LiTFSI addition shows an ionic conductivity of 3.49×10^{-5} at 25℃, which is higher than that of the PEBA 2533 based SPE with 20wt% LiTFSI addition (e.g., 3.0×10^{-5} S cm^{-1} at 25 ℃) [26]. It should be noted that higher ionic conductivity can be realized without sacrificing mechanical strength of SPEs by adopting different PEBA polymer matrixs. It means that the SPEs with higher ionic conductivity can be fabricated by adopting the higher mechanical strength of polymer matrix and much more LiTFSI additions. In addition, the Ea of PEBA 4033-40wt% LiTFSI SPE is ca. 0.64 eV. In order to adjust the mehcanical properties of SPEs, Al_2O_3 nanoparticles were

adopted as the filler, and the ion conductivities of CPEs with 1 wt%, 2 wt%, and 3 wt% Al_2O_3 additions were tested. As shown in Figure 4.12, ionic conductivities of CPEs all decrease after the addition of Al_2O_3 nanoparticles comparing with that of PEBA 4033-40wt% LiTFSI SPE. More precisely, the ionic conductivity of CPEs increases with the increase of Al_2O_3 content from 1 wt% to 2 wt%, and decreases when the Al_2O_3 content is further increased to 3 wt%. However, although the ionic conductivity varies with the increase of Al_2O_3 content, the change in ionic conductivity is slight. It means that the variation of ionic conductivity is possibly caused by the mechanical strength difference of CPEs.

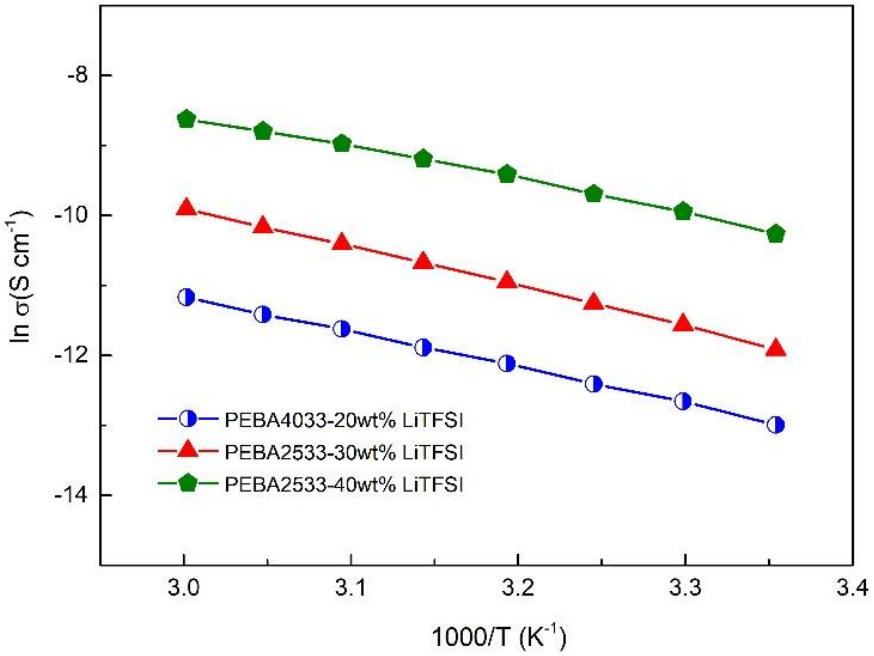

Figure 4.11 Ionic conductivities of SPEs vs. temperature (solvent evaporation temperature: 90 °C).

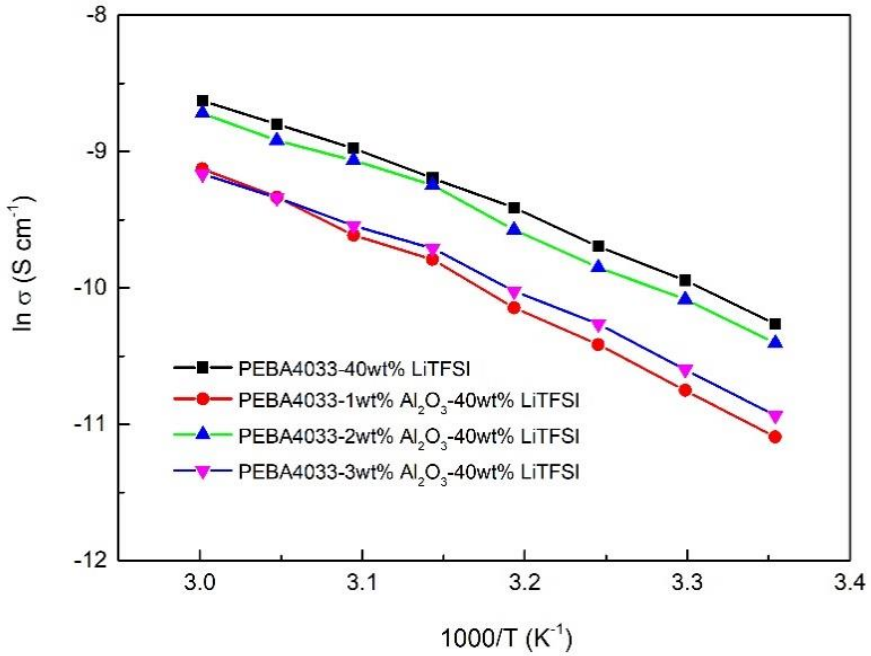

Figure 4.12 Ionic conductivities of CPEs vs. temperature (solvent evaporation temperature: 95 °C).

4.3.4 Cycle stability of ASSLMBs

Long-term cycling stability is critical for the industrial application of ASSLMBs. Figure 4.13 shows the cycling performance of ASSLMB assembled with PEBA 4033-40wt% LiTFSI SPE and $LiFePO_4$ cathode (areal capacity: 1.5 mAh cm^{-2}). As we can see, the capacity increases at first due to the enhancing contact between SPE and cathode, and then decreases due to the uncontrolled growth of Li dendrite with the increase of cycle number. Meanwhile, the increased voltage platform during charging process after 50th cycles shown in Figure 4.14 also proves the degradation of interface contact in anode side, which is consistent with the decreased CE. Here, mechanical strength of SPEs is thought as an important factor for the uniform deposition of Li, therefore, in order to improve the cycling performance of ASSLMBs, Al_2O_3 nanoparticle was adopted as the filler to adjust the mechanical strength of SPEs. Figures

4.15 and 4.16 display the cycling performance and voltage profile of ASSLMB assembled with PEBA 4033-3wt% Al_2O_3-40wt% LiTFSI CPE separately. It is demonstrated that the cycling performance is enhanced after the addition of Al_2O_3 nanoparticles. In addition, the Li symmetrical cell was also assembled to explore the anode interface contact bahavior during the plating and stripping process. It is found that the Li symmetrical cell can work stably over 200 h at 0.1 mA cm^{-2} and 60 ℃ as shown in Figure 4.17. In general, stable cycling of ASSLMB is realized by using PEBA 4033-3wt% Al_2O_3-40wt% LiTFSI CPE, which proves the excellent Li dendrite suppression ability of PEBA 4033 based CPE even using high-loading cathode.

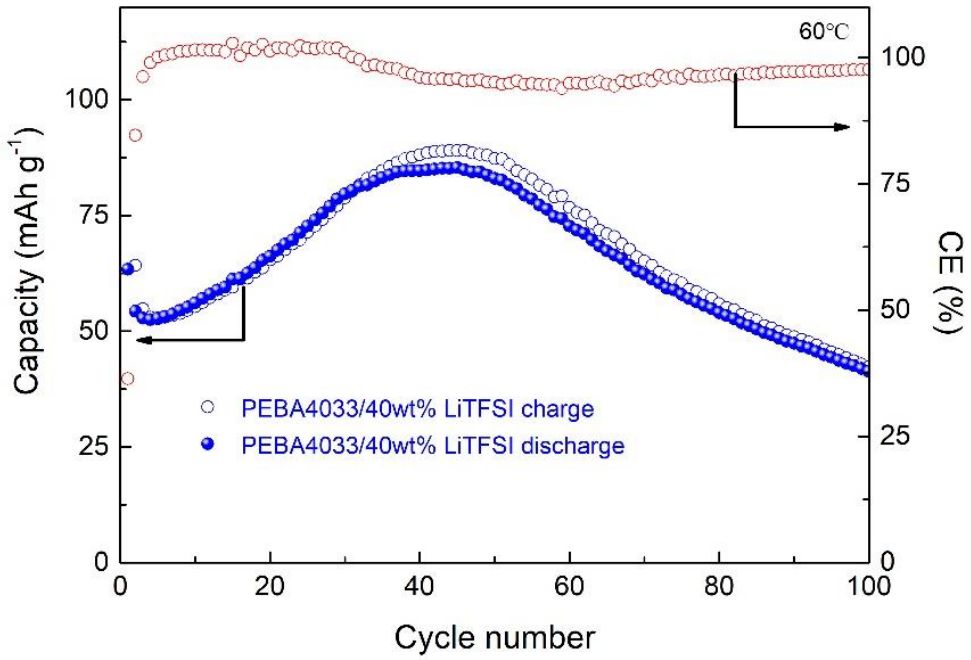

Figure 4.13 Cycling performance of the Li/PEBA 4033-40wt% LiTFSI/$LiFePO_4$ cell at 0.1 mA cm^{-2} and 60 ℃ (areal capacity: 1.5 mAh cm^{-2}; solvent evaporation temperature: 70 ℃).

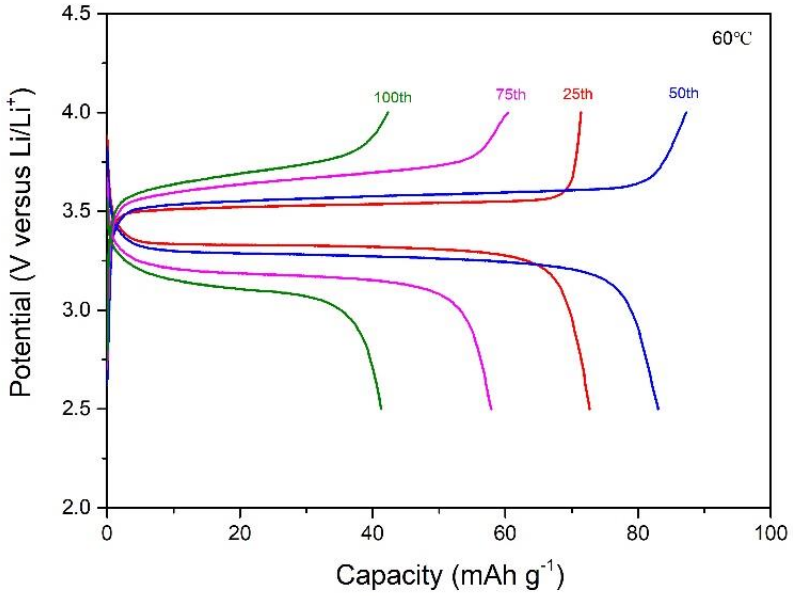

Figure 4.14 Voltage profile of the Li/PEBA 4033-40wt% LiTFSI/$LiFePO_4$ full cell at the current density of 0.1 mA cm^{-2} and 60 ℃ (areal capacity: 1.5 mAh cm^{-2}; solvent evaporation temperature: 70 ℃).

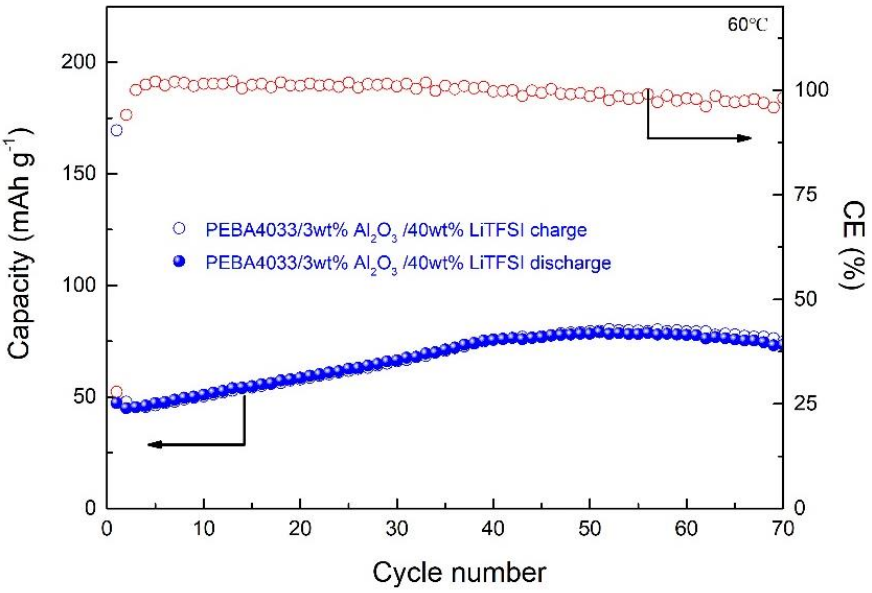

Figure 4.15 Cycling performance of the Li/PEBA 4033-3wt% Al_2O_3-40wt% LiTFSI/$LiFePO_4$ cell at 0.1 mA cm^{-2} and 60 ℃ (areal capacity: 1.5 mAh cm^{-2}; solvent evaporation temperature: 70 ℃).

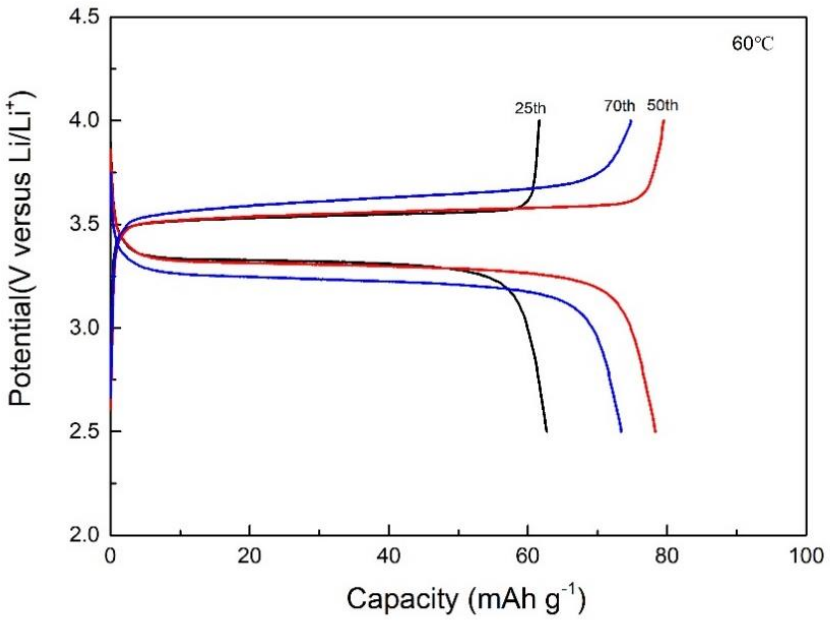

Figure 4.16 Voltage profile of the Li/PEBA 4033-3wt% Al_2O_3-40wt% LiTFSI/$LiFePO_4$ full cell at the current density of 0.1 mA cm^{-2} and 60 ℃ (areal capacity: 1.5 mAh cm^{-2}; solvent evaporation temperature: 70 ℃).

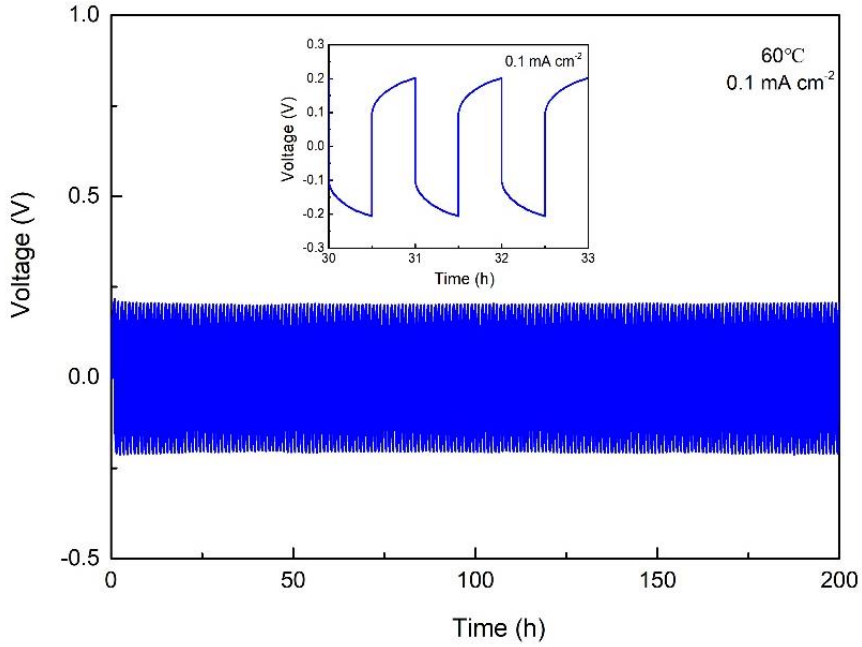

Figure 4.17 Galvanostatic cycling curve of the Li/PEBA 4033-3wt% Al_2O_3-40% LiTFSI /Li symmetrical cell at 0.1 mA cm^{-2} and 60 ℃ (solvent evaporation temperature: 70 ℃).

Although the cycling performances of ASSLMBs can be improved significantly with the addition of Al_2O_3 nanoparticles into PEBA 4033 based SPEs, but there are several obstacles still to hinder the application of ASSLMBs, such as rapid attenuation of capacity and low CE. Considering the close relationship between mechanical strength of SPEs and the heating history during the preparation process. Effects of solvent evaporation temperature during the CPEs preparation process on the battery cycling performance were also investigated for further enhancing the performance of ASSLMBs. Figures 4.18, 4.19 and 4.20 show the cycling performance of ASSLMBs assembled with PEBA 4033-3wt% Al_2O_3-40% LiTFSI CPEs, which were prepared at the solvent evaporation temperature of 80 ℃, 85 ℃ and 90 ℃, respectively. As shown in Figure 4.18, the CE is lower than 100%, which can be attributed to the chemical reaction in anode caused by the uncontrolled Li dendrite growth. After that, fast reduction of specific capacity happens. However, the specific capacity reduction of the ASSLMBs assembled with CPEs fabricated at the solvent evaporation temperature of 85 and 90 ℃ are mitigated obviously. Moreover, the CE also increases with the increase of solvent evaporation temperature. It means that the chemical reactions are easier to occur at anode side and result in the reduction of specific capacity and CE when the CPE prepared at low solvent evaporation temperature was adopted. The mechanism is still unclear, and in our opinion, the mechanical strength determined by the heating history makes great effects on the Li dendrite suppression ability of CPEs and battery performance.

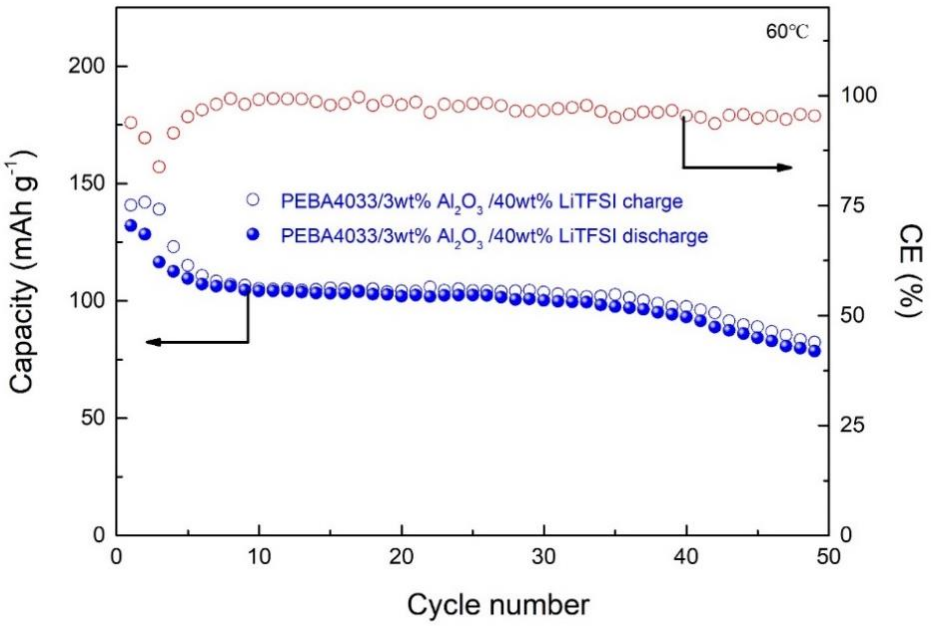

Figure 4.18 Cycling performance of the Li/PEBA 4033-3wt% Al_2O_3-40wt% LiTFSI/$LiFePO_4$ cell at 0.1 mA cm^{-2} and 60 ℃ (areal capacity: 1.5 mAh cm^{-2}; solvent evaporation temperature: 80 ℃).

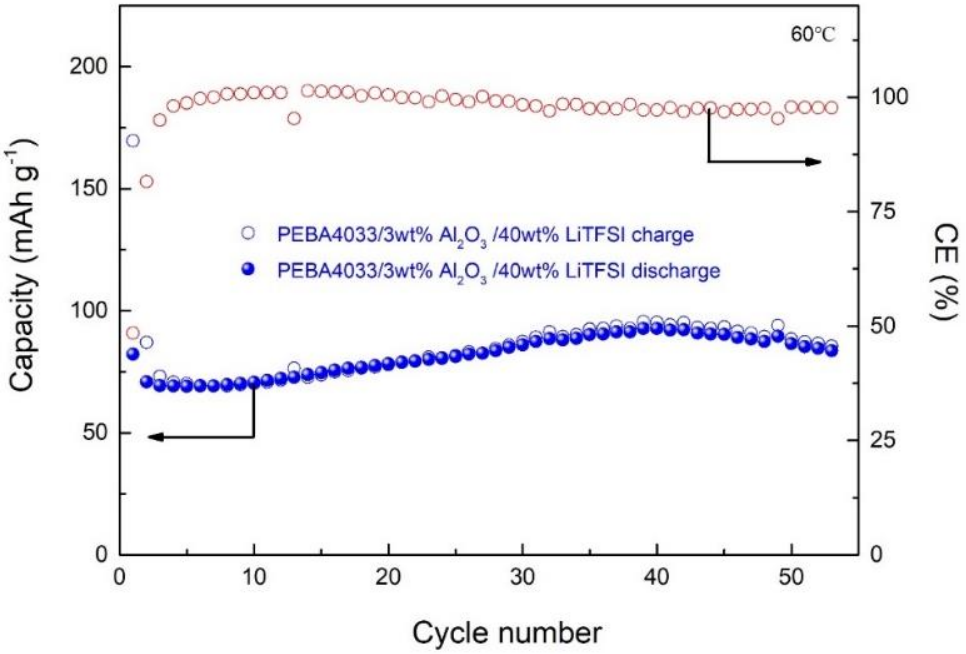

Figure 4.19 Cycling performance of the Li/PEBA 4033-3wt% Al_2O_3-40wt% LiTFSI/$LiFePO_4$ cell at 0.1 mA cm^{-2} and 60 ℃ (areal capacity: 1.5 mAh cm^{-2}; solvent evaporation temperature: 85 ℃).

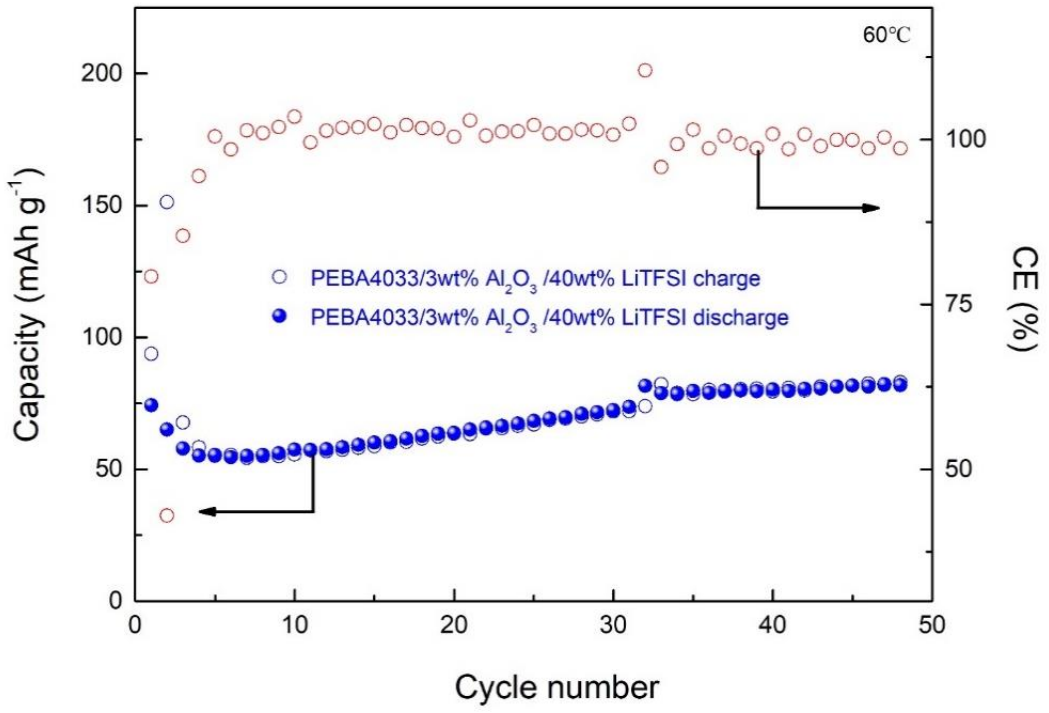

Figure 4.20 Cycling performance of the Li/PEBA 4033-3wt% Al_2O_3-40wt% LiTFSI/$LiFePO_4$ cell at 0.1 mA cm^{-2} and 60 ℃ (areal capacity: 1.5 mAh cm^{-2}; solvent evaporation temperature: 90 ℃).

4.4 Conclusions

In this study, the PEBA 4033-based SPE with LiTFSI as the Li salt was fabricated via a casting method. By XRD characterizations, it is proved that the crystal phase of PA12 can transfer from α phase to γ phase with the increase of LiTFSI content, and transfer back to α phase with the increase of temperature. In addition, the obtained SPE with 40wt% LiTFSI dopped possesses an ionic conductivity of 3.49×10^{-5} S cm^{-1} at 25 ℃. The performances of ASSLMBs assembled with PEBA 4033-40wt% LiTFSI SPE and PEBA 4033-3wt% Al_2O_3-40wt% LiTFSI CPE ($LiFePO_4$ cathode: 1.5 mAh cm^{-2}) were compared and enhanced battery performance was realized by using CPE. Moreover, effects of solvent evaporation temperature on battery performance were also investigated by using PEBA 4033-3wt% Al_2O_3-40wt% LiTFSI CPEs, and it is found that the CE of ASSLMB increases with the increase of solvent evaporation temperature

during the CPE preparation process at the range of 80-90 ℃. In addition, excellent Li plating and stripping performance of PEBA 4033-3wt% Al_2O_3-40wt% LiTFSI electrolyte was also proved based on the Li symmetrical battery. In general, the ASSLMBs assembled with PEBA 4033 based SPEs display excellent cycling performance even with high-loading cathode.

References

[1] Y. Chen, K. Wen, T. Chen, X. Zhang, M. Armand, S. Chen, Recent progress in all-solid-state lithium batteries: The emerging strategies for advanced electrolytes and their interfaces, Energy Storage Mater. 31 (2020) 401-433.

[2] X. Judez, G. G. Eshetu, C. Li, L. M. Rodriguez-Martinez, H. Zhang, M. Armand, Opportunities for rechargeable solid-state batteries based on Li-intercalation cathodes, Joule 2 (2018) 2208-2224.

[3] C. Fang, J. Li, M. Zhang, Y. Zhang, F. Yang, J. Z. Lee, M.-H. Lee, J. Alvarado, M. A. Schroeder, Y. Yang, B. Lu, N. Williams, M. Ceja, L. Yang, M. Cai, J. Gu, K. Xu, X. Wang, Y. S. Meng, Quantifying inactive lithium in lithium metal batteries, Nature 572 (2019) 511-515.

[4] C. Jin, O. Sheng, M. Chen, Z. Ju, G. Lu, T. Liu, J. Nai, Y. Liu, Y. Wang, X. Tao, Armed lithium metal anodes with functional skeletons, Mater. Today Nano 13 (2021) 100103.

[5] X. Tao, J. Wang, Z. Ying, Q. Cai, G. Zheng, Y. Gan, H. Huang, Y. Xia, C. Liang, W. Zhang, Yi Cui, Strong sulfur binding with conducting magnéli-phase Ti_nO_{2n-1} nanomaterials for improving lithium-sulfur batteries, Nano Lett. 14 (2014) 5288-5294.

[6] X. Tao, J. Wang, C. Liu, H. Wang, H. Yao, G. Zheng, Z. W. Seh, Q. Cai, W. Li, G. Zhou, C. Zu, Y. Cui, Balancing surface adsorption and diffusion of lithium-polysulfides on nonconductive oxides for lithium-sulfur battery design, Nat. Commun. 7 (2016) 1-9.

[7] J. B. Park, C. Choi, S. Yu, K. Y. Chung, D. W. Kim, Interfacial framework via self-discharge mechanism for stable lithium metal anode with superior rate, Adv. Energy Mater. 11 (2021) 2101544.

[8] J. Liu, Z. Bao, Y. Cui, E. J. Dufek, J. B. Goodenough, P. Khalifah, Q. Li, B. Y. Liaw,

P. Liu, A. Manthiram, Y. S. Meng, V. R. Subramanian, M. F. Toney, V. V. Viswanathan, M. S. Whittingham, J. Xiao, W. Xu, J. Yang, X.-Q. Yang, J.-G. Zhang, Pathways for practical high-energy long-cycling lithium metal batteries, Nat. Energy 4 (2019) 180-186.

[9] P. Albertus, S. Babinec, S. Litzelman, A. Newman, Status and challenges in enabling the lithium metal electrode for high-energy and low-cost rechargeable batteries, Nat. Energy 3 (2018) 16-21.

[10] C. P. Grey, J. M. Tarascon, Sustainability and in situ monitoring in battery development, Nat. Mater. 16 (2016) 45-56.

[11] J. Luo, C. Wang, H. Wang, X. Hu, E. Matios, X. Lu, W. Zhang, X. Tao, W. Li, Pillared mxene with ultralarge interlayer spacing as a stable matrix for high performance sodium metal anodes, Adv. Funct. Mater. 29 (2018) 1805946.

[12] M. Armand, J. M. Chabagno, M. J. Duclot, Polymeric solid electrolytes in proceeding of the 2nd international meeting on solid state electrolytes, St. Andrews, UK, 1 (6) September 1978.

[13] K.-H. Chen, K. N. Wood, E. Kazyak, W. S. LePage, A. L. Davis, A. J. Sanchez, N. P. Dasgupta, Dead lithium: mass transport effects on voltage, capacity, and failure of lithium metal anodes, J. Mater. Chem. A 5 (2017) 11671-11681.

[14] W. S. LePage, Y. Chen, E. Kazyak, K.-H. Chen, A. J. Sanchez, A. Poli, E. M. Arruda, M. D. Thouless, N. P. Dasgupta, Lithium mechanics: roles of strain rate and temperature and implications for lithium metal batteries, J. Electrochem. Soc. 166 (2019) A89-A97.

[15] Y. Lu, C.-Z. Zhao, H. Yuan, X.-B. Cheng, J.-Q. Huang, Q. Zhang, Critical current density in solid-state lithium metal batteries: mechanism, influences, and strategies, Adv. Funct. Mater. 31 (2021) 1-33.

[16] J. Kasemchainan, S. Zekoll, D. S. Jolly, Z. Ning, G. O. Hartley, J. Marrow, P. G. Bruce, Critical stripping current leads to dendrite formation on plating in lithium anode solid electrolyte cells, Nat. Mater. 18 (2019) 1105-1111.

[17] S. Wenzel, T. Leichtweiss, D. Krüger, J. Sann, J. Janek, Interphase formation on lithium solid electrolytes-An in situ approach to study interfacial reactions by photoelectron spectroscopy, Solid State Ionics 278 (2015) 98-105.

[18]A. Manthiram, X. Yu, S. Wang, Lithium battery chemistries enabled by solid-state electrolytes, Nat. Rev. Mater. 2 (2017), 16103.

[19] L. Miara, A. Windmuller, C. L. Tsai, W. D. Richards, Q. L. Ma, S. Uhlenbruck, O. Guillon, G. Ceder, About the compatibility between high voltage spinel cathode materials and solid oxide electrolytes as a function of temperature, ACS Appl. Mater. Interfaces 8 (2016) 26842-26850.

[20] M. Ihrig, R. Ye, A.M. Laptev, D. Grüner, R. Guerdelli, W. S. Scheld, M. Finsterbusch, H.-D. Wiemh¨ofer, D. Fattakhova-Rohlfing, O. Guillon, Polymer-ceramic composite cathode with enhanced storage capacity manufactured by field-assisted sintering and infiltration, ACS Appl. Energy Mater. 4 (2021) 10428-10432.

[21] J. G. Kim, B. Son, S. Mukherjee, N. Schuppert, A. Bates, O. Kwon, M. J. Choi, H. Y. Chung, S. Park, A review of lithium and non-lithium based solid state batteries, J. Power Sources 282 (2015) 299-322.

[22] Z. Huang, W. Pang, P. Liang, Z. Jin, N. Grundish, Y. Li, C.-A. Wang, A dopamine modified $Li_{6.4}La_3Zr_{1.4}Ta_{0.6}O_{12}$/PEO solid-state electrolyte: enhanced thermal and electrochemical properties, J. Mater. Chem. A 7 (2019) 16425-16436.

[23] Z. Li, X. Guo, Integrated interface between composite electrolyte and cathode with low resistance enables ultra-long cycle-lifetime in solid-state lithium-metal batteries, Sci. China Chem. 64 (2021) 673-680.

[24] R. Ye, M. Ihrig, E. Figgemeier, D. Fattakhova-Rohlfing, M. Finsterbusch, Aqueous processing of $LiCoO_2$-$Li_{6.6}La_3Zr_{1.6}Ta_{0.4}O_{12}$ composite cathode for high-capacity solid-state lithium batteries, ACS Sustainable Chem. Eng. (2023).

[25] M. Ihrig, E. Dashjav, A. M. Laptev, R. Ye, D. Grüner, M. Ziegner, P. Odenwald, M. Finsterbusch, F. Tietz, D. Fattakhova-Rohlfing, O. Guillon, Increasing the performance of all-solid-state Li batteries by infiltration of Li-ion conducting polymer into LFP-LATP composite cathode, J. Power Sources 543 (2022) 231822.

[26] C. Liu, Y. He, X. An, N. Kitiphatpiboon, X. Du, X. Hao, A. Abudula, G. Guan, A poly (ether block amide) based solid polymer electrolyte for solid-state lithium metal batteries. J. Colloid Interf. Sci. 630 (2023) 595-603.

[27] E. Tocci, A. Gugliuzza, L. D. Lorenzo, M. Macchione, G. D. Luca, E. Drioli, Transport properties of a co-poly(amide-12-b-ethylene oxide) membrane: a comparative study between experimental and molecular modelling results, J. Membr. Sci. 323 (2008) 316-327.

[28] S. M. Aharoni, n-Nylons: their synthesis, structure, and properties, John Wiley & Sons Incorporated 1997.

[29] S. Rhee, J. L. White, Crystal structure and morphology of biaxially oriented polyamide 12 films, J. Polym. Sci. B Polym. Phys. 40 (2002)1189-1200.

[30] K. Inoue, S. Hoshino, Crystal structure of nylon 12, J. Polym. Sci. Polym. Phys. Ed. 11 (1973) 1077-1089.

CHAPTER 5 Conclusions and Prospects

5.1 Conclusions

ASSLMBs assembled with LMA, SPEs and various cathode materials is one kind of electrochemical energy storage devices that outperform traditional LIBs assembled with liquid electrolytes and graphite anode materials, in terms of higher energy density, higher safety, and more environmental friendly. In this study, PEBA based SPEs were prepared with the casting method, and used to assemble the ASSLMBs. The performances of ASSLMBs assembled with PEBA 2533 based SPEs were tested and DFT calculation was conducted for revealing the mechanism behind the excellent battery performance. Furthermore, Al_2O_3 nanoparticles were adopted to improve the mechanical strength of PEBA 2533 based SPEs and enhanced cycling performance, which was realized with the low-loading cathode (0.15 mAh cm^{-2}). Finally, PEBA 4033 based SPEs were prepared and modified with Al_2O_3 nanoparticles to fabricate the ASSLMBs using the high-loading cathode (1.5 mAh cm^{-2}). The main conclusions are summarized as follows:

(1) The PEBA 2533-20% LiTFSI SPE with an ionic conductivity of 3.0×10^{-5} S cm^{-1} at 25 ℃ was adopted to assemble the ASSLMBs with the $LiFePO_4$ cathode. Electrochemical performance tests of Li/SPE/$LiFePO_4$ cell showed that the battery remained 94% of its maximum capacity (127.5 mAh g^{-1}) at the rate of 0.5 C and 60 ℃ after 200 cycles. Based on the calculations, it is found that the amide group in the PEBA has stronger electron donating ability than the ether group. Moreover, the effect of extra electrons on $TFSI^-$ anions was also investigated, and it is proved that $TFSI^-$ anion can be activated with the existence of extra electrons by comparing the bond lengths of $TFSI^-$ and $TFSI^-+e^-$. As such, a mechanism was proposed, in which $TFSI^-$ can be activated with the attack of electrons from both the amide groups and the Li anode

during the charging process with the generation of LiF enriched SEI layer. In addition, the voltage polarization was observed in a symmetrical Li/SSE/Li cell at the current density of 0.2 mA cm^{-2}. Thus, an SEI damage mechanism accounting for the voltage polarization was also proposed. It is considered that improving interface contact and cycling at limited current density should be two effective solutions for battery performance improving.

(2) The PEBA 2533-based SPE with LiTFSI as the Li salt and Al_2O_3 nanoparticles as the solid plasticizer was prepared via a casting method. It is found that the obtained SPE with 3wt% Al_2O_3 dopped had an ionic conductivity of 3.57×10^{-5} S cm^{-1} at 25 ℃. When it was applied to fabricate ASSLMBs with the $LiFePO_4$ based cathode, the obtained optimal Li/SPE/$LiFePO_4$ cell remained 94.9% of its maximal capacity (133.9 mAh g^{-1}) at 60 ℃ with 0.1 mA cm^{-2} even after 650 cycles and the average CE was also as high as 99.84%. In addition, the fabricated Li/ PEBA 2533-20% LiTFSI-3wt% Al_2O_3/Li symmetrical cell also showed excellent cycling stability (1000 h). In addition, by XPS characterizations, self-aggregation layer (SAL) of PA12 was discovered, which should contribute to promoting the robustness of LiF enriched SEI layer so that PEBA 2533-based SPEs exhibit excellent Li dendrite suppression ability. Thus, the PEBA based SPEs have potential for the application of it in ASSLMBs.

(3) The PEBA 4033-based SPE with LiTFSI as the Li salt was fabricated via a casting method. By XRD characterizations, it is proved that the crystal phase of PA12 can transfer from α phase to γ phase with the increase of LiTFSI content, and transfer back to α phase with the increase of temperature. In addition, the obtained SPE with 40wt% LiTFSI dopped possessed an ionic conductivity of 3.49×10^{-5} S cm^{-1} at 25 ℃. The performances of ASSLMBs assembled with PEBA 4033-40wt% LiTFSI SPE and PEBA 4033-3wt% Al_2O_3-40wt% LiTFSI CPE ($LiFePO_4$ cathode: 1.5 mAh cm^{-2}) were

compared and it is found that the enhanced battery performance was realized by using CPE. Moreover, effects of solvent evaporation temperature on battery performance were also investigated by using PEBA 4033-3wt% Al_2O_3-40wt% LiTFSI CPEs, and it is known that the CE of ASSLMB increases with the increase of solvent evaporation temperature during the CPE preparation process at the range of 80 to 90 ℃. In addition, excellent Li plating and stripping performance of PEBA 4033-3wt% Al_2O_3-40wt% LiTFSI electrolyte was also proved based on the Li symmetrical battery. In general, the ASSLMBs assembled with PEBA 4033 based SPEs display excellent cycling performance even with high-loading cathode.

5.2 Prospects

Although significant efforts have been performed for the development of SPEs for the acceleration of industrial application of ASSLMBs, almost all the SPEs cannot meet the requirements of industrial application due to the limited ionic conductivity, uncontrolled Li dendrite growth, and robust suface contact. Thus, innonative solutions for solving these issues are still needed urgently. The following points should be considered for further development of SPEs to promote the scale up of ASSLMBs.

1. Enhanced surface contact

To date, Sufficient surface contact in the cathode side is still a problem when the SPE is used. Therefore, creative cathode structure design is needed to guarantee both the ionic conductivity and electron conductivity reliable.

2. Ion conductivity of SPEs

Considering the ion transfer mechanism of SPEs, high temperature is always necessary for the charging and diacharging of ASSLMBs. Thus, higher ionic conductivity at room temperature is expected. Addition of ceramic ion conductor which possesses higher ion conductivity at room temperature is one of the most promising

solutions.

3. Li dendrite suppression

The uncontrolled growth of Li dendrites as the main obstacle of ASSLMBs application is still unsolved. Construction of robust SEI layer is a promising solution for the Li dendrite suppression. Thus, the investigation of the formation mechanism of SEI is of great importance.

CURRICULUM VITAE

Personal details

Name: Changlin Liu

Nationality: China

Date of birth: 2 Janunary 1992

Email: chang_lin_liu@sina.com

Educations

September, 2020- July, 2023	D.Eng. (Safety Science and Technology), Hirosaki University, Japan
September, 2015- July, 2018	M.Sc. (Department of Chemical Engineering), Taiyuan University of Technology, China
September, 2011- July, 2015	B.Sc. (Department of Chemical Engineering), Changchun University of Technology, China

Experiences

July, 2018- August, 2019	Sungrow Renewables Development Co., Ltd.
September, 2019- June, 2020	Great Wall Motor Co., Ltd.

Scholarship and Awards

1. Excellent Student Award, Hirosaki University, March 2023.
2. China Scholarship Council (CSC) (October 2020-september 2023).

List of Publications and Presentations

Publications

1. **Changlin Liu,** Yang He, Xiaowei An, Zhijun Wu, Xiaogang Hao, Qiang Zhao, Abuliti Abudula, Guoqing Guan, Effect of nano Al_2O_3 addition on cycling performance of poly(ether block amide) based solid-state lithium metal batteries, Resources Chemicals and Materials, 2 (2023) 167-176.

2. **Changlin Liu**, Yang He, Xiaowei An, Nutthaphak Kitiphatpiboon, Xiao Du, Xiaogang Hao, Abuliti Abudula, Guoqing Guan, A poly(ether block amide) based solid polymer electrolyte for solid-state lithium metal batteries, Journal of Colloid & Interface Science, 630 (2023) 595-603.

3. Yang He, **Changlin Liu**, Zhengkun Xie, Pairuzha Xiaokaiti, Gang Chen, Zhongbao Feng, Yutaka Kasai, Abuliti Abudula, Guoqing Guan, Construction of cobalt sulfide/molybdenum disulfide heterostructure as the anode material for sodium ion batteries, Advanced Composites and Hybrid Materials, 6 (2023) 85.

4. Yang He, **Changlin Liu**, Shang Peng, Juan Zhang, Gang Chen, Zhongbao Feng, Qiang Zhao, Abuliti Abudula, Guoqing Guan, Micro-flower-like MoS_2-modified Co_9S_8 heterostructure as anode material for sodium-ion batteries with superior reversibility and rate capacity, Journal of Materials Science & Technology, 145 (2023) 210-220.

5. Yang He, **Changlin Liu**, Zhengkun Xie, Jiwei Wang, Gang Chen, Qiang Zhao, Abuliti Abudula, Guoqing Guan, Prussian blue analog derived cobalt sulfide nanoparticles embedded in N/S Co-doped carbon frameworks as a high-performance anode material for sodium-ion batteries, ACS Applied Energy Materials, 5 (2022) 8697-8708.

6. Jinggang Zhao, Peifen Wang, Jing Wang, **Changlin Liu**, Junli Wang, Lei Shi, Guangwen Xu, Abuliti Abudula, Guoqing Guan, Biostarch-assisted synthesis of microscopic heterogeneous manganese-cobalt oxides for efficient catalytic combustion of toluene, Chemical Engineering Journal, in press.
7. Jinggang Zhao, Peifen Wang, **Changlin Liu**, Qiang Zhao, Junli Wang, Lei Shi, Guangwen Xu, Abuliti Abudula, Guoqing Guan, Nanosheet-state cobalt-manganese oxide with multifarious active regions derived from oxidation-etching of metal organic framework precursor for catalytic combustion of toluene, Journal of Colloid & Interface Science, 629 (A) (2023) 706-722.
8. Nutthaphak Kitiphatpiboon, Meng Chen, Xiumin Li, **Changlin Liu**, Shasha Li, Junli Wang, Shang Peng, Abuliti Abudula, Guoqing Guan, Heterointerface engineering of Ni_3S_2@NiCo-LDH core-shell structure for efficient oxygen evolution reaction under intermittent conditions, Electrochimica Acta, 435 (2022) 141438.
9. Xiyan Yue, Jiajia Wang, Zhengkun Xie, Yang He, Zhao Liu, **Changlin Liu**, Xiaogang Hao, Abuliti Abudula, Guoqing Guan, Controllable synthesis of novel orderly layered $VMoS_2$ anode materials with super electrochemical performance for sodium ion batteries, ACS Applied Materials & Interfaces, 13 (2021) 26049-26054.

International presentations

1. **Changlin Liu**, He Yang, Abudula Abuliti, Guan Guoqing, “Electrochemical Characteristics of All Solid-state Lithium Metal Batteries Based on Poly(ether block amide) 4033 Electrolyte,” International Chemical Engineering Symposia 2023, Tokyo University of Agriculture and Technology (TUAT), March 15-17.

2. **Changlin Liu**, Xiaowei An, Natthaphak Kitiphatpiboon, Yang He, Abuliti Abudula, Guoqing Guan, “Electrochemical Characteristics of Solid-state Lithium Metal Batteries Based on PEBAX Electrolyte,” 19th Asia Pacific Confederation of Chemical Engineering (APCChE 2022) Congress, August 9-12, Kuala Lumpur Convention Centre, Kuala Lumpur, Malaysia. (On line)

3. Yang He, **Changlin Liu**, Shang Peng, Juan Zhang, Katsuki Kusakabe, Abuliti Abudula, and Guoqing Guan, “MoS_2-modified Co_9S_8 Heterostructure as Anode Material for Sodium-ion Batteries,” International Symposium on Chemical Engineering (ISChE) 2022, Fukuoka, Japan, December 2-4, 2022.

Domestic presentations

1. **Changlin Liu**, Natthaphak Kitiphatpiboon, Abuliti Abudula, and Guoqing Guan, “Electrochemical Characteristics of Solid-state Lithium Metal Batteries Based on PEBAX Electrolyte,” 令和 4 年度化学系学協会東北大会、2022 年 9 月 17 日(土)～18 日（日)、岩手大学、盛岡。

2. 何 楊、 **劉 長林**、 張 娟、阿布 里提、官 国清, “CoS/MoS_2 Heterostructure as Anode Material for Sodium-ion Batteries with Superior Reversibility and Rate Capacity,” 化学工学会第 88 年会、東京農工大学、2023 年 3 月 15-17 日。

List of Patents

1. **劉長林**、官国清、関　和治、阿布里提、“全固体リチウムイオン電池用固体電解質及びその製造方法並びに全固体リチウムイオン電池、”出願番号：特願2022-062001、出願日：2022 年４月１日.